ADVANCED FUNCTIONAL MATERIALS
www.afm-journal.de

Stimuli-Responsive Liquid Crystal Elastomers: From Materials to Applications

Jiao Liu, Hao-Yi Jiang, Jing-Qi Tian, Yuqi Tang, Chi-Bo Feng, Xin-Yu Zhou, Zhi-Jun Huang, Bing-Xiang Li, Yan-Qing Lu,* and Quan Li**

Liquid crystal elastomers (LCEs) are well-known for their significant, reversible, and anisotropic shape changes when exposed to different external stimuli due to their crosslinked polymer networks that merge the elastic properties of rubbers with the anisotropic characteristics of liquid crystals. LCEs with stimuli-responsive behaviors are preferable for applications in robotics, bio-medics, electronics, optics, and energy. In this review, the state-of-the-art advances in stimuli-responsive LCEs are reviewed, including thermo-responsive LCEs, photo-responsive LCEs, electro-responsive LCEs, and other responsive LCEs, such as chemical-responsive LCEs, magnetic-responsive LCEs, humidity-responsive LCEs, radio-frequency -responsive LCEs, ultrasonic-responsive LCEs, and photothermal-responsive LCEs, all of which have contributed to the resurgence in LCE research. The LCEs exhibit remarkable performance, spanning several orders of magnitude. They typically achieve actuation strains of 5–500%, stresses of 0.01–20 MPa, and fast response speeds, making them promising systems for actuators and artificial muscles. Furthermore, the applications of these responsive LCEs in information encryption, force sensors, and material transportation are demonstrated, which have significant potential for further development of the next-generation advanced functional materials. Finally, this review concludes with a summary and perspective on the current challenges and emerging research opportunities for high-performance LCEs endowed with remarkable properties.

1. Introduction

Stimuli-responsive polymeric materials have garnered significant attention due to their lightweight, excellent processability, and biomimetic responses to external stimuli, which demonstrate potential applications in integrated sensors, soft robots, and actuators.[1–12] Polymers exhibiting liquid crystal (LC) phases are particularly intriguing materials, showing great promise in fields such as soft robotics,[13–16] information security,[17–19] and sensing,[20–24] due to their ability to reversibly alter sizes and shapes in response to stimuli including heat, light, electricity, or magnetic fields.[25–29] LCs are a mesophase, an intermediate state between solid and liquid,[30] characterized by both the fluidity of a liquid and the orderliness of a crystal.[31,32] LCs are typically divided into two categories: thermotropic LCs and lyotropic LCs.[33–40] The former exhibits a mesophase as the temperature varies, while the latter forms a mesophase as a result of changes in solvent concentration. When a crystalline substance is heated to its melting point, the molecules lose their positional order, while their orientational order stays intact. Upon further heating, the material loses its intermolecular orientational order and transitions into an isotropic state. Polymers with LC phases contain LC main-chain polymers (LCPs), glassy LC polymer networks (LCNs), LC elastomers (LCEs), etc.,[41] as shown in Figure 1. Among them, LCPs are typically high-performance polymers characterized by a low dielectric constant and excellent heat resistance, capable of forming LC phases due to rigid rod-like molecular structures and intramolecular interactions. LCNs feature a network structure with moderate to dense crosslinking, demonstrating high-performance characteristics similar to those of LCPs. However, when stimulated, the ordering of LCNs decreases slightly in

J. Liu, H.-Y. Jiang, J.-Q. Tian, C.-B. Feng, X.-Y. Zhou, Z.-J. Huang, B.-X. Li
College of Electronic and Optical Engineering and College of Flexible Electronics (Future Technology)
Nanjing University of Posts and Telecommunications
Nanjing 210023, China
E-mail: bxli@njupt.edu.cn

The ORCID identification number(s) for the author(s) of this article can be found under https://doi.org/10.1002/adfm.202524606

DOI: 10.1002/adfm.202524606

J. Liu, Y.-Q. Lu
National Laboratory of Solid State Microstructures and Collaborative Innovation Center of Advanced Microstructures and College of Engineering and Applied Sciences
Nanjing University
Nanjing 210093, China
E-mail: yqlu@nju.edu.cn

Y. Tang, Q. Li
Institute of Advanced Materials and School of Chemistry and Chemical Engineering
Southeast University
Nanjing 211189, China
E-mail: quanli3273@gmail.com

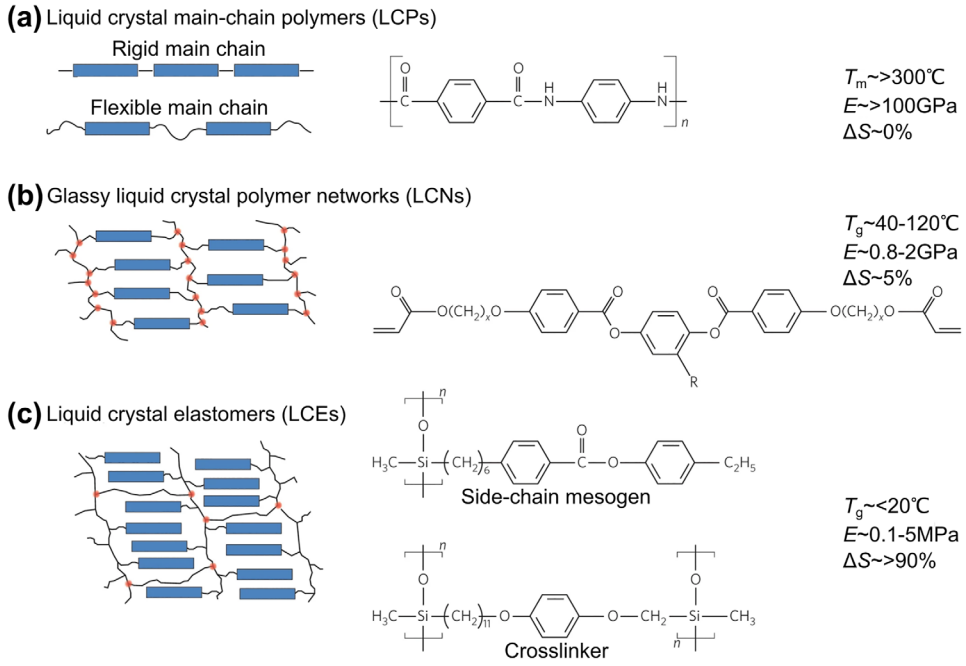

Figure 1. Examples of liquid crystal polymers (LCPs), polymer networks (LCNs), and elastomers (LCEs). Reproduced with permission.[29] Copyright 2015, Springer Nature.

comparison to LCPs. LCPs, LCEs, and LCNs represent a class of stimuli-responsive materials capable of programmable shape changes. LCEs are typically regarded as crosslinked LCPs. Nevertheless, their response to stimuli differs from that of highly crosslinked, glassy polymers, which are formed through the polymerization of concentrated multifunctional LC monomers and are known as LCNs. In the wider category of crosslinked LCPs, the magnitude of the stimulus response is linked to an increase in the molecular weight between crosslinks (MW_c), which in turn leads to enhanced chain mobility in LCEs. These materials are distinguished by their chemical compositions, crosslinking densities, and thermomechanical properties (**Figure 1**). Most LCEs are lightly crosslinked polymer networks that incorporate either main or side chain mesogens, with a low overall crosslink density.[42–44] A thermochromism behavior [45] integrates shape memory properties with photochemical phase transitions, achieving a substantial light-induced contraction of 81% by controlling the storage and subsequent release of strain energy in linear LCP fibers. The switching segment, within its highly ordered structure, effectively traps the stress-induced strain energy, which is then swiftly released through reversible trans-cis photoisomerization that disrupts the lamellar LC phase, resulting in the ultralarge contraction. Wu and coworkers[46] constructed a photoactuator capable of being healed and reprocessed, based on entangled, non-crosslinked azopolymer chains with high molecular weight, which exhibits reversible solid-to-liquid transitions. Photoinduced bending in the azopolymer actuators occurs due to the trans-cis isomerization of the azopolymers on the irradiated surface. The healability and reprocessability of photoactuators enhance their lifetimes, making them crucial for material reuse and recycling, while offering a novel approach to the development of smart materials. They display significant reversible changes in shapes and colors at the macroscopic level under exposure to stimuli, in contrast to LCPs and LCNs.[47–50]

LCE, initially synthesized by Finkelmann,[51] is composed of long-chain molecules with weak crosslinking that undergo conformational changes when exposed to a small force, imparting the material both soft elasticity and viscoelasticity.[49,52–55] LCEs, capable of experiencing reversible, complex, and programmable shape changes when exposed to external stimuli, show great potential for applications in fields such as smart robots, bioinspired technologies, sensors, and information encryption.[56–60] During the transition from the LC phase to the isotropic state induced by an external stimulus, significant and reversible macroscopic shape changes occur between two distinct shapes due to changes in molecular ordering.[56] The ordering of mesogens in LCEs can be disrupted by exposure to external stimuli, causing mechanical and optical responses, including thermal,[61,62] electrical,[63,64] magnetic,[65,66] photonic,[67–70] chemical,[71,72] and mechanochromic responses[73,74] Moreover, integrating different functional dopants, such as carbon black particles, carbon nanotubes, liquid metals,[74–76] magneto-thermal dopants,[66] and photo-thermal dopants,[77] improves the thermal response rates, remote controllability, and programmability of LCEs. Apart from these properties, LCEs also exhibit intricate functions, including bending,[78–80] curling,[81] twisting,[82–84] oscillations,[85–88] out-of-plane actuation deformation,[89] and mechanical color change responses. [90,91] It is important to highlight that the reversible and anisotropic responses are exclusively observed in single-domain LCEs where all mesogens are aligned.[92] In contrast, LCEs produced without extra treatment are typically multidomain, with mesocrystals exhibiting local order within subdomains, while maintaining macroscopic isotropy.[93] The transition from a polydomain to a monodomain chain structure in LCEs shows great

potential for energy-absorbing applications due to the mechanical energy dissipation. Moreover, the reversible response of monodomain LCEs to external stimuli makes them highly suitable for different applications.

To address this issue, various techniques have been developed to fabricate aligned single-domain LCEs, including mechanical alignment, external field alignment, surface alignment, and anisotropic desolvation. The most commonly used alignment methods depend on the mechanical alignment of gel networks or viscous monomer solutions,[94] especially for the uniaxial alignment of thin films and fibers. Nonetheless, achieving mechanical alignment of spatially intricate patterns remains challenging, despite recent efforts showing some spatial control through multiaxial mechanical forces.[95] Other alignment techniques leverage the antimagnetic and dielectric anisotropies of mesogen monomers. The orientation of LCs can be controlled by applying an oriented surface, which induces anisotropy in the morphology or chemical structure of the surface, thereby transforming the LC material into an anisotropic form. Techniques such as cloth rubbing,[96] micropatterning,[97] and photolithography[98] have been used to achieve spatially complex patterns with intricate designs.

In recent years, researchers have explored various aspects of the chemistry and materials processing of LCE materials,[99] including different alignment methods (such as mechanical alignment, surface-enforced alignment, field-assisted alignment, and rheological alignment),[27,100] the preparation and properties of LCEs, thermally and photogenerated macroscale mechanical responses,[29] 4D printed LCEs with stimuli-responsive properties,[101,102] and their applications in smart soft actuator systems.[1,103] Prior research has extensively covered the fundamentals of LCEs,[104] including versatile actuation modes,[99,102,105] material-structure-function relationships,[106] bio-inspired color mechanisms,[107] shape-programming challenges,[108] and various soft actuators about adjustable stiffness, mechanical responsiveness, and their applications.[107] This review deliberately diverges from conventional focus on material design, fabrication, or actuation mechanisms. Instead, it establishes a unified framework spanning materials, fabrication, various stimuli-responsive performance, and applications, enabling direct cross-comparison among diverse material systems and device architectures. To the best of our knowledge, no reviews have yet comprehensively embraced the emerging topic of the different responsive behaviors of LCEs. Therefore, it is crucial to provide an easy-to-access overview of multiple-responsive LCEs to external stimuli and their applications, as this is essential for advancing their development and encouraging further innovation. In this review, we provide a state-of-the-art account on the recent advancements in multiple-responsive LCEs, including thermal-responsive LCEs such as thermochromic LCEs, thermal-responsive shape changes, and thermal-responsive soft actuators; photoresponsive LCEs, including photochromic cholesteric LCEs (CLCEs), photo-induced shape changes, photo-induced soft actuators, and photo-induced microactuators; electrical-responsive LCEs, such as electrochromic CLCEs, electro-induced shape changes, and electro-induced soft actuators; and other types of responsive LCEs (**Figure 2**). We also discuss the practical applications of these multiple-responsive LCEs in areas such as information encryption, force sensors, and material transportation, all of which hold great potential for the advancement of next-generation functional materials. Finally, this review concludes with an outlook on the existing challenges and prospects for high-performance LCEs with remarkable properties. Notably, the primary challenges of LCEs have been emphasized, with potential solutions suggested based on the cutting-edge research findings. The perspectives provided on this topic are anticipated to promote the further development of responsive LCE materials.

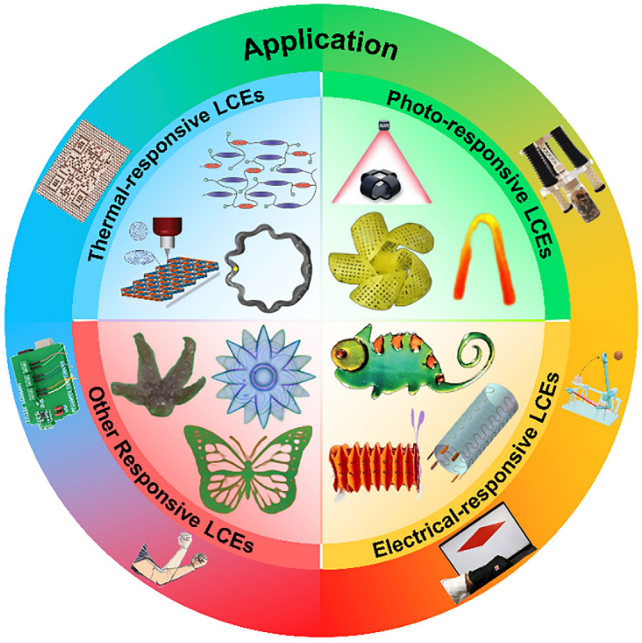

Figure 2. Schematic illustration of thermal-responsive, photo-responsive, electrical-responsive, and other types of stimuli-responsive LCEs and their applications.

2. LCE Fabrication

LCEs are crosslinked polymer networks that integrate the flexibility of rubbers with the anisotropic properties of LCs. Initially proposed by de Gennes in 1975, polymeric materials that maintain liquid crystallinity could show a significant response to stimuli, similar to the cooperative expansion and contractile behavior of muscle fibers. Finkelmann and coworkers were the first to synthesize these novel materials as a nematic side-chain elastomer by using a hydrosilylation reaction by attaching vinyl mesogenic pendant groups to a siloxane polymer backbone in 1981.[109] In 1994, Finkelmann developed a two-step crosslinking technique to create monodomain LCEs, which consequently made LCEs an important area of research in material science. Nevertheless, this crosslinking approach faces inherent challenges that limit practical applications. The issues arise from the inability to control the reaction kinetics during the alignment phase: applying the load too early to a fragile gel causes it to break, while waiting too long during the ongoing crosslinking process leads to poor alignment and significant disorder. Subsequently, polymerization techniques hydrosilylation, free-radical polymerization of acrylate, and polyaddition

reactions involving epoxy and acid have been employed to produce LCEs with diverse architectures.[110] In recent years, the have seen considerable advancements, particularly with the integration of thiol-based click chemistry in the fabrication of LCEs, such as the two-step thiol-acrylate reaction. In contrast to hydrolysis, this chemistry depends on the nucleophilic Michael addition of thiol-acrylate and acrylate photopolymerization. The polymerization process employed to form LCP chains and crosslink them into LCE networks encompass reactions, such as the epoxy-acid reaction,[111] epoxy-thiol reaction,[112] amine-acrylate reaction with hydrogen bonding,[113] thiol-isocyanate reaction,[114,115] and the acrylate homopolymerization used for crosslinking. The concept of LCE systems crosslinked through dynamic covalent chemistry allows the elastomers to be reshaped after complete crosslinking. Thermally activatable dynamic covalent chemistry reactions include Diels–Alder reaction,[116] thiol–Michael adduct equilibrium,[117] urea–amine exchange,[118] transcarbomylation,[119] transcarbonation,[120] thiourethane bond exchange,[121] vinylogous urethane–amine exchange,[122] siloxane exchange,[123] olefin metathesis,[124] triazolinedione click reactions,[125] transalkylation,[126] and nucleophilic exchange of quaternary anilinium salts.[127] Furthermore, 4D printing involves the additive fabrication of stimulus-responsive materials, allowing 3D structures to transform between pre-designed shapes. This method not only simplifies the production of conventional LCE actuators but also facilitates the construction of intricate LCE structures with multi-level mesogen alignment, offering researchers significant versatility in designing LCE actuators with complex structures.

3. Thermo-Responsive LCEs

3.1. Thermochromic CLCEs

LCEs attract significant attention due to the stimuli-responsive behavior enabled by the coupling of order and viscoelasticity. LCEs, which maintain the cholesteric phase (also known as CLCEs), are flexible polymeric materials with a periodic structure that exhibits selective reflection. Generally, there are two common methods for the preparation of CLCEs: anisotropic deswelling and enforced alignment. A well-aligned CLCE, capable of shape reconfiguration, through a polymerization process using diacrylate LC monomers and a dithiol (BDMT), was successfully synthesized (**Figure 3a**).[128] These CLCEs display selective reflection, which can be thermally adjusted by over 200 nm across the visible spectrum by incorporation of photosensitive chiral dopants. The optical response is closely related to the thermomechanical expansion of CLCE films. When heated, the reflection color of the films shifts from blue to red, moving to longer wavelengths. The extent of thermochromism of the CLCEs is mainly determined by the crosslink density, which is controlled by the concentration of BDMT.

The thermochromism behavior observed in CLCEs originates from a thermally induced displacement of the helical pitch, which corresponds to a deformation along the pitch. This structural alteration is the direct cause of the macroscopic color change. The selective reflection band of CLCE has a central wavelength (λ_C), which is defined by the helix's pitch length (P) and the average refractive index ($\bar{n}$). Their relationship is given by Equation 1:

$$\lambda c = \bar{n} P \tag{1}$$

The product of the chiral monomer's helical twisting power (HTP) and its concentration [c] is inversely related to the resulting pitch length.

$$P = \frac{1}{HTP \times [c]} \tag{2}$$

Increasing the BDMT concentration from 0.5 to 0.9 mol can reduce the crosslink density, thereby influencing the LCE's thermomechanical properties. Concurrently, heating the film from 25 to 200 °C induces a color shift from blue-green to red, which is associated with a shift in the reflection wavelength from 500 to 700 nm, indicating the thermal modulation of the CLCE's helical structures. Therefore, the thermochromic responses of the CLCE are dictated by factors such as its crosslink density, the concentration of chiral dopants, and the temperature, all of which influence the heterogeneity in the pitch distribution. The thermochromic behaviors can be modulated by adjusting the crosslink density, supramolecular concentration, and initial reflection wavelength. The addition of dimeric hydrogen-bonded mesogens moves the temperature-dependent tuning of the reflection wavelength toward lower temperatures. Moreover, once heating disrupts the hydrogen bonds, the thermochromic response is sharpened. In samples with a lower pitch-to-thickness ratio, heating can even lead to the complete disappearance of the reflection band. These findings highlight the unique potential of CLCEs for manipulating light, paving the way for novel applications in textiles, optics, and architecture. Moreover, in order to enhance the tunability and reaction rate, CLCEs with intra-mesogenic supramolecular bonds were developed.[129] Particularly, LC monomers derived from dimerized oxy-benzoic acid (OBA) were selected, leading to red-shifting thermochromism in selective reflection as the content of OBA increases. When the concentration reaches or exceeds a certain threshold, the selective reflection in the CLCEs can vanish upon heating, similar to an on-off "switching" effect. Likewise, as the temperature increases, the selective reflection of the CLCEs moves toward the red (Figure 3b), owing to the increasing film thickness and the helical pitch. This research is anticipated to facilitate practical applications in low-temperature sensitive optical components and thermal indicators for food packaging and smart window coatings. Thermochromic materials are increasingly used in various applications, and improving the selectivity and tunability of thermochromism would be particularly beneficial, especially in built environment applications. The thermochromic behavior of the CLCE results in solid-state components that simultaneously alter both specular and diffuse reflectance, thus paving the way for innovative applications in textiles, optics, and architecture. Additionally, CLCEs that incorporate intra-mesogenic supramolecular bonds could serve functional purposes in temperature-sensitive optical components, reliable thermal indicators for food packaging, and smart window coating. LCE lattices with thermally controllable deformation have promising applications in energy-absorbing structures, microfluidic actuation, mechanical computing, and soft robotics.

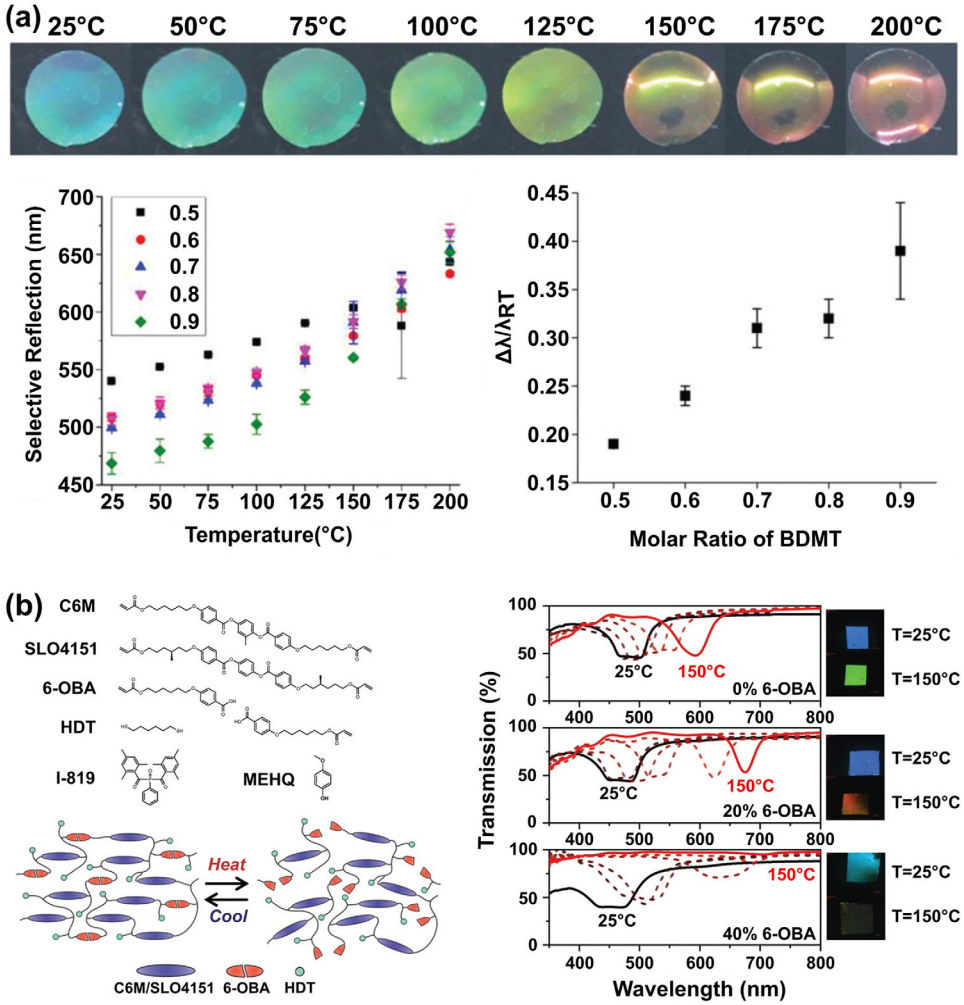

Figure 3. a) Thermochromism observed in a typical CLCE film. Reproduced with permission[128] Copyright 2019, John Wiley and Sons. b) Optical properties of CLCEs during heating. Reproduced with permission.[129] Copyright 2023, John Wiley and Sons.

The unique capabilities of LCEs to manipulate light open up new possibilities for applications in textiles, optics, and architecture.

3.2. Thermo-Responsive Shape Changes

LCEs have been considered as stimuli-responsive materials with promising applications in soft robotics,[24,130,131] artificial muscles,[132–134] shape-shifting structures,[135] and tissue engineering.[136] Main-chain LCEs consist of elastomeric networks with rigid LC moieties, known as mesogens, which undergo actuation when heated above their nematic-to-isotropic transition temperature (T_{NI}),[132,134,135] when exposed to light[137,138] or chemical gradients.[139,140] LCEs show significant, reversible contractions when exposed to temperatures above and below their T_{NI}, which is achieved by programming the director's alignment in the nematic state. To date, techniques have been developed to program director alignment, including command surfaces for producing thin films with a pixelated director field,[134,135,141] magnetic alignment,[139,142] 3D printing,[143–148] and mechanical alignment.[24,132] A flexible 3D printing platform for fabricating LCE lattices in both homogeneous and heterogeneous topologies, with spatially programmable nematic directional ordering and localized compositions, was presented.[148] These lattices undergo reversible shape-morphology changes above and below their T_{NI}, depending on their compositional topology. By directly printing LCE inks with different actuation temperatures, triangular honeycomb lattices are created, with each pillar featuring a unique LCE oriented in a guiding arrangement parallel to the pillar's direction (**Figure 4a**). Additionally, stretching and magnetic fields are commonly used to align LCEs into monodomain or single-crystal orientations, while temperature variation induces dimensional alteration (tensile strain) in uniaxially aligned LCEs.[42] However, these alignment techniques offer limited spatial control over orientation and resolution.

Typically, the shape and actuation of LCEs become permanent once the irreversible chemical crosslinking procedure is completed. However, recent studies show that introducing dynamic covalent bonds into LCE networks provides a novel approach to modifying mesogen alignment through covalent bond exchange, allowing for reprogrammability.[111,149–153] The challenge is that

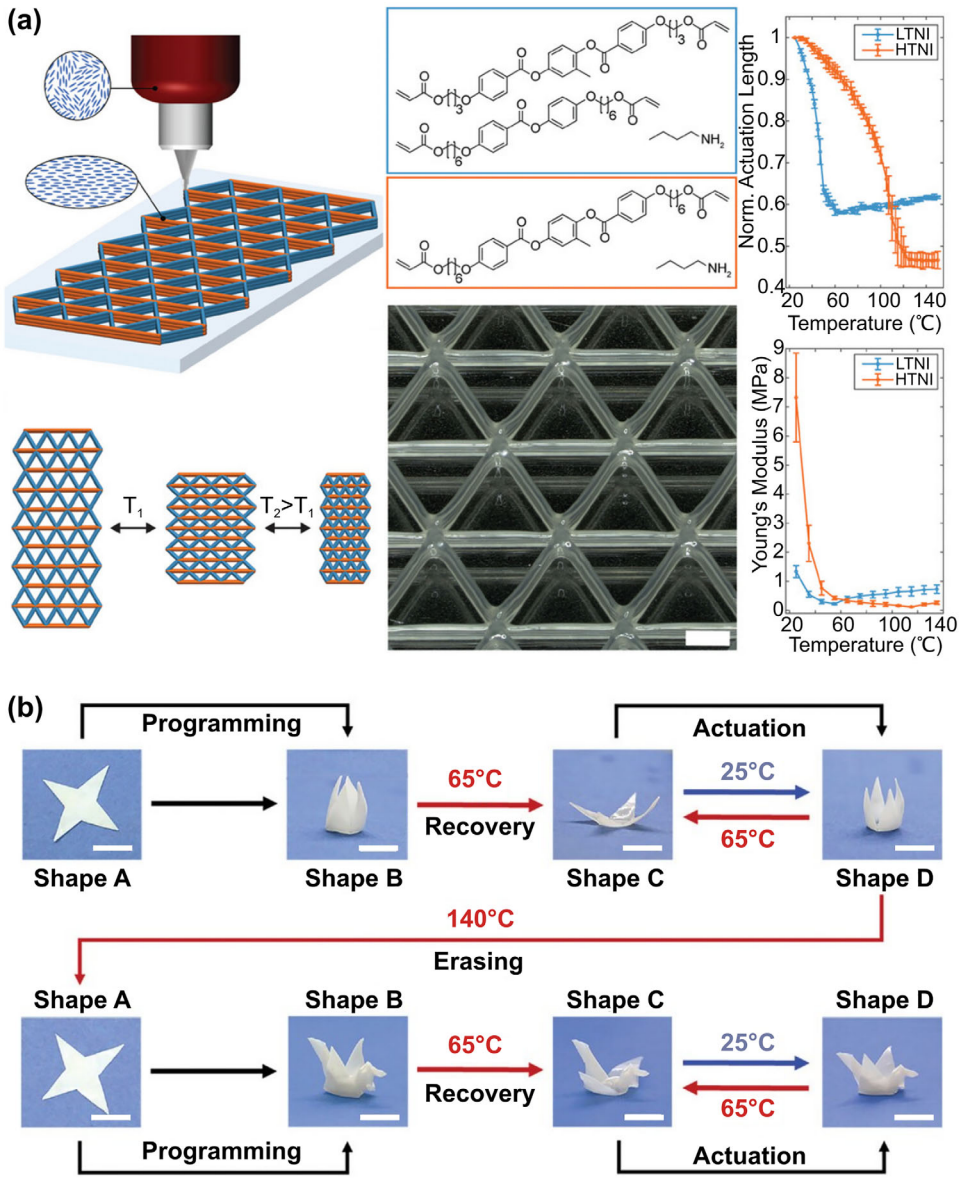

Figure 4. a) Printing LCE lattices. Reproduced with permission.[148] Copyright 2024, John Wiley and Sons. b) Demonstration of actuation programming and reprogramming. Reproduced with permission.[158] Copyright 2022, John Wiley and Sons.

activating dynamic bonds often requires extreme conditions, and multi-cycle reprogramming is often hindered by network deterioration and catalyst depletion. The isotropization temperature (T_i) is crucial because it determines the actuation temperature and influences other characteristics, significantly impacting the performance of LCE applications. LCEs need to be heated above their transition temperature from the nematic to the isotropic phase. Under this condition, the materials show elastomeric properties and require continuous external force to preserve their alignment and avoid returning to their original shape. Zheng and colleagues[154] developed a controlled radical diffusion method that allows for geometrically insensitive programming of actuation. This approach enables LCEs to be molded into intricate shapes using soft elasticity, while mesogen alignment is achieved by immersing the LCE in a solution of a free-radical initiator in water. This method enables the scalable and versatile production of sophisticated LCE actuators, marking a considerable leap forward in the field of soft robotics. Leveraging the synergistic effects of solvents and dynamic covalent bonds, Ji and coworkers[155] proposed a facile method to rejuvenate non-fresh LCEs, which involves transforming the irreversibly crosslinked LCE into a dynamic vitrimer through swelling with transesterification catalysts, allowing it to return to its original form for controlled regrowth. The solvent employed for swelling induces a physical change in the non-fresh LCEs, causing a transition from the LC phase to the isotropic phase. At the same time, the transesterification catalyst promotes the topological reorganization via dynamic covalent band exchange. This approach offers a post-modification technique for rejuvenating and reusing self-growing LCEs, holding potential for the development of

high-performance materials for advanced soft growing robotics. Conventional physical methods, such as annealing, are unsuitable for adjusting the actuation temperature. This is because the new T_i achieved through annealing reverts to its original value upon heating above T_i, but actuation itself requires temperatures exceeding T_i. The actuation temperature of a fully crosslinked LCE is predetermined upon its synthesis. Consequently, it can only be altered by modifying the chemical structures—a process that typically necessitates a complete restart from the molecular design stage. Ji and coworkers[156] discovered that reversible reactions of dynamic covalent bonds enable the retention of different T_i achieved through annealing in covalently adaptable LC networks, such as LC vitrimers. This reversible tunability of T_i allows a single, fully crosslinked LCE to yield diverse soft actuators with distinct actuation temperatures, thereby enabling one device to be adapted for varying thermal requirements. A new method for reprogramming is to spray a thermoplastic layer over an LC layer.[157] However, due to the significant influence of layer thickness on performance, the bilayer structure is limited to thin-film actuators and unsuitable for 3D actuators with complex geometries. The dual-phase LCE networks that combine a crystalline melting transition with an LC transition were developed.[158] Within this system, the crystalline phase functions as an "alignment framework", maintaining mechanical deformation through a shape memory mechanism and ultimately leading to mesogen alignment within the LC phase (Figure 4b). This approach employs a physical shape memory transition to organize mesogens, enabling quick reprogramming within seconds and offering remarkable versatility in designing 3D-printed LCEs with unlimited programmable actuation modes.

3.3. Thermo-Responsive Soft Actuators

Incorporating soft materials into robotics represents one of the most promising pathways for advancing biomimetic systems. A significant advancement in this integration is material-driven locomotion, which mimics the evolutionary progress of living organisms to crawl, walk, jump, and fly. Soft materials have been used for walking and crawling,[14,26,159–161] but jumping or storing elastic energy to launch like animals have been rarely investigated.[162–165] A method to quickly release stored energy is by inducing mechanical instability in soft materials.[166] The snap-through transition in soft actuators[167] has been investigated through variations in crosslink density,[168] light,[169,170] humidity,[171] pressure,[172] etc. Snap-through is commonly found in biological systems, mechanical devices, and consumer goods, which occur in responsive materials due to mechanical instability induced by external stimuli.[173] This behavior in CLCEs arises from patterning the nematic direction through the material thickness and combining it with spatial variations in stimulus exposure, resulting in mechanical instabilities.[143,174,175] The localized orientation of the director in LCEs and mechanical components with a full-thickness functional gradient was successfully produced (**Figure 5a**).[176] The laminates are composed of two different thick LCE film components: one was synthesized using radical-mediated 1,4-bis-[4-(6-acryloxyhexoxy)phenyl]-2-methylbenzene and benzyl mercaptan, yielding a rigid LCE with a high crosslinking density. The other was fabricated by mixing acrylate and mercaptan, resulting in a softer LCE with a lower crosslinking density. Each film is manufactured into a 7 mm square with a +1 topological defect. By compressing these LCE films together, the alignment of the defect center with the edges is achieved, enabling a laminated device with a gradual modulus gradient. The high-modulus surface is positioned down on a heating surface at 160 °C, allowing the film to initially deform into a cone shape. The LCE film's curvature subsequently flips as a result of mechanical instability, creating an inverted cone and a sharp jump in the component's center. Figure 4a illustrates the leaping behavior of LCEs due to this abrupt change. The transition generates force and acceleration, allowing the LCE to jump off the surface in less than 6 ms, achieving a height over 200 times its thickness and 2.5 times the width of the LCE component. In response to stimuli, the LCEs can reversibly shrink or expand by transitioning between nematic and isotropic states.[177,178] Many bistable soft active structures based on LCEs, including doubly clamped buckling strips,[170,174,179,180] cylindrical shells,[169] twisted ribbons,[181] and circular bilayered rings,[182] show the light- or heat-induced snapping.

Harnessing snapping, a natural instability phenomenon (e.g., Venus flytraps), has gained increasing attention in the field of autonomous soft robots. However, the development of self-sustained snapping and snapping-driven autonomous motion in soft robots has been seldom explored. The bistable, ribbon ring-like structures to facilitate self-sustained snapping in a collection of soft LCE wavy rings through the continuous thermal and photothermal activation were produced (Figure 5b).[183] The self-sustained snapping drives the rings to flip continuously, producing autonomous dancing or crawling motions on both land and underwater. The 3D, self-supporting wavy rings exhibit a highly symmetric or asymmetrically twisted shape, with adjustable geometric asymmetries. The crawling velocity can be modified by changing the geometric asymmetries, with the maximum speed achieved at the greatest asymmetry. The twisting soft robots that incorporate inherent physical intelligence, enabling flexible and autonomous movement in diverse unstructured environments, without relying on onboard or external control systems or human intervention, were prepared (Figure 5c).[181] The soft robots are made of twisted LCE ribbons with a straight centerline that respond to heat, enabling them to absorb thermal energy from their surroundings and traverse various outdoor hard surfaces and different granular substrates without slipping. These actions include climbing loose sandy slopes, navigating sand ripples, and escaping from buried sand. This study presents an innovative approach to designing the embodied physical intelligence, utilizing twisting geometry and snap-through instability to enhance adaptive interactions between soft robots and the environment. Figure 5c shows that it self-rolls constantly at a speed of 0.4 mm s^{-1} to climb the gently curved car roof.

4. Photo-Responsive LCEs

4.1. Photochromic CLCEs

Compared to temperature and other stimuli, light has been considered a promising method for distant, localized, and free-form actuations that do not alter the surrounding medium. A crucial aspect of an object is its color, which is essential to the

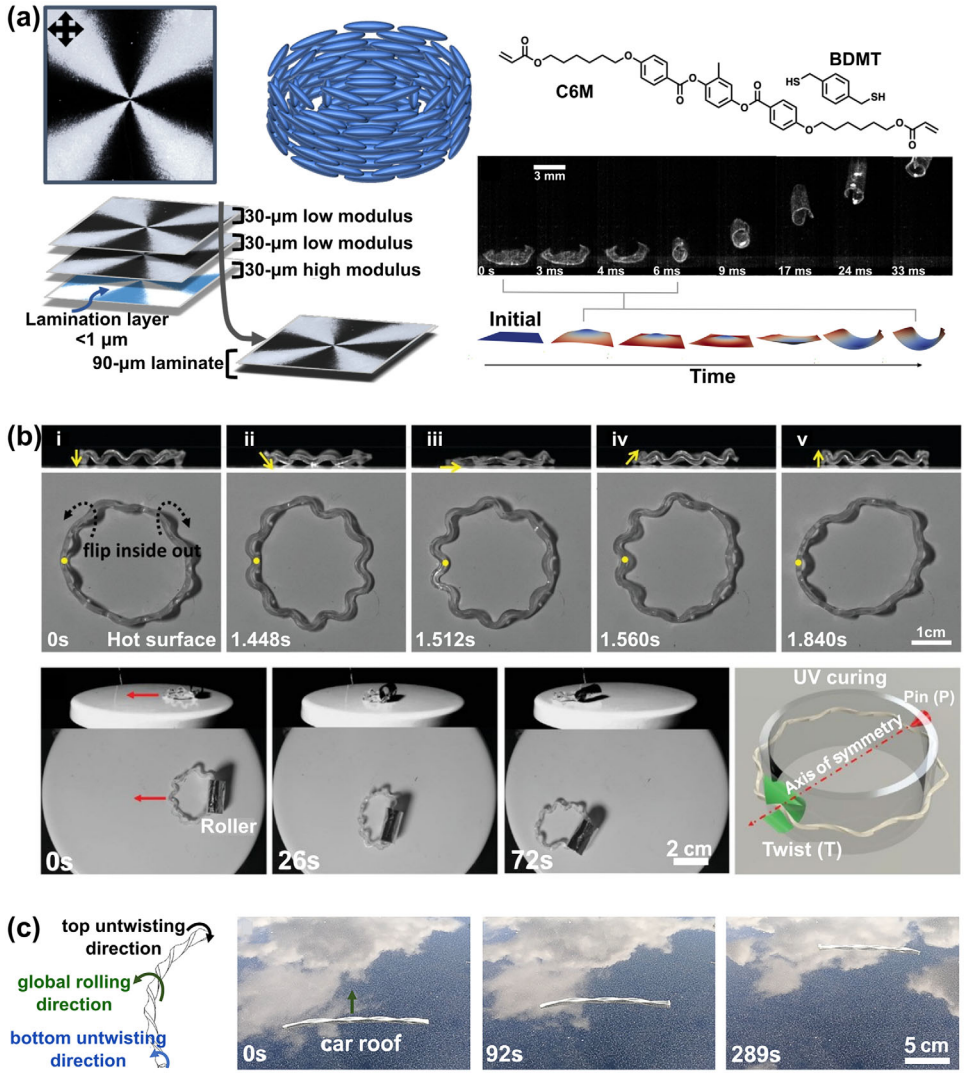

Figure 5. a) Leaping LCEs. Reproduced with permission.[176] Copyright 2023, The American Association for the Advancement of Science. b) Time-lapsed optical side-view and top-view images of the self-dancing ring at 120 °C, and the originally immobile dancing wavy ring self-crawls forward after adding a lightweight roller to reduce rear friction. Reproduced with permission.[183] Copyright 2022, John Wiley and Sons. c) Demonstration of self-rolling while climbing a car roof outdoors. Reproduced with permission.[181] Copyright 2022, National Academy of Sciences.

communication of information through symbols, pictures, and designs in contemporary information technology.[184–189] To realize both shape-morphing and color-changing abilities in cholesteric and nematic LCEs doped with chromic dyes or aggregation-induced emission (AIE) molecules, researchers have recently combined conventional molding methods with mechanical or surface alignment strategies.[90,190–194] A photoswitchable titanium-based nanocrystal (TiNC)/LCE composite ink suitable for 4D printing was developed, enabling reprogrammable photochromic and photomotive properties within a single structure.[188] When exposed to oxygen and UV radiation, the printed TiNC/LCE composite can reversibly transition from white to black due to the photochromic quality of the TiNC. A customized UV light mask was employed to inscribe the letters "LCE" on a printed TiNC/LCE composite surface (**Figure 6**a). By using another UV light mask, the composite sheet can be cleaned and overwritten with a high-resolution barcode after exposure to air. The phase transition between the monodomain and isotropic phases, involving a fully reversible change in molecular organization from long-range order to random orientation, governs both the shape-recovery actuation and visibility of LCEs. Reversible high-resolution phase patterning of LCE in different phases was realized with remarkable controllability through the use of laser-induced dynamic crosslinking technology (Figure 6b).[189] When the LCE is exposed to a UV laser, the crosslinking occurs in the isotropic phase within the irradiated area, which restricts the molecular motions. As a result, the crosslinked LCE maintains its transparency and exhibits isotropic phase characteristics below the T_{NI}. To address this issue, the material of 2-Methylene-propane-1,3-bis(thioethyl acrylate) (MBTA) was added to the LCE networks, allowing the incorporation of allyl sulfide functional groups. Chain exchanges between these allyl

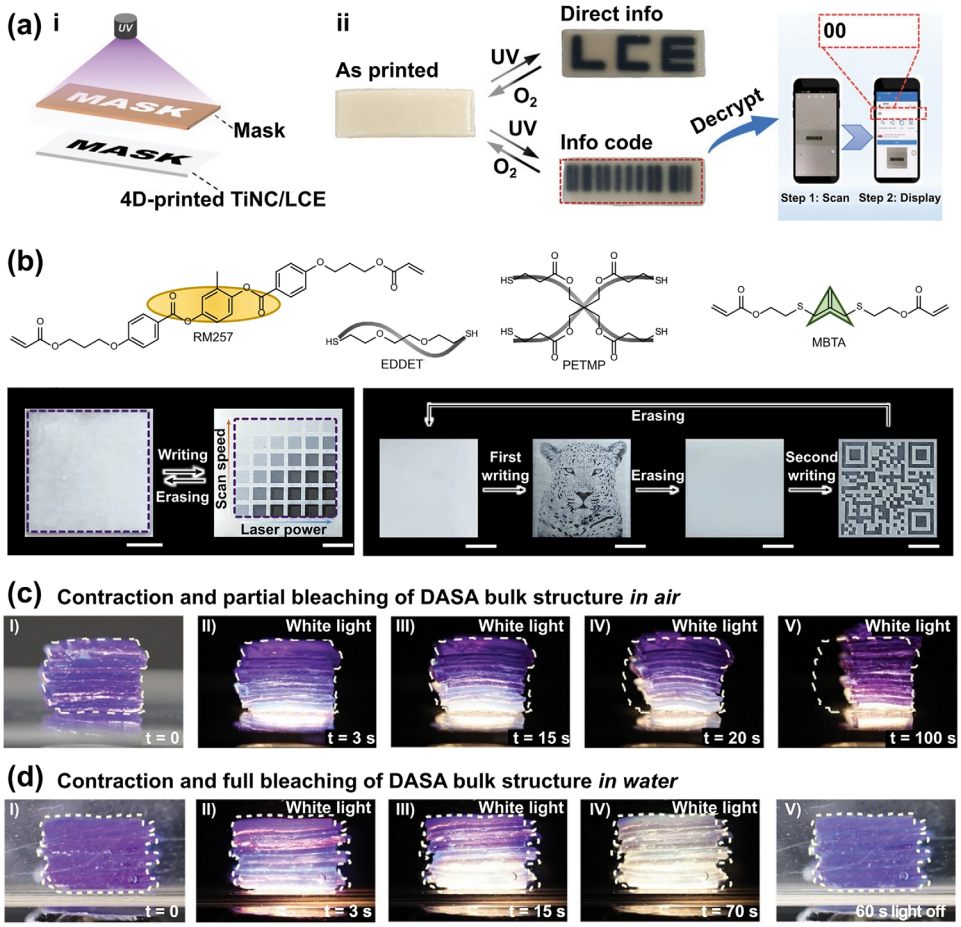

Figure 6. a) Optical reprogrammable color mode facilitates image display and encryption of information. Reproduced with permission.[188] Copyright 2023, John Wiley and Sons. b) Molecular structures and pictures of LCEs going through the printing process with different laser settings and the erasing procedure that follows. Reproduced with permission.[189] Copyright 2022, Springer Nature. c,d) Under white light irradiation, the width of the 3D structure undergoes contraction and masking: c) in air and d) underwater. Reproduced with permission.[199] Copyright 2024, John Wiley and Sons.

sulfide groups through RAFT (Reversible Addition-Fragmentation Chain Transfer) reactions facilitate stress relaxation within the crosslinked network. Free radicals produced by photoinitiators under UV laser irradiation initiate RAFT reactions between the allyl sulfide groups, resulting in the erasure process at elevated temperatures with a higher-power laser than the one used during the writing process. The LCE was modified into a multi-domain phase through the RAFT process, enabling controlled release during the writing process. After cooling to room temperature, the modified multi-domain LCE reverts to its opaque properties. Thus, the reversible patterning of heterogeneous phases inside homogeneous LCE films is created (Figure 6b). Moreover, photonic switches can be used to induce phase transitions of the LCEs, along with long-wavelength light from the visible to near-infrared range.[195,196] For example, azobenzene derivatives in conjunction with upconversion[197] or triplet–triplet annihilation mechanisms have been employed to build red-light-regulated systems.[198] A unique post-functionalization procedure by incorporating donor-acceptor Stenhouse adduct (DASA) into siloxane-based LCEs was designed (Figure 6c,d).[199] When exposed to low-intensity visible light, these LCEs exhibit 2D planar actuation and bleaching by incorporating DASA, which overcomes the conventional incompatibility with LCEs, allowing the fabrication of films with appropriate thickness. The LCEs' bending and contraction occur when exposed to high-intensity visible light. Under 300 mW cm^{-2} illumination, the material contracts vertically while expanding horizontally, although the bleaching is not uniform. The samples are submerged in water to create a reservoir for dispersing photothermal energy, which reduces the thermal-driven response of DASA. This helps prevent the formation of colored states and enhances light transmission. Under these conditions, within 70 s of light exposure, the 3D structure completely turns white, which contracts along the nematic direction while expanding in the orthogonal plane, with a change smaller than that observed in air. After the color fades almost instantly, the structure and color nearly return to their original state. This work lays the foundation for the development of LCE-based actuators beyond thin film and UV-light dependent systems. Through careful control of the structural design and light exposure, a single 4D-printed TiNC/LCE object can be programmed, erased, and reprogrammed both globally and locally, enabling the creation of desired photocontrollable color patterns and 3D structures, like barcode designs and

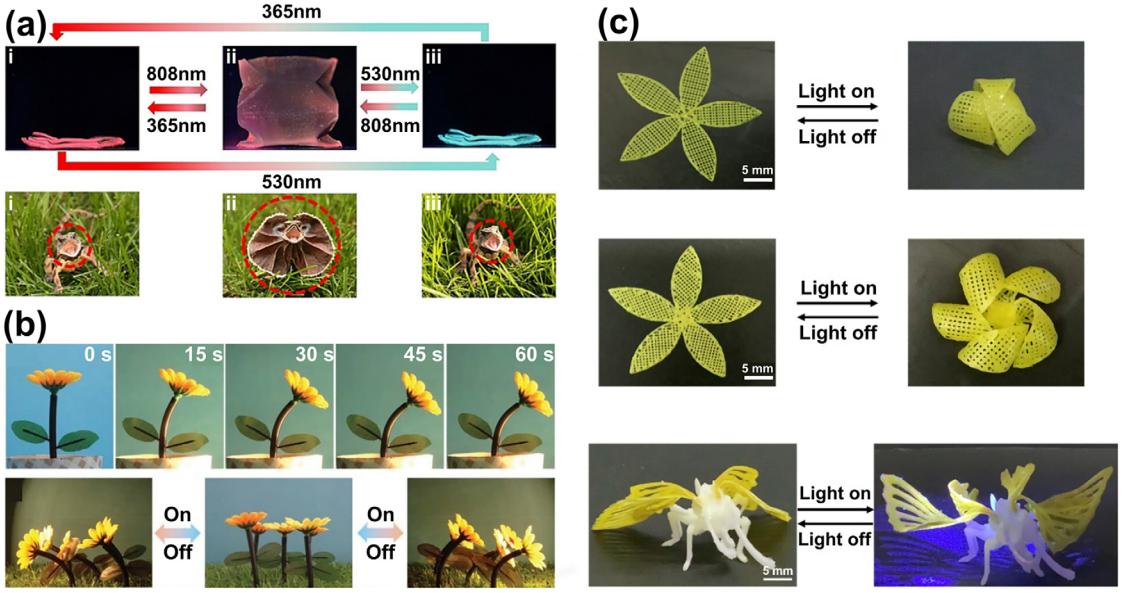

Figure 7. a) Photographic images of frill-necked lizards displaying their frills in either spread-out or folded positions. Reproduced with permission.[192] Copyright 2021, John Wiley and Sons. b) Bionic sunflower supported by the stem of the MXene-LCE hose driver. Reproduced with permission.[205] Copyright 2022, John Wiley and Sons. c) Photoresponsive biomimetic functions of 3D-printed LCE. Reproduced with permission.[206] Copyright 2024, American Chemical Society.

origami- and kirigami-inspired forms. This study introduces an innovative approach to the development of adaptive structures with distinctive and adjustable multifunctional capabilities, offering promising applications in fields such as biomimetic soft robotics, intelligent construction, camouflage, and multi-level information storage. Local phase patterning methods and permanent phase programming enable temporary information encryption at body temperature, enhancing the capabilities of LCE devices for use in wearable technologies.

4.2. Photo-Responsive Shape Changes

Bioinspired smart materials with complex deformations have attracted significant attention in fields of science and technology.[192,200–206] Li, Yang, and coworkers[192] incorporated terminally functionalized AIE-active tetraphenylethylene (TPE) derivatives and photochromic spiropyran (SP) derivatives into LCE networks through covalent bonding to achieve synergistic photochromic luminescence and programmable soft actuator functions (**Figure** 7a). The SP segments can undergo reversible isomerization, transitioning between a non-fluorescent closed form and a red fluorescent open state upon continuous exposure to UV and visible light. This research not only demonstrates photochromic luminescence via the use of functionalized TPE and SP derivatives but also reveals that the motions of the LCEs can be controlled by manipulating the alignment of the mesogens. The synergistic control over 3D shape deformation and color-selective luminescence was achieved.[205] Figure 7b illustrates the cooperative mechanism of motion and luminescence change, mimicking the biological functions of the fringed lizard. A novel photopolymerizable MXene nanoscale monomer was designed with high compatibility and efficient photothermal conversion within an LCE matrix. By performing in situ free radical photopolymerization of the MXene nanoscale monomer, the crosslinked LCE polymer networks were formed, resulting in a biomimetic light-responsive MXene-enhanced LCE tubular actuator with omnidirectional self-orientation capabilities. These polymerizable MXene nanoscale monomers act as both photosensitizers and photothermal nanotransducers, while also significantly enhancing the mechanical properties of the LCE tubular actuator. The MXene-LCE tubular actuators are capable of quickly sensing, tracking, and interacting with incident light in three dimensions. Their exceptional light-tracking precision is attributed to their unique hollow structure, radially symmetric shape, and integrated self-shadowing photothermal mechanical feedback. Furthermore, a biomimetic light-seeking sunflower with a stem composed of the MXene-LCE tubular actuator is fabricated. This system effectively tracks diffuse light and maintains its phototropic angle even under extended illumination (Figure 7b). Most of these systems rely on molecular photoswitches, such as diarylethene,[207,208] dithienylcyclopentene,[209] and azobenzene.[210–213] Azobenzene undergoes trans-cis isomerization upon exposure to UV light and reverts to its stable state when heated or illuminated with light of different wavelengths. The molecular motors were integrated into the backbone of LC oligomers, serving as an ink to print LCEs with photoresponsive biomimetic capabilities.[206] These light-driven molecular motors were selected as essential components of 3D printing photosensitive ink. A pair of photoresponsive flowers was designed and fabricated (Figure 7c). In the first case, the petal size was 5 × 15 mm^2 and made of two layers, with the printing orientation aligned at 0°/90° to the long axis, respectively. The designed flower was printed, cured, and dried, and then the final sample was subjected to UV light, which made the petals completely close within 60 s. When the light source was turned off, the

petals reverted to the original opening state, simulating the natural opening and closing of the flowers. Interestingly, altering the printing directions of the petals to 45°/135° relative to the long axis in the double-layer structure results in UV exposure triggering coiling, which causes the petals to close in a helical shape. The direction and manner in which the petals close are greatly influenced by the predefined printing pattern, including factors like the number of layers and the angles between them. This research paves the way for the future advancement of responsive materials with more sophisticated and intricate actuation capabilities. Self-oscillation refers to the continuous periodic movement of an object driven by a non-periodic stimulus. Priimagi, Yang, and coworkers[214] fabricated light-powered self-oscillators from LCN actuators that are capable of three basic modes of motion: bending, twisting, and contraction-expansion. By taking advantage of the time delay inherent in the material's response, which is essential for maintaining the periodicity of oscillation, a versatile self-oscillator has been achieved by simultaneously integrating different oscillation modes through the manipulation of the excitation beam's position. The generalized model and the demonstrated freestyle self-oscillator collectively offer new perspectives into the fundamental principles of soft matter mechanics. Sitti, Priimagi, and their coworkers[180] developed locomotion patterns resembling those of marine invertebrates by leveraging the natural light responsiveness and molecular anisotropy of monolithic liquid crystal gels (LCGs). By inducing localized deformations through precise spatiotemporal light patterns, a range of underwater locomotion modes such as crawling, walking, jumping, and swimming is achieved. The physico-mechanical properties of LCGs are fundamental to achieving diverse, light-driven underwater locomotion. This capability introduces a new design toolbox for creating efficient untethered soft robots for fluidic environments. In order to achieve autonomous physical intelligence (API) with self-regulated capabilities, He and coworkers[215] introduced an innovative method for generating nonlinear time-lag feedback in materials, showcasing how a constant stimulus can produce delayed responses that propel autonomous motion. The feedback systems trace the evolution of physically intelligent robots. Moreover, the strategies for embedding API into soft robots for diverse environments are proposed, and future challenges that extend beyond simple locomotion are discussed.

4.3. Photo-Responsive Soft Actuators

Animals utilize jumping as a vital form of locomotion to enhance their mobility, evade predators, and adapt more effectively to their environment, which inspires scientists to develop leaping robots based on biological principles. The robots are made of lightweight materials, and the structural layouts facilitate quick energy storage and release,[169,216–219] including dielectric elastomer actuators,[220–222] chemical actuators,[223,224] pneumatic actuators,[225] and motors.[226,227] A light-driven soft leaping robot, leveraging a double-fold LCE ribbon actuator combined with a three-leaf folding structure, was developed (**Figure 8a**).[228] This robot demonstrates significant potential in terms of jumping height, distance, and maximum take-off speed. Moreover, by simply changing the ribbon's fold angles, the leaping direction of the soft robots can be efficiently regulated. The changes in folding angles can alter the direction of the ribbon's unfolding force, thereby influencing the robot's jumping direction. The azimuth angle β of the double-folded LCE robot progressively increases from 3.6° to 67.0° as the folding angle increases from 0° to 44.2° (Figure 8a). This strategy improves the performance of jumping actuators, which is anticipated to have a wide-ranging impact on the strength, continuity, and adaptability of future soft robots.

Although a variety of leading robots have been reported in literature,[171] these robots generally necessitate modifications in external stimuli, such as temperature and light, to trigger jumping motions.[169,176,228–232] An LCE robot capable of self-sustained multimodal locomotion, with the particular mode of movement controlled by substrate adhesion or remote light stimulation, was introduced (Figure 8b).[233] Particularly, the LCE performs continuous snapping actions, enabling its self-sustained rolling motion in a constant gradient thermal field. By fine-tuning substrate adhesion, the LCE robot demonstrates reversible shifts between rolling and jumping modes. Moreover, the rolling motion can be dynamically controlled via light stimulation, allowing for a range of movements such as turning, slowing down, stopping, reversing, and navigating around complex obstacles. This concept of incorporating on-demand gate control opens up new possibilities for the design of further autonomous soft robots. A highly soft, low-driven temperature light-responsive LC gel with inherent light responsiveness that can mimic locomotion patterns of marine invertebrates was developed (Figure 8c).[180] Various underwater locomotion modes, such as crawling, walking, jumping, and swimming, were triggered by localized deformations by selective spatiotemporal light illumination. By slightly salting the water to increase its density, the LC gel construct can swim through consecutive arrhythmic stroke and relaxation cycles. These findings emphasize the crucial influence of the physico-mechanical characteristics of LC gels in different types of light-driven robotic underwater movement. Moreover, recent work has shown that LCE can achieve auto-switchable multimodal performance as a higher level of such photo-responsive intelligence. He and coworkers[234] also designed a light-responsive soft actuator with an engineered asymmetry and a dynamic structure, integrating two unique internal feedback loops governed by inherent bifurcation. As a result, the actuator is capable of dynamically switching among three motion modes— tracking, undulation, and oscillation, while independently adjusting to changes in environmental conditions like light intensity, viscosity, and temperature. Moreover, this multimodal functionality broadens the range of environmental interactions, paving the way for applications in areas like fluid dynamics, electronics, and environmental monitoring, beyond mere locomotion. This progress in physical intelligence marks a milestone in the development of next-generation autonomous soft robotics, paving the way for systems with superior autonomy and unprecedented adaptive capabilities.

Microactuators can accurately control and manipulate small-scale objects and systems, making it possible to develop miniature microelectromechanical systems[228,235,236] for use in miniature robotics,[237–241] biomedical devices,[242–244] and integrated electronics.[245] However, most of the complex microscale motions require each point along a trajectory to be deliberately encoded into the material during manufacture[80,144,239,246–248] or directly controlled in real time by successive changes in

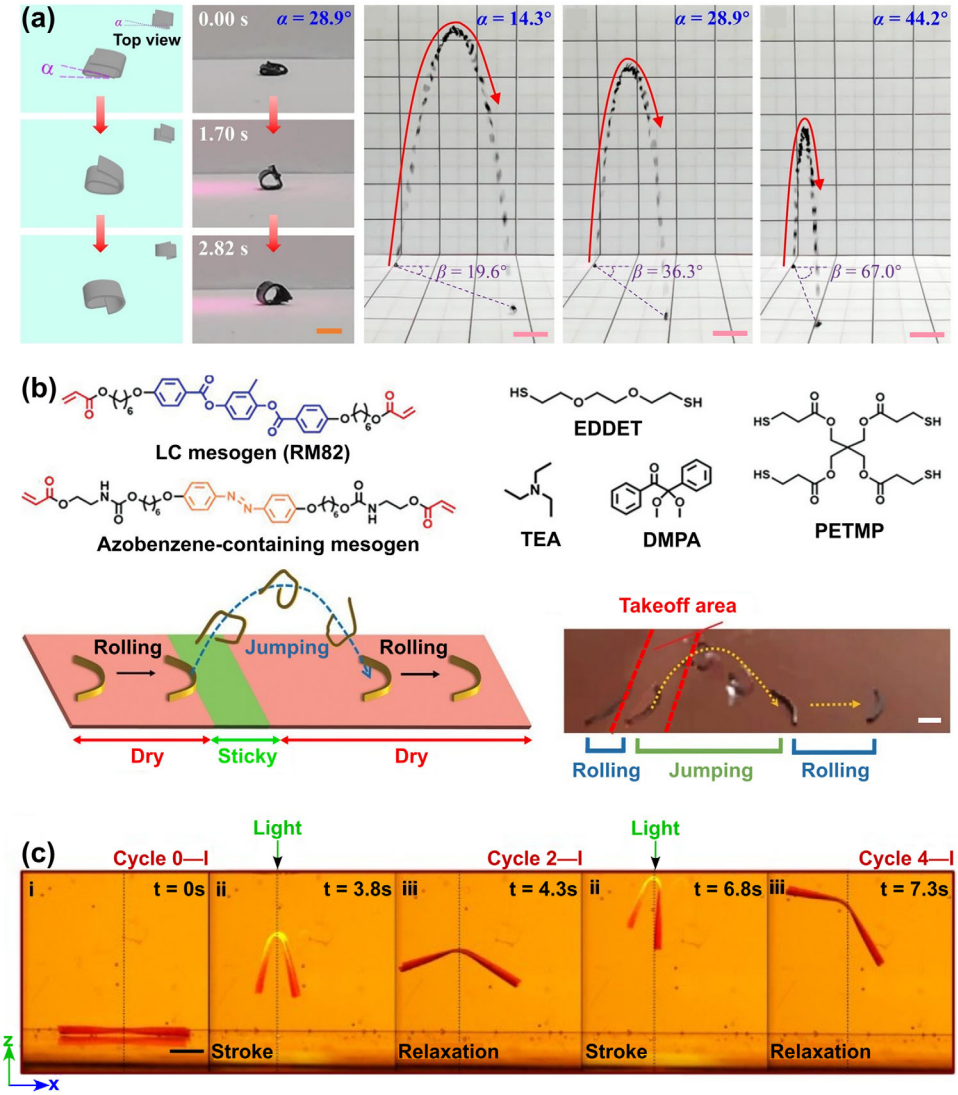

Figure 8. a) Photographs illustrating jump behaviors at various crease angles. Reproduced with permission.[228] Copyright 2023, John Wiley and Sons. b) Molecular structures and the integrated autonomous rolling and jumping motions. Reproduced with permission.[233] Copyright 2024, John Wiley and Sons. c) Swimming of a liquid crystal gel cantilever structure during consecutive illumination cycles. Reproduced with permission.[180] Copyright 2020, National Academy of Sciences.

external stimuli.[70,248–251] The soft micro-robots made from photoresponsive LCEs were developed,[70] which can be powered by structured monochromatic light to perform complex biomimetic movements, leveraging light's wireless, scalable, and spatiotemporally selective properties (**Figure 9a**). Researchers have developed artificial micro-swimmers that generate traveling wave motions for self-propulsion, eliminating the need for external forces or torques. Furthermore, micro-robots are constructed by photolithographically patterning disks, with the nematic director oriented perpendicular to the disk surface. These basic structures experience thickness compression along with in-plane expansion. The aligned LCEs used for these disks exhibit a typical contraction of ≈20%. Crucially, their axial symmetry implies that there is no preferential direction of motion within the plane of the disk. As a result, the disk's orientation can be manipulated in two dimensions based on the direction of the induced wave deformation. Additionally, projecting a rotating fan-shaped light field as an azimuthal traveling wave around the same micro-robot enables controlled rotation without causing translational movement. Through self-regulating processes, a variety of intricate and non-reciprocal brush-like trajectories in a single material system were developed (Figure 9b,c).[252] When a micropost made of photoresponsive LCEs, with mesogens oriented at an angle to the structure's axis, is exposed to steady light, dynamic movements can be triggered. The light causes a transition from order to disorder, converting the structure into a complex bimorph that twists and bends through a multi-layered opto-chemo-mechanical process. This study has broad implications for autonomous multimodal actuators and enhances fundamental understanding of self-regulated systems.

Drawing inspiration from the natural phenomenon of pilo-erection, where hair stands up on biological skin, light-fueled

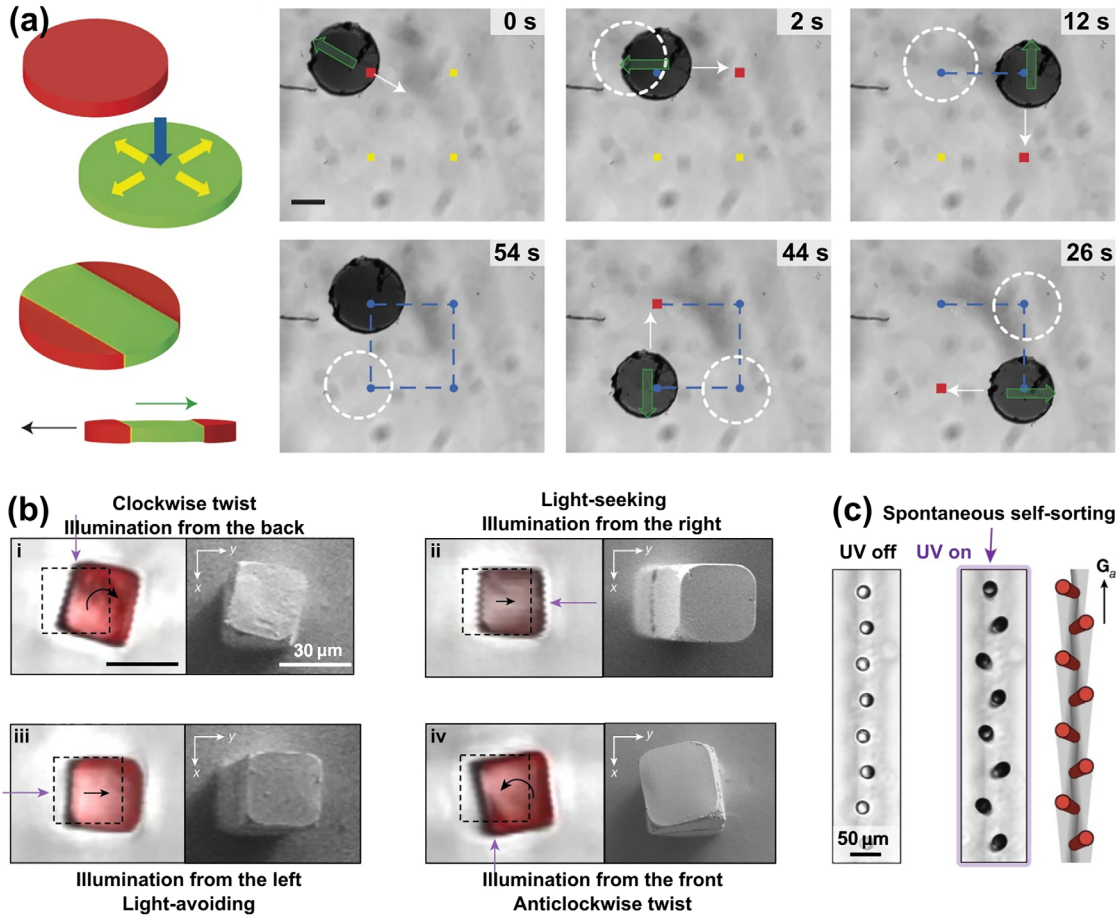

Figure 9. a) In-plane movement control of a disc-shaped microrobot. Reproduced with permission.[70] Copyright 2016, Springer Nature. b,c) In a micropost with oblique director alignment, various fundamental deformation modes are induced under irradiation with different directions. Reproduced with permission.[252] Copyright 2022, Springer Nature.

artificial goosebumps to activate passive microstructures were developed (**Figure 10**).[18] They used photoresponsive LCEs as the reactive artificial skin to drive 3D-printed passive polymer microstructures. Upon exposure to a programmable femtosecond laser, the LCE skin produces localized artificial goosebumps, precisely activating the adjacent microstructures. This type of microactuation can adjust the angles of micro-mirrors to regulate light reflection and break down self-assembled microstructures driven by capillary forces both locally and globally. This approach enables accurate, targeted, and controllable manipulation of microstructures, paving the way for advancements in programmable micromachine technology.

5. Electro-Responsive LCEs

5.1. Electrochromic CLCEs

Structure color can be generated using soft materials with the interaction between light and nanoperiodic dielectric structures.[253–259] The elastomer can be transformed into the form of CLCEs by using the reaction medium and monomer ingredients, which can produce flexible and stretchable chiral photonic elastomers (CPEs) that can self-organize into helical nanostructures.[260–263] The color of chiral nanostructures in LCEs can be tuned by stretching, with dynamic polychromatic control via electrical signals.[264–267] Recently, a CPE that can be electronically controlled in multiple colors was developed (**Figure 11a**).[266] The stretchable and synchronized multicolor separation from a uniform beginning color is realized by adjusting heterogeneous elastic moduli inside the CPEs, which can be investigated by using a mixed CPE structure incorporated into a dielectric elastomer actuator (DEPA). For practical applications, the CPEs on the DEPA are further organized into a 3x3 pixel array to show electrically controlled multicolor pixel binning switching. A chameleon-inspired photonic skin is created on a stretchable substrate, featuring multimodal CPEs with an initial uniform color. Under biaxial stretching, the initially monochromatic red chameleon skin transforms into a vibrant version, displaying localized color separation similar to the dynamic shifts seen in real chameleon skin. Drawing inspiration from the chameleon's actively tunable color systems, an innovative smart skin composed of a photonic crystal nanostructure, a carbon nanotube (CNT) coating, and LCEs (Figure 11b) was developed.[267] This intelligent skin integrates structural color tunability with multiple functionalities, including sensing and actuation, into a single architecture. Under an electric voltage, the smart skin

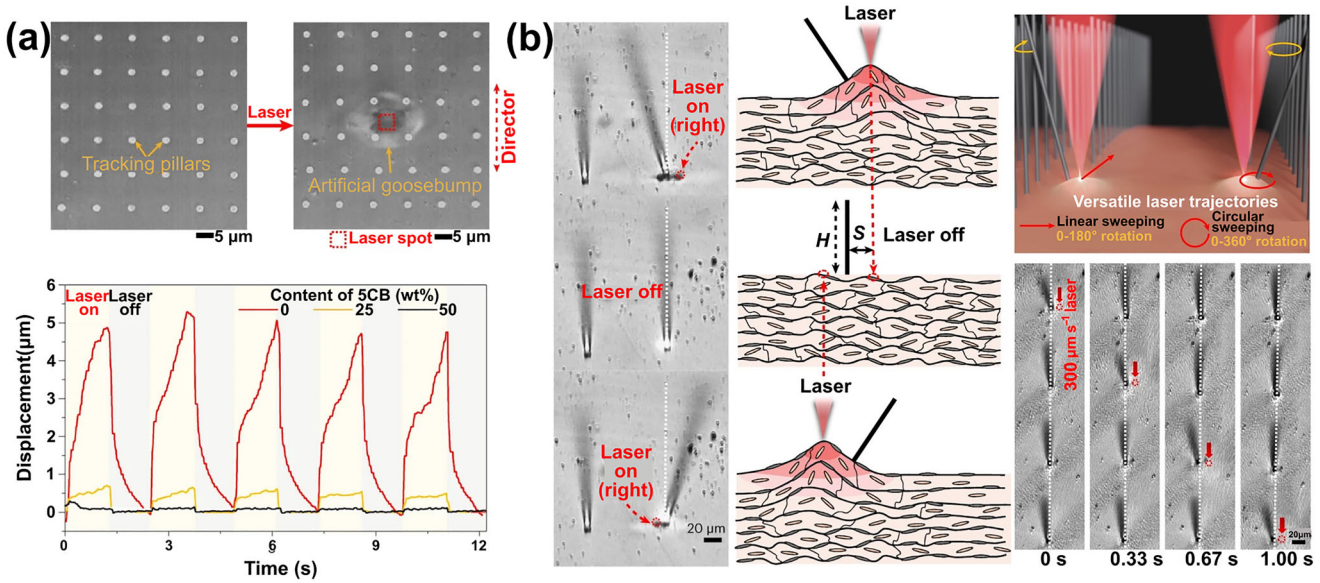

Figure 10. a) Generation of localized artificial goosebumps on the LCE skin using a femtosecond laser. b) Light-activated goosebump-driven passive microhairs with two degrees of freedom motion. Reproduced with permission.[18] Copyright 2024, Springer Nature.

exhibits a contraction effect due to the thermoelectric effect, induced by the photonic crystal structures, LCE-based actuators, and CNT coating, resulting in the visible color changes. This research is anticipated to open new pathways for creating active tunable structural color systems, pushing the advancements of structural color-based devices and systems. A hybrid LCE structure integrated with dielectric elastomer actuators enables electrically stretchable multicolor separation, leading to the development of chameleon-inspired photonic e-skin for various device applications. Additionally, the ability to switch multicolor concealed camouflage and control invisible photonic e-skin enhances the performance of numerous potential photonic applications. The adjustable structural color system automatically modulates the color based on the surrounding colors, paving the way for the creation of dynamic tunable structural color systems and promoting the advancement of structural color-based technologies and devices.

5.2. Electro-Responsive Shape Changes

The dielectric elastomers (DEs), which are exposed to an external electric field, can expand and shrink in-plane. By using customized material design,[268,269] patterned electrode coatings,[270,271] and rigorous external constraint,[272,273] this in-plane actuation can be transformed into a variety of out-of-plane motions. Three approaches have been used to tackle issues related to actuation strain and device fabrication: adjusting the mechanical characteristics of constraints or dielectric materials,[274–276] optimizing electric field parameters,[277–280] and selectively activating different components within assembled devices.[281] The LC dielectric elastomer capable of altering its dielectric driving mode in response to thermally induced shape changes was developed (**Figure 12a**).[276] The two shapes that emerge from the LC's phase transition demonstrate different bending stiffnesses, resulting in various driving modes after applying an electric field. Additionally, when the transesterification reaction is triggered by heating, the permanent shape can be altered through dynamic network rearrangement. The temporary repeatable shape is determined by the deformation that occurs during the solvent evaporation process. Meanwhile, the space charge mechanism allows for a considerably lower electric driving field and facilitates a bidirectional driving mode. The horn-shaped LCE alternates between a flat membrane and a serrated structure as a result of temperature changes. The varying bending stiffness of these geometries, once coated with flexible electrodes, results in two different dielectric actuation modes when exposed to an external electric field. The actuator bends to the left or right when the electric field is reversibly altered, causing the petals of the moving element to flex inward or outward. This unique flexibility in actuation modes under a low electric field provides a wide range of design possibilities for practical soft robots.

Two distinct active material systems were combined (Figure 12b):[269] the quick and effective actuation of dielectric elastomers and the shape programmability of LCEs. The molecular alignment and localized elastic anisotropy are imparted to LCEs through a top-down photoalignment technique. The linearly driven LCE monoliths are capable of achieving strain rates greater than 120% per second, with an energy conversion efficiency of 20%, and can lift loads over 700 times the weight of elastomers. The electric actuation mechanism offers distinct advantages for miniaturization, including shape programmability, improved efficiency, and greater flexibility, making it ideal for soft robotics and beyond. The flexible tubular actuators using a novel artificial muscle material were developed, which can be easily patterned with programmable strain derived from LCEs (Figure 12c,d).[24] Under applied electrical voltage, the tubular actuator can perform bending actuation in multiple directions and achieve significant (≈40%) uniform contraction.

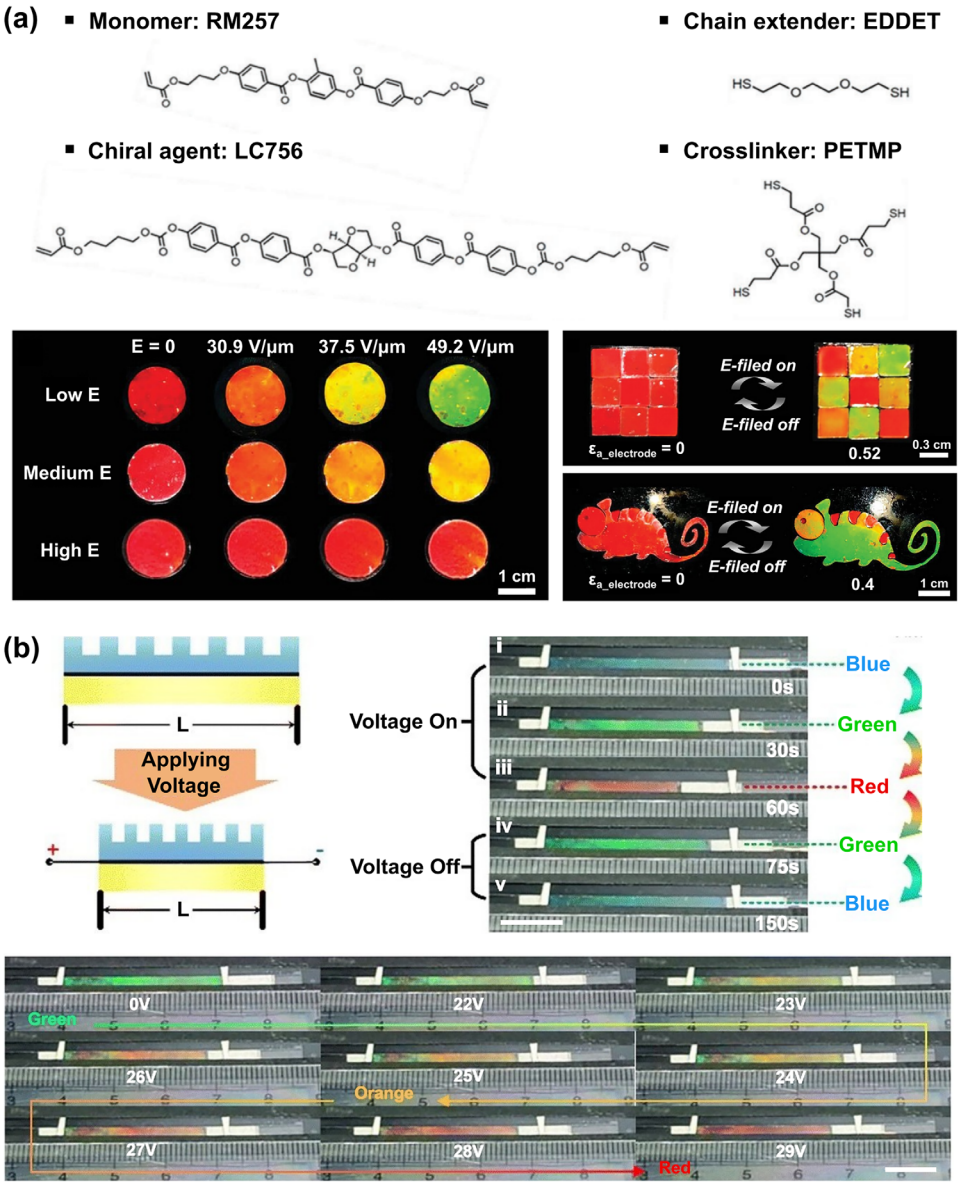

Figure 11. a) Chemical structure of raw materials for stretchable CPE precursors and reflection color of CPEs variation under different electric fields and electrically changeable multicolor graphics in pixel structure and chameleon pattern. Reproduced with permission.[266] Copyright 2023, John Wiley and Sons. b) Smart skin changes in length and color when a particular external voltage is applied. Reproduced with permission.[267] Copyright 2024, Royal Society of Chemistry.

By employing several tubular actuators, a multifunctional soft gripper and an untethered soft robot are constructed.

5.3. Electro-Responsive Soft Actuators

Electric actuators have significant advantages over stimuli-responsive materials.[76,282–285] Recent studies focus on combining stretchable resistive heaters with LCEs to enhance the control of electrical signals.[76,283,286] An artificial muscle fiber with enhanced mechanical properties, known as a dual-network liquid crystal elastomer (DNLCE), was developed by introducing a pure LC monomer network into a crosslinked self-network LCE (SNLCE) (**Figure 13**a).[286] The rigid auxiliary networks function as a sacrificial bond, effectively dissipating excess mechanical energy and aligning along the molecular chains of the primary network, thereby enhancing the mechanical performance and actuation load of DNLCE fibers. To enhance controllability, the DNLCE is coated on the surface of CNT fibers and forms a helical structure by inserting twisted wires to fabricate CNT@DNLCE coiled fibers driven by the electrothermal effect. Compared to CNT@SNLCE coiled fibers, this design improves the constant-length stress and actuation load without sacrificing the contraction stroke. Additionally, the CNT@DNLCE artificial muscle fibers are applied in the weaving of origami structures to achieve multiple motion modes. For instance, the 2D origami

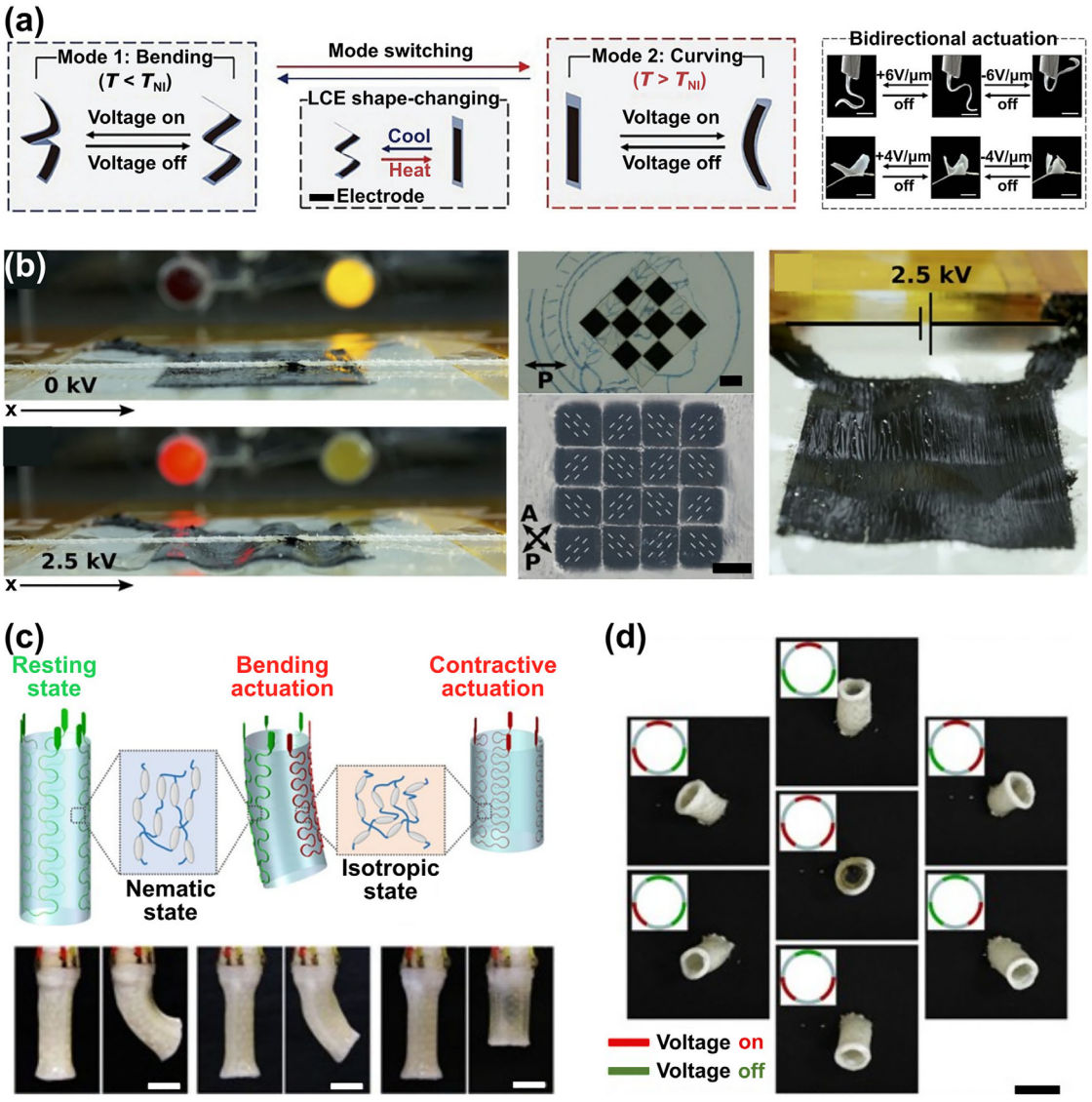

Figure 12. a) Mode-switching of dielectric actuations based on reversible LCE shape-changing. Reproduced with permission.[276] Copyright 2024, John Wiley and Sons. b) Uniaxial out-of-plane buckling LCEs and pixelated dielectric LCE actuator. Reproduced with permission.[269] Copyright 2019, The American Association for the Advancement of Science. c,d) Multimodal actuation of a tubular actuator based on LCEs. Reproduced with permission.[24] Copyright 2019, The American Association for the Advancement of Science.

structure is folded into a rectangular shape, utilizing the asymmetric friction between the feet and the wooden substrate to allow the caterpillar robot to move forward on various terrains. When voltage is applied, the caterpillar robot contracts under the action of fiber contraction, causing the rear foot to move forward while the front foot remains stationary. After the stimulus is removed, the crawling robot can revert to its initial state, with the front foot moving forward and the rear foot remaining stationary on a smooth surface, enabling it to crawl in an organized manner. This design, based on CNT@DNLCE artificial muscle fibers, provides new functionalities and application potential for bionic robots. An energy-efficient crawling robot inspired by caterpillars was fabricated, which is capable of exhibiting multiple crawling modes (Figure 13b).[287] This function is achieved through electric heating generated by soft heaters made of silver nanowire networks, which are patterned and integrated into a thermal bimorph actuator based on LCEs. By employing a patterned and distributed heating mechanism along with programmable heating, distinct temperature distributions are established, facilitating a curvature distribution along the robot's body. The competition between friction at the robot's front and rear ends and the ground allows for the modulation of temperature and curvature profiles, leading to varying frictional forces between the front and rear sections and the ground. This work demonstrates the potential of LCE-based actuators in soft robotics, advancing the development of adaptable, biomimetic crawling mechanisms. To facilitate the comparison of advanced LCE systems and the selection of optimal materials, **Table 1** provides examples of performance metrics across various responsive LCE soft actuators.

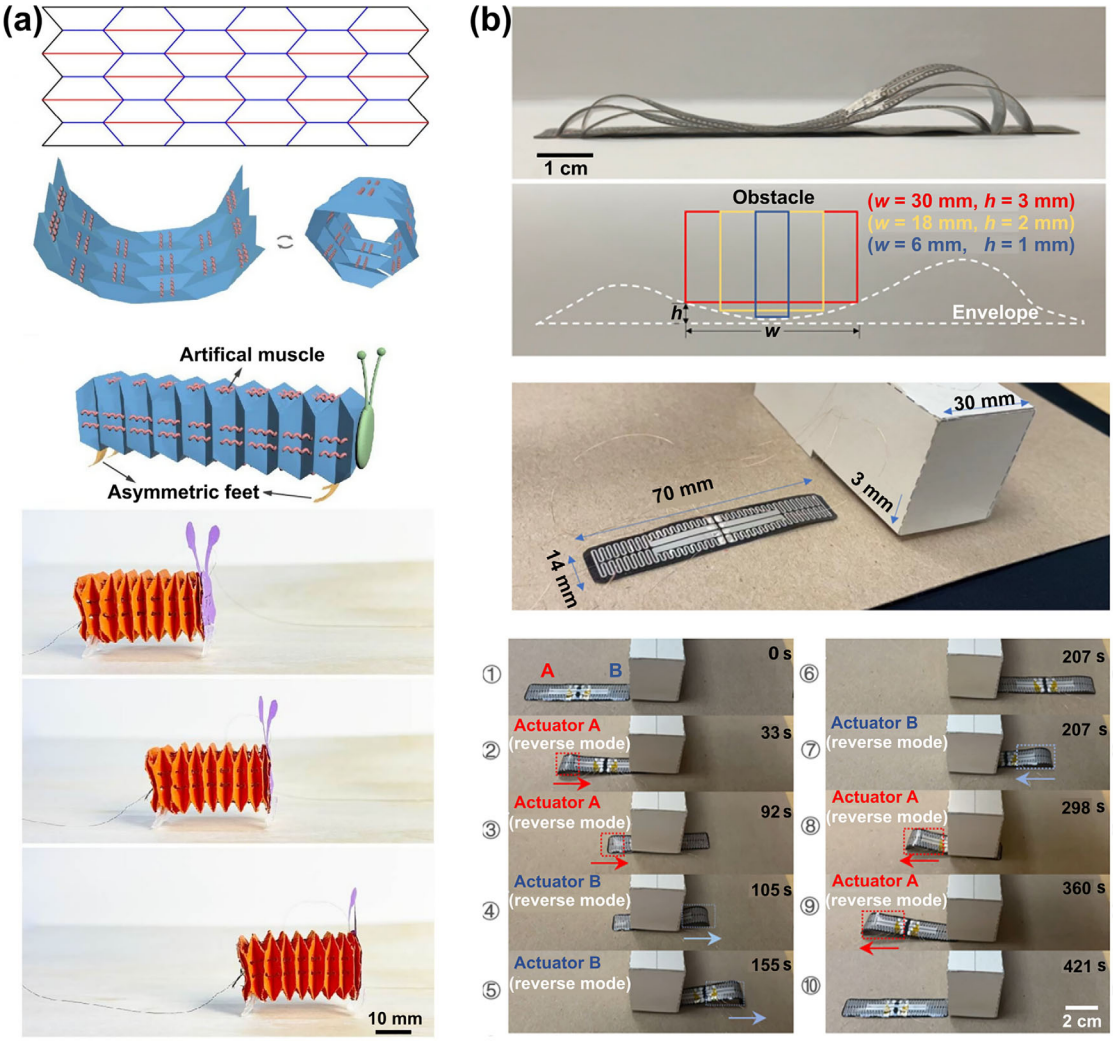

Figure 13. a) Application of the CNT@DNLCE artificial muscle fibers. Reproduced with permission.[286] Copyright 2024, American Chemical Society. b) Demonstration of the crawling robot moving through a shallow or deep gap. Reproduced with permission.[287] Copyright 2023, The American Association for the Advancement of Science.

6. Other Responsive LCEs

6.1. Chemical-Responsive LCEs

Mechanical color change refers to a color alteration resulting from mechanical deformation, which serves as a valuable characteristic for offering users direct and visually noticeable indications of environmental changes. Compared to electromechanical devices, mechanical color-changing sensors provide a direct method for detecting external stimuli. CLCEs, force-induced color-changing materials, have been widely studied due to their 1D periodic spiral shape, enabling predictable and reversible mechanical color changes across the visible spectrum.[29,80,91,191,288,289] By introducing dynamic covalent boronic ester bonds into the polymer network, a crosslinked CLCE that exhibits mechanical responsiveness, shape programmability, and self-healing capabilities was developed, whose reflection color can be dynamicallyand reversibly altered over the whole visible spectrum (**Figure 14a**).[90] As the applied strain increases from 0% to 120%, the reflectance peak wavelength gradually changes from 659 to 468 nm. The stretching and releasing cycles were repeated more than 100 times, with no significant signs of deterioration. This innovative approach enhances the functionality of CLCEs, providing significant potential for applications in smart materials and adaptive devices. A strain sensor based on a main-chain CLCE with high stretchability was designed, which is capable of distinguishing the direction, position, and magnitude of deformation under in-plane bending (Figure 14b).[290] The main-chain CLCE film exhibits a red, green, to blue color gradient in the direction perpendicular to the long axis of the film as the bending curvature increases. The preparation of suitable LCE fibers for textile applications is challenging due to the tendency of these fibers to fragment into droplets during processing, caused by Plateau-Rayleigh instability. To address this issue, a simple method to produce CLCE fibers from an oligomeric precursor that is diluted with a solvent was

Table 1. Examples of some responsive LCE soft actuators.

Stimulus	Processing route	Representative metric ranges	Prototypical applications	Refs.
Thermo-responsive soft actuators	Leaping, snap-through in a freestanding film	Strain rate (0.54% per °C); Stimuli-induced response (6 ms); Reaching a height over 200 times the material's thickness and 2.5 times the width of the LCE.	Material design and geometrical constraints	[176]
	Twisting for a soft, intelligent, autonomous robot	As *T* increases from 80 to 180 °C, rolling speed increases from ≈1.5 to ≈3.8 mm s^{-1}; Below T_{NI}, the ribbon rolls slowly at ≈0.5 mm s^{-1}; Above T_{NI}, it unrolls into a flat strip and stops rolling.	The design of embodied physical intelligence for adaptive soft robot-environment interactions	[181]
Photo-responsive soft actuators	Light-driven soft jumping robot	Jumping height (87 body length (BL)), jumping distance (65 BL), and maximum take-off velocity (930 BLs^{-1}); The actuators go through the flipping processes within 3 s; NIR laser (power density: 1.14W cm^{-2}).	Smart materials and soft intelligent robots	[228]
	Biomimetic swimming and versatile locomotion	The microrobot undergoes a net displacement of 110 µm at a speed of 2.1 µm s^{-1}; Moving backward, the microrobot displaces 120 µm at 2.8 µm s^{-1}.	Microrobotic technologies and advanced microrobotic	[70]
	Self-regulated non-reciprocal motions	Non-linear "dancing" actuation at 115 mW cm^{-2}; twisting to tilting at medium intensity; At maximum light intensity, it evolves into an asymmetric, stroke-like movement.	Soft robotics, micro-walkers, sensors, and cell culture scaffolds provide robust information encryption.	[252]
	Precise and two-degree-of-freedom motion, including 0–360 degrees of rotation	These microstructures have submicrometer-scale resolution (down to 100 nm).	Information storage applications	[18]
Both thermal- and photo-responsive soft actuators	Dancing and motion in free-standing wavy rings	Quickly snaps within 112 ms at flipping angle ≈135°; The fastest crawling speed ≈0.95 mm s^{-1}.	Adaptive autonomous soft crawler, hydrogels, shape memory polymers, and magnetic elastomers	[183]
	Multimodal autonomous locomotion	LCE arches up over 1.6 s. and collapses very rapidly (within 0.1 s); An initial increase in speed with increasing width, peaking at ≈9.3 mm s^{-1}.	Further autonomous soft robots	[233]
Electro-responsive soft actuators	Programmable liquid Crystal dielectric elastomer with multimodal actuations	LCE shape-changing strain (47.5%) and actuation angle (20°at 8 Vμm^{-1}).	Soft robotics	[276]
	Shape-programmable dielectric LCE actuators	The linearly actuated LCE monoliths achieve strain rates over 120% per second with an energy conversion efficiency of 20% while moving loads over 700 times the elastomer weight.	Soft robotics	[269]
	LCE-based soft tubular actuator with multimodal actuation	LCE-based tubular actuator with multiple actuation modes, controlled by 1.0 to 3.0 V; The tubular actuators exhibit multidirectional bending and up to ≈40% homogenous contraction.	Soft robot with on-board power source and microcontroller	[24]
	High-strength LCE fibers	The double-network LCE shows considerable improvements in tensile strength (313.9%) and maximum actuation stress (342.8%); The maximum energy density reaches 1207.1 J kg^{-1} under the 32 MPa actuation load; The contractile stroke retains 98.8% of its value after 2000 cycles.	Artificial muscle fibers and origami structures	[286]
Both thermal- and electro-responsive soft actuators	Bidirectional crawling robot with multiple locomotion modes	The locomotion speed depends on the applied current (from 5 to 30 mA) and actuation frequency (from 0.064 to 0.264 Hz); Under 30 mA and 0.2 Hz, forward and reverse locomotion speeds are 0.5 and 0.72 mm s^{-1}, respectively.	Smart and multifunctional soft robots	[287]

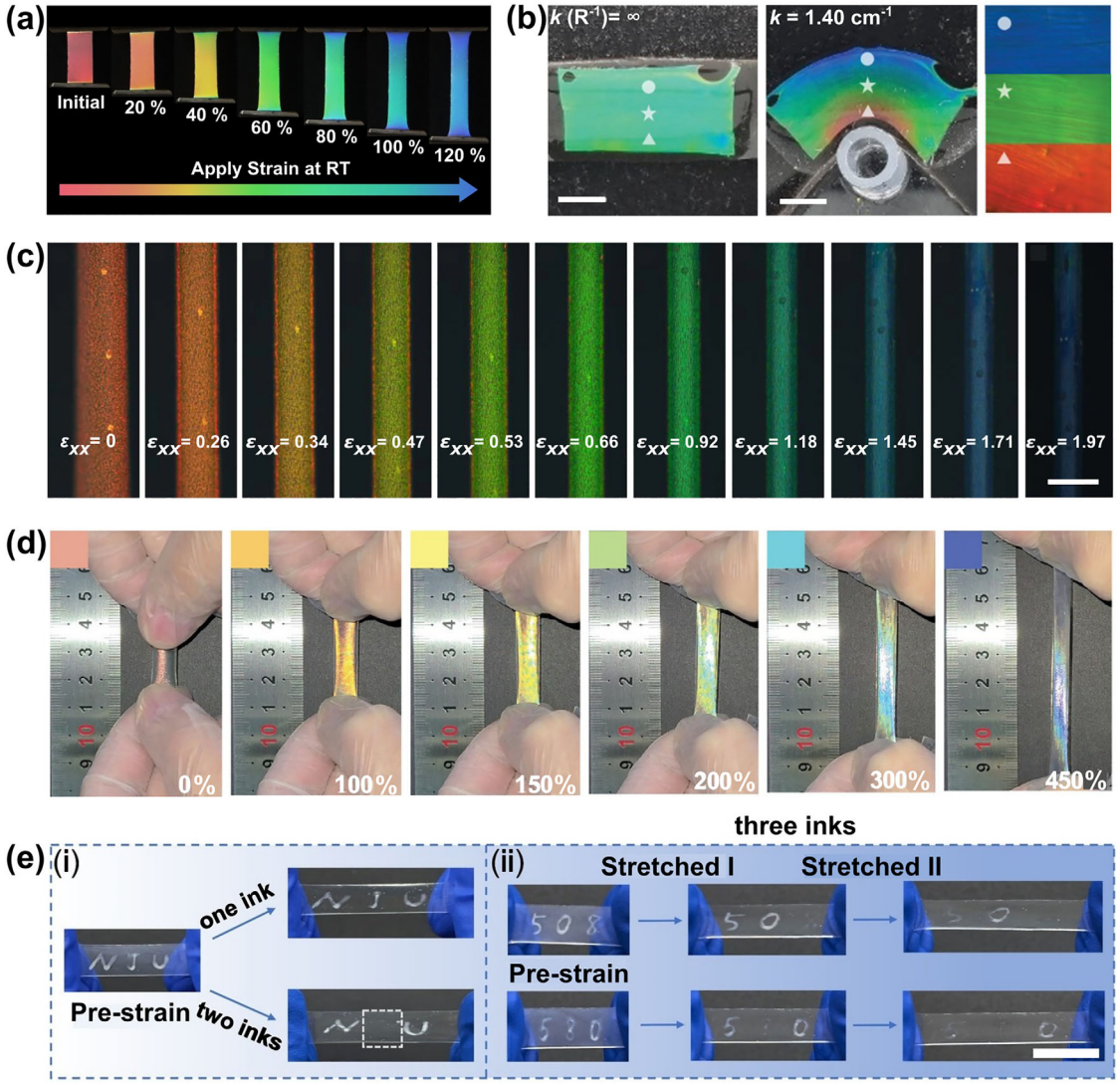

Figure 14. a) Photographs of a CLCE film undergoing mechanical stretching. Reproduced with permission. Copyright 2022, John Wiley and Sons.[90] b) The CLCE membrane changes color when bent in-plane. Reproduced with permission.[290] Copyright 2022, John Wiley and Sons. c) Reflection POM pictures of CLCE fibers under elongational strain. Reproduced with permission.[291] Copyright 2022, Springer Nature. d) Digital photos of the CNCs/PDES elastomer during the stretching process. Reproduced with permission.[292] Copyright 2022, John Wiley and Sons. e) Images of the multi-level strain response of LCE. Reproduced with permission.[17] Copyright 2023, John Wiley and Sons.

proposed (Figure 14c).[291] CLCE fibers demonstrate a remarkable mechanochromic response, covering the full visible color spectrum, when stretched up to 200%. To evaluate its long-term durability in practical conditions, the reflection spectra of the fiber were recorded and subjected to 100 cycles. This approach successfully balances the viscoelastic qualities, allowing for continuous filament extraction while delaying Plateau-Rayleigh instability until the helical structure is fully created. When the obtained filament surface is stretched to 200%, the CLCE fibers change from red to blue. The straightforward concept has potential applications in wearable devices, displays, and soft robotics.

A cellulose nanocrystal (CNC) was incorporated into a polymerizable deep eutectic solvent (PDES) via in situ polymerization to develop skin-like elastomers (Figure 14d).[292] This method utilizes dynamic interfacial hydrogen bonding and an elastic ionic-conductive PDES matrix, effectively overcoming the brittleness and non-tunable pitch constraints of CNC-based elastomers. The resultant material exhibits excellent self-healing capabilities throughout a strain range of 0–500% and a broad spectrum of strain-induced dynamic structural color. As the sample is uniformly stretched from 0% to 450%, its structural color transitions sequentially from red to orange, yellow, green, and blue. The constructed LCEs can be applied in information encryption, mostly through their reversible shape or structural color changes. However, these techniques have limitations in multi-level information encryption, and there are few studies on how the optical transparency of LCEs changes.[190,293,294] In the absence of applied stress, LCEs can be polymerized into an opaque polydomain state. The polydomain-monodomain transition occurs in LCEs, transitioning to a transparent state when the domains

are macroscopically aligned in the stretching direction.[29,64,295] It is anticipated that multi-level information encryption and information display can be integrated using the optical features of the LCEs under external stimulation. A straightforward approach for producing dual-responsive materials that can switch between opaque and transparent states under strain or temperature was proposed (Figure 14e).[17] The mechanical and thermal properties of the LCEs can be altered by varying the contents of long-chain flexible spacer groups. The stress and strain at break were measured at 1.51 MPa and 635%, respectively. The energy loss from the relaxation of the polydomain structure was confirmed by the stress-strain hysteresis during cyclic stretching and releasing between 20% and 400%. This strain-induced change in transmittance of the LCE was both reversible and reproducible for up to 200 cycles, with the sample nearly recovering its original state after resting for 20 min. Information can be encoded and decrypted at different strains or temperatures by using LCE inks, allowing for multi-level information security. This study offers new perspectives on the development of advanced encryption materials that are versatile and highly secure for applications.

LCEs with dynamic crosslinking through metal-ligand coordination networks, involving incorporating tridentate pyridine functional groups into the side chains of a main-chain LCP, were developed (**Figure 15a**).[296] The chelation between the tridentate pyridine and metal ions serves as a robust interaction site, acting as a crosslinking point. The partial reversibility of the dissociation and reassociation between the metal ions and ligands facilitates the repetitive programming of mesogen orientation. Importantly, the metal-ligand bonds can completely dissociate at elevated temperatures, allowing the LCE network to dissolve in solvents. This property enables the LCEs to be reshaped into desired geometries via solution casting. A strategy to monitor the kinetic growth of CLC polymers through structural color changes was proposed.[297] These color changes are attributed to the Michael addition reaction of thiols and acrylates, leading to the creation of oligomers. By performing light polymerization on different regions of the coating at various time intervals, multicolored patterns can be obtained. The distinct colors represent different crosslinking densities and polymer chain lengths. A flower-shaped coating with low crosslinking density was fabricated on the substrate, showing high flexibility, and reversible swelling and recovery. When the flower is immersed in acetone, it becomes invisible. In contrast, upon drying, the flower reappears, and this process is completely reversible (Figure 15b). This work presents a novel approach to modulate optical and responsive properties, offering new possibilities for the development of camouflage and anti-counterfeit materials.

6.2. Magnetic-Responsive LCEs

Magnetic polymer materials are fabricated through the incorporation of magnetic particles in a polymer matrix and preprogrammed by magnetism.[298,299] When exposed to a magnetic field, these materials exhibit rapid deformation, with a short response time, excellent biocompatibility, and magnetic field penetration, showing promising potential for biomedical applications.[27,292,300–303] Recently, magnetic LCEs have been developed to achieve multi-responsiveness and enhance multitasking capabilities.[28,65,249,304] A novel soft composite film based on LCEs as its primary flexible matrix was developed by incorporating magnetic microparticles (MMPs) within it to achieve remote magnetic control, enabling constraint-free in situ reconfiguration (**Figure 16a**).[65] Additionally, the responsiveness of LCEs to environmental stimuli, such as temperature changes and UV illumination, enhances their multi-degree-of-freedom control characteristics, showcasing great potential for multi-responsive, multifunctional, and reconfigurable soft robotics applications. This composite material enables the construction of reconfigurable magnetic soft miniature machines that can adapt to varying environmental conditions. Incorporating LCEs and MMPs into monolithic structures adds a new aspect to soft machine design, significantly improving their functionality in complex environments, particularly for miniature soft robots that can adapt to environmental changes while being controlled remotely. A novel magnetic LCE (magLCE), characterized by its nematic order and magnetization strength, was introduced and programmed independently through extrusion printing (Figure 16b).[305] The magLCE is formed by embedding ferromagnetic particles like NdFeB in the LCE matrix. By adjusting the printing speed, the nematic order of the extruded LCE ink can be programmed, while the magnetization strength can be controlled by manipulating the magnets, resulting in dual anisotropy. Additionally, thermally induced shrinkage could interfere with deformation caused by the magnetic field. When a magnetic field is applied at 20 °C, the strip initially changes from a straight shape to an "M" shape. Afterward, further heating causes the strip to curl, leading to a more complex "M" shape (Figure 16b). However, if heating is applied first, the straight strip coils along its length, which increases its structural rigidity. When a magnetic field is later applied, it causes only minor deformation to the curled strip, enabling a slight "M" shape with minimal deflection. The macroscopic deformation induced by the magnetic field had minimal impact on the nematic order at the microscopic level, as confirmed by the consistent maximum contraction strain (≈35%). In a 120-cycle test at 120 °C, the bending angle remained unchanged before and after cyclic actuation. By leveraging the programmable dual anisotropy characteristics, precise control over the response of the LCE can be achieved, providing a basis for future applications in intelligent materials and adaptive structures.

6.3. Humidity-Responsive LCEs

Multi-responsive LCE materials have been developed, including those responsive to humidity,[72,157,306–308] solvent,[296,297] and gas,[91,307] which hold significant promise for the production of non-contact electronic devices and intelligent bionic systems.[309,310] A hydrogen-bonded CLC monomer mixture capable of fabricating 4D photonic microactuators with humidity and temperature responsiveness using two-photon polymerization printing technology was designed.[306] This CLC monomer mixture consists of reactive mesogenic monomers, chiral dopants, monofunctional acrylates, and carboxylic mesogens. The carboxylic functionalized molecules in the system serve as supramolecular crosslinkers via hydrogen bonding, endowing the microactuators with sub-micrometer resolution. The polymerized CLC mixture can undergo alkaline treatment to

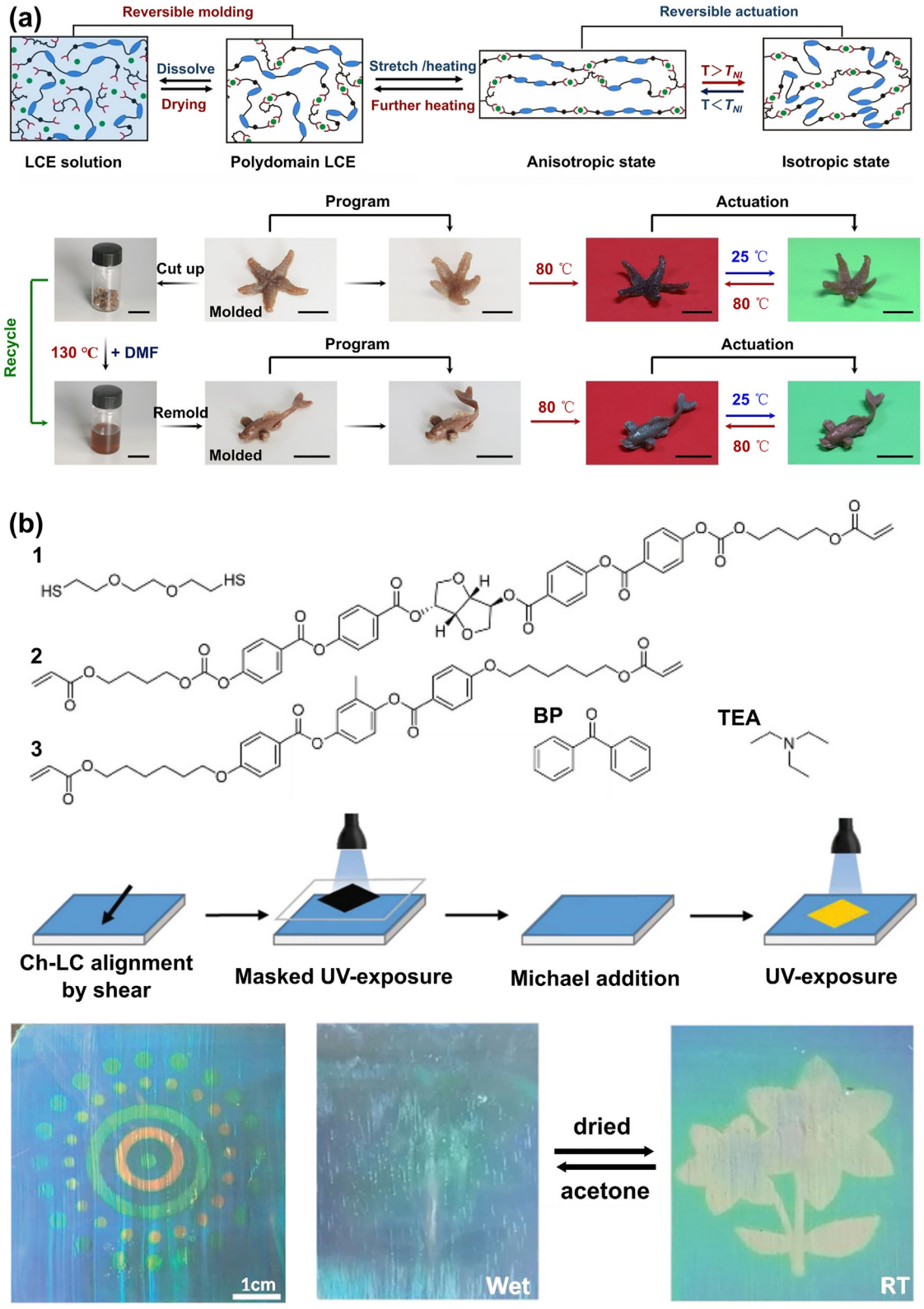

Figure 15. a) Reprocessing and remolding of LCE-Ni 3D actuator. Reproduced with permission.[296] Copyright 2024, John Wiley and Sons. b) Patterned coating on glass showing dual responsiveness to solvents and temperature. Reproduced with permission.[297] Copyright 2019, John Wiley and Sons.

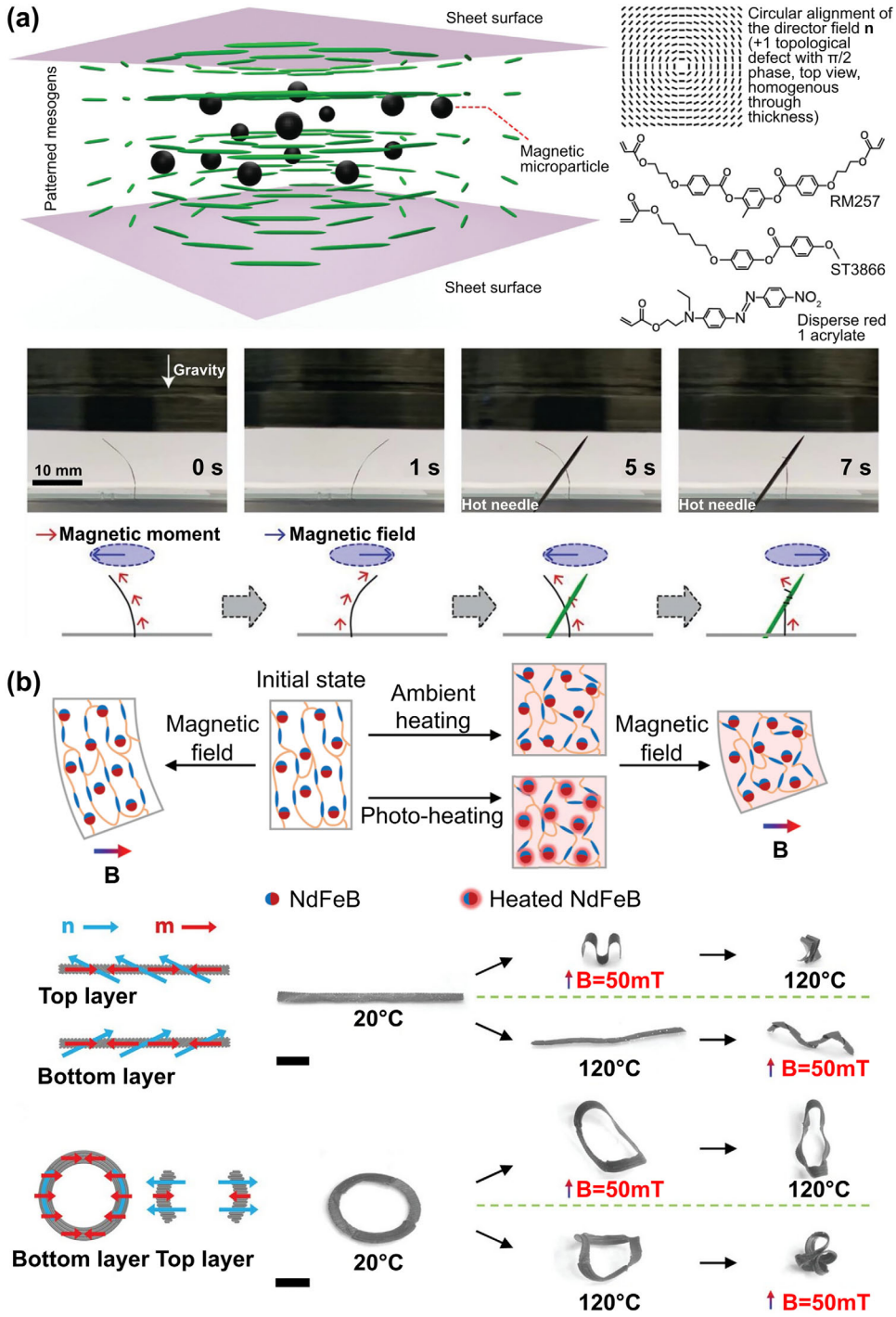

Figure 16. a) Schematic illustrations of the composite film for circular alignment of the director field of the LCE base matrix and demonstration of a vine-plant-inspired filament and a reconfigurable magnetic spring. Reproduced with permission.[65] Copyright 2021, John Wiley and Sons. b) Multimodal shape morphing of magLCE with dual anisotropy. Reproduced with permission.[305] Copyright 2023, John Wiley and Sons.

disrupt hydrogen bonds, thereby imparting dual responsiveness to variations in humidity and temperature. This characteristic enables the printed "flower" shapes to change significantly under different temperature and humidity conditions (**Figure** 17a). The response at 75% RH shows reversibility over ten cycles, ranging between 25 (12–18% expansion) and 20 °C (25–30% expansion). The polymer network can expand or contract in response to external environmental changes, leading to alterations in height and reflective color of the "flower". A novel linear LCP with light- and humidity-responsive properties was introduced by combining the advantages of ring-opening metathesis polymerization with post-polymerization modification.[308] As the

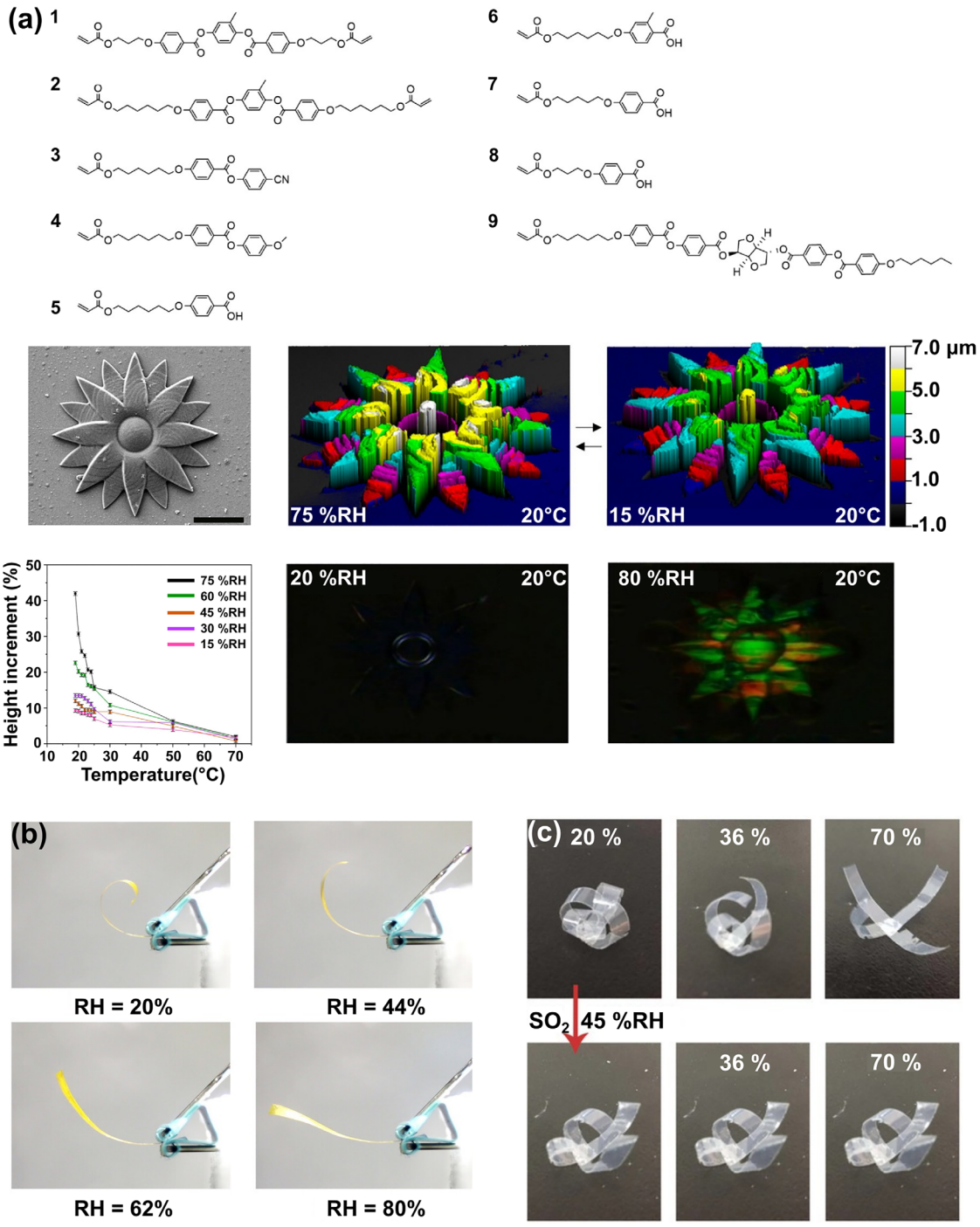

Figure 17. a) Chemical structures of reactive mesogenic monomers for preparing the photonic photoresist and color changes and actuating characteristics of flowers under different humid conditions. Reproduced with permission.[306] Copyright 2020, American Chemical Society. b) Humidity controls the bending of LCE strips. Reproduced with permission.[308] Copyright 2023, John Wiley and Sons. c) The reversible opening/closing of flowers (top) and the flowers becoming inactive after exposure to sulfur dioxide gas (bottom). Reproduced with permission.[307] Copyright 2019, John Wiley and Sons.

relative humidity (RH) of the environment surrounding increases from 20% to 80%, the swelling of the hygroscopic carboxylate-treated side causes the curved bands to gradually unfold into a flat shape (Figure 17b). A monolayer LCE membrane that exhibits dual responsiveness to humidity and sulfur dioxide (SO_2) gas was developed.[307] To achieve mesogen alignment, the film was elongated to 200% strain at 60 °C and held for 10 min to fully relieve the stress induced during the stretching. The humidity sensitivity of this membrane can be modulated by exposure to SO_2, while the response time to SO_2 is significantly

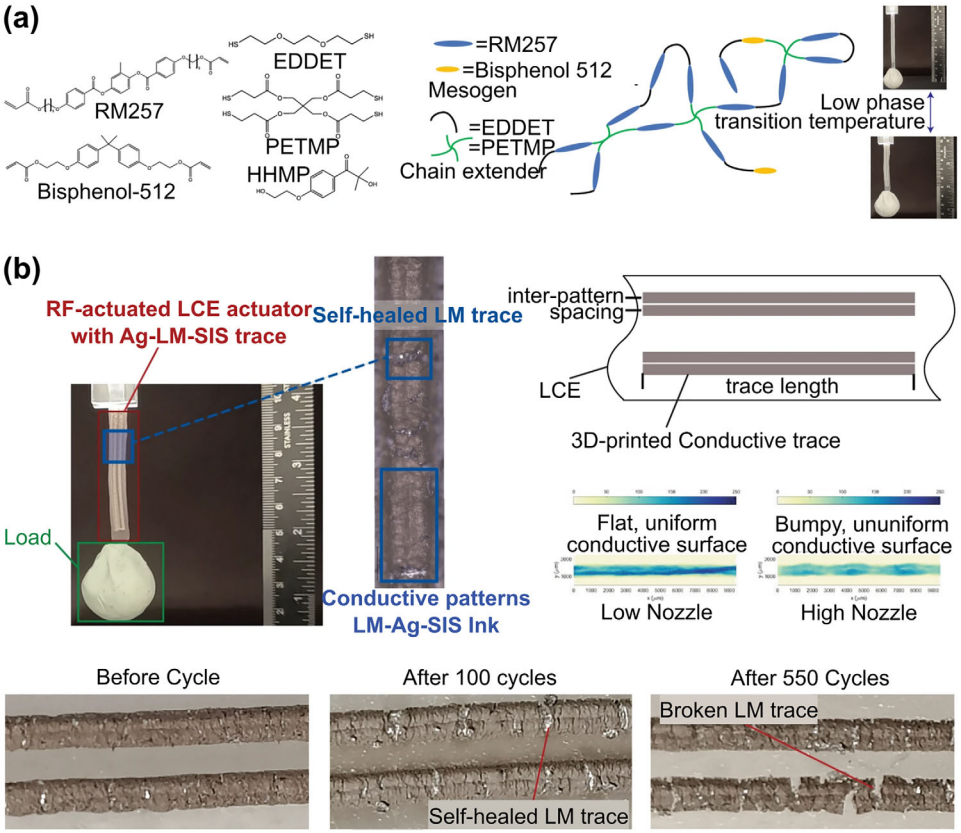

Figure 18. a) Chemical structures and b) characterization of RFact's frequency-selective actuator. Reproduced with permission.[311] Copyright 2025, Springer Nature.

influenced by the environmental RH. They successfully endow the LCN membrane with humidity-responsive characteristics by treating one side of the membrane with potassium hydroxide solution. When this humidity-responsive membrane is exposed to an SO_2 atmosphere, the acidification reaction of the carboxylate on the membrane surface results in the cessation of its humidity responsiveness. This innovative material is utilized to fabricate artificial flowers with dual sensitivity. In the absence of SO_2, RH variations cause flowers to open and close reversibly, mimicking natural behaviors of flowers that open in humid environments and close in dry conditions. However, in the SO_2 atmosphere, when the flowers come into contact with moisture, they deform and subsequently become inert to humidity changes, demonstrating irreversible motion (Figure 15c). Both reversible and irreversible, controlled by SO_2, making the LCE film valuable for designing and fabricating multifunctional devices.

6.4. Radio-Frequency-Responsive LCEs

Using on-board batteries or wired connections to external power sources to power soft robots in such environments can greatly limit their mobility. Similarly, wireless actuation methods face limitations due to short-range operation, line-of-sight operation, or the unintended activation of multiple actuators. Majidi, Kumar, and coworkers[311] developed a radio-frequency system that enables frequency-selective actuation of LCE actuators (**Figure 18**). The LCE actuator is a flexible robotic system designed for efficient and targeted movement, driven by thermal energy without the need for batteries. They designed LCE actuators that operate at low actuation temperatures and integrate conductive circuits that resonate and generate heat when exposed to specific radio-frequency excitations within the 2.40 GHz range. Efficient beamforming is achieved through a wireless actuation platform capable of inferring the wireless channel and directing signals toward the actuator.

6.5. Ultrasonic-Responsive LCEs

Ji and coworkers[312] achieved ultrasonic welding of reprogrammable silver nanowire-LCE composites (AgNW-LCEs) without the need for any additional reagents (**Figure 19**). By integrating silver-disulfide coordination with ultrasonic welding (UW) technology, high-frequency vibrations at the interface initiate a robust double-network welding process between the AgNWs and the dynamic LC networks. The UW process allows for the integration of monolithic AgNW-LCEs into heterostructured actuators within 0.68 s. The LCE composite with 2 wt% AgNWs exhibits enhanced mechanical performance, achieving an elongation of 214% and a tensile strength of 2.18 MPa. Enabled by the in situ photothermal effect of AgNWs, the AgNW-LCE

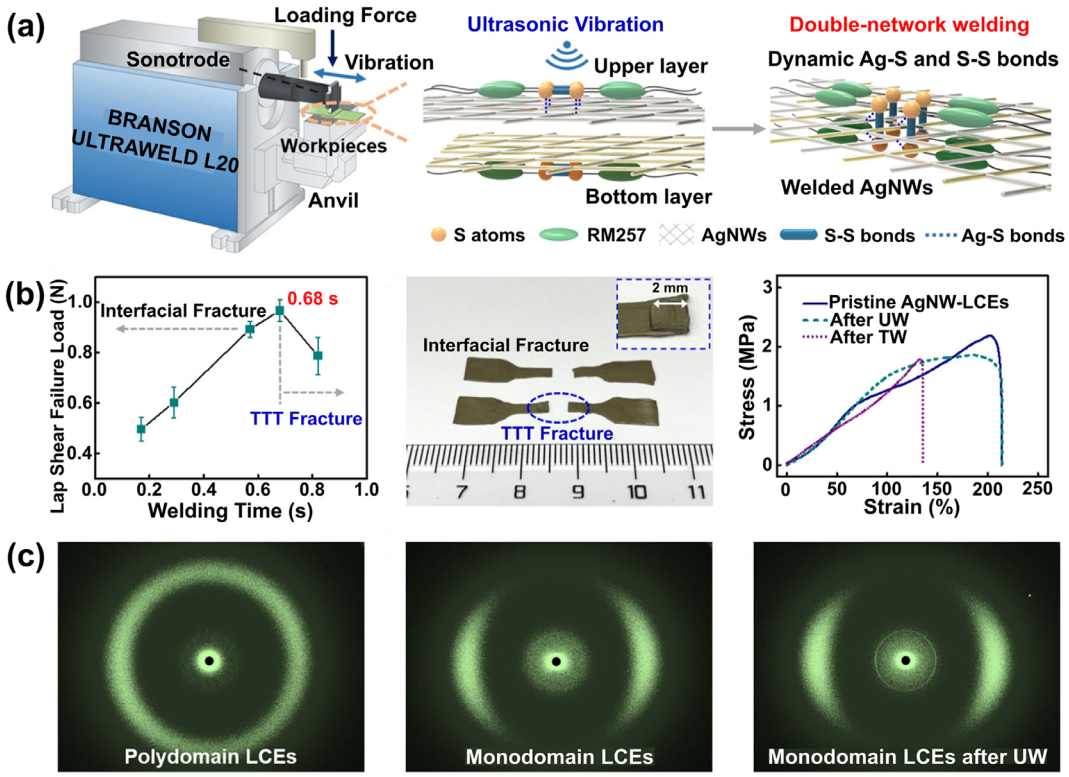

Figure 19. a) The working mechanism of the UW system. b) Relationship between lap shear failure load and welding time. c) 2D XRD patterns of (left) polydomain AgNW–LCEs and monodomain AgNW–LCEs (middle) before and (right) after UW. Reproduced with permission.[312] Copyright 2023, American Chemical Society.

actuator undergoes reversible contraction and expansion, achieving a strain of ≈32% during multiple cycles of IR irradiation and cooling. Moreover, the ultrasonic welding of AgNW-LCEs also yielded outstanding healing performance, with ≈100% strain recovery and ≈85% stress recovery, thanks to the strong double-network welding mechanism of AgNWs and dynamic LC networks. The presented approach provides a viable strategy for fabricating soft and multi-responsive actuators from advanced polymer materials. Zhang, Sun, and Li[313] proposed an ultrasonics sonochemistry method that facilitates a one-step process, integrating hydrosilylation polyaddition polymerization with crosslinking reactions to synthesize polysiloxane main-chain LCEs (MC-LCEs). Utilizing the remarkable effect of acoustic cavitation, polyaddition polymerization and crosslinking are readily conducted at ambient temperature using routine ultrasonic equipment, producing the LCE network in ≈30 min. The synthesized MC-LCEs exhibit superior quality, outstanding material properties, and remarkable stimuli-responsive actuations. This fabrication technique outperforms traditional thermal processing in speed, convenience, and effectiveness, enabling cost-effective large-scale production of polysiloxane-based MC-LCEs.

6.6. Photothermal-Responsive LCEs

Yang and coworkers[314] developed a single-layer, multi-responsive soft actuator that can undergo 3D deformation and exhibit dynamic structural color changes (**Figure 20a**). This was achieved via a precisely controlled evaporation method, which forms a Janus structure in the CLCE by depositing reduced graphene oxide (RGO). The single-layer structural color actuator transitions directly from a flat shape to 3D configurations via the photothermal effect. This capability stems from the RGO, which not only enhances the CLCE's mechanical strength and color intensity of the CLCE while also imparting responsiveness to NIR light through effective photothermal effects. CLCE-30 exhibits an appropriate tensile strength and a 130% elongation at break, making it a viable matrix material for CLCEs. Additionally, the RGO/CLCE film's photothermal deformation induced by NIR light remained consistent and reliable after 100 cycles. This distinct architecture allows the materials to execute multiple cycles of reversible 3D deformation, providing a clear route for the development of advanced single-layer 3D soft actuators. Chen, Wang, and coworkers[315] developed a novel class of light-reconfigurable LCEs (PUOLCE) (Figure 20b). These materials incorporate multifunctional dynamic covalent organic photothermal molecules as chain extenders, which also act as photothermal agents and dynamic bond precursors. Upon near-NIR irradiation, the resulting photothermal effect triggers rapid exchange reactions in the dynamic oxime carbamate bonds, enabling efficient material welding. Leveraging the NIR-assisted welding strategy, PUOLCE-based units can be assembled into various complex actuators exhibiting novel deformation modes. Furthermore, these assembled actuators can be reconfigured on demand under NIR illumination to perform different

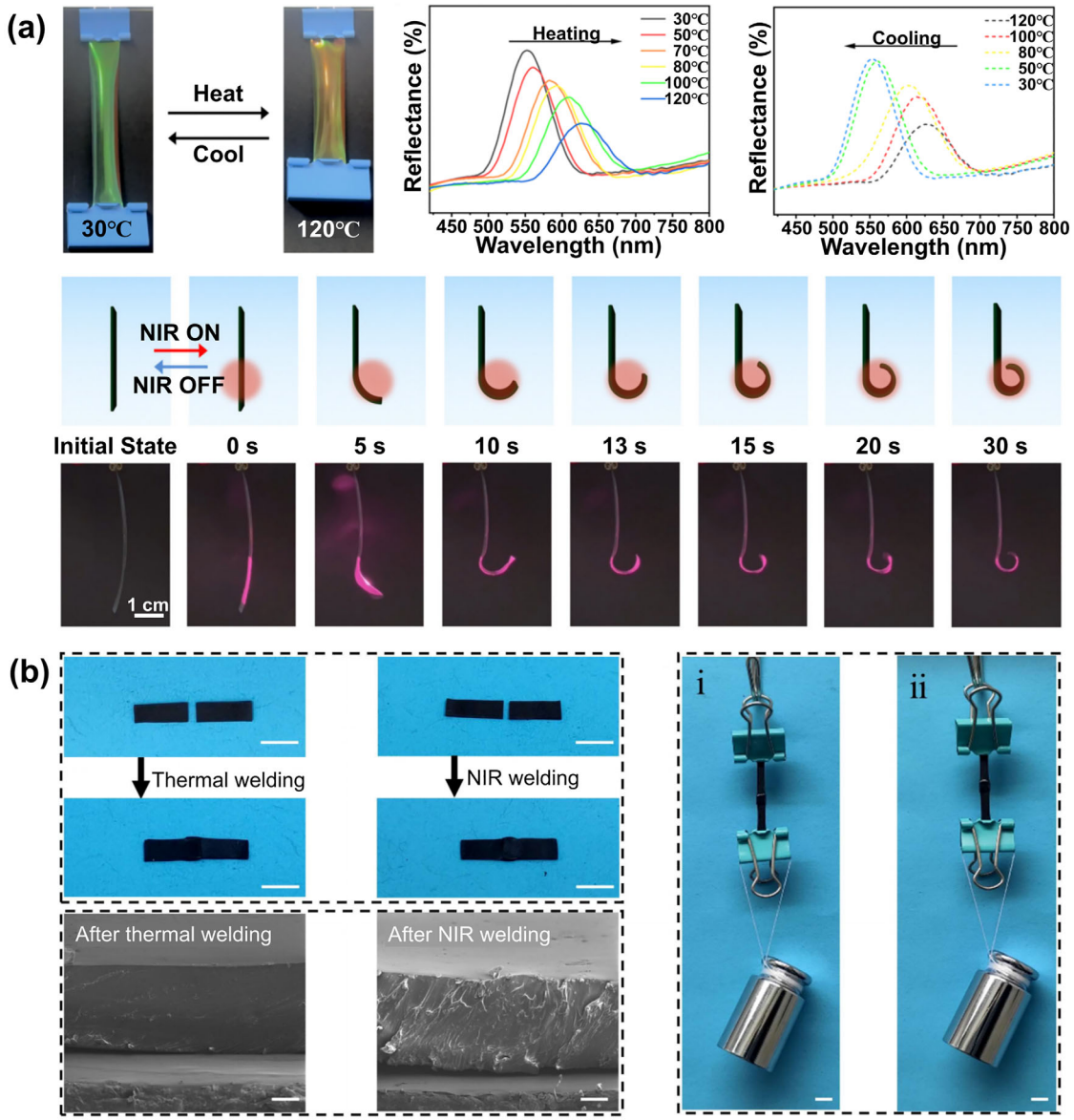

Figure 20. a) Photographs of the RGO/CLCE film at different temperatures. Reproduced with permission.[314] Copyright 2014, Royal Society of Chemistry. b) Photos of the welding process of PUOLCE2 film. Reproduced with permission.[315] Copyright 2025, John Wiley and Sons.

mechanical tasks. The PUOLCE demonstrates the maximum stress value, reaching 11.7 MPa, and its toughness was found to be 1557 kJ m^{-3}. The photothermal conversion efficiency of PUOLCE was determined to be 16.1% at 200 mW cm^{-2}, 14.2% at 500 mW cm^{-2}, and 10.5% at 800 mW cm^{-2}. In contrast to other typical photothermal-responsive LCEs, the PUOLCE film showed a highly competitive photothermal response rate, with no decrease in equilibrium temperature observed after 5 cycles of NIR light at an intensity of 500 mW cm^{-2}. Additionally, the photothermal actuation performance remained unchanged after 30 cycles of testing, indicating that the PUOLCE film exhibited excellent photothermal conversion efficiency and stability. The outstanding photothermal effect enables the photo-welding approach by activating dynamic oxime-carbamate bonds through NIR irradiation. This study thus offers a foundation for designing adaptive soft actuators capable of programmable shape-shifting functions.

7. Applications

7.1. Information Encryption

As communication technology advances rapidly, the importance of information security grows, driving the progress of responsive materials and technologies for anti-counterfeiting, encryption, and information protection.[17,18] Recently, significant efforts have been directed toward the development of advanced anti-counterfeiting materials and encryption methods, including photonic crystals,[316–320] structural-color materials,[321–323] rewritable materials,[324,325] wrinkles,[326–328]

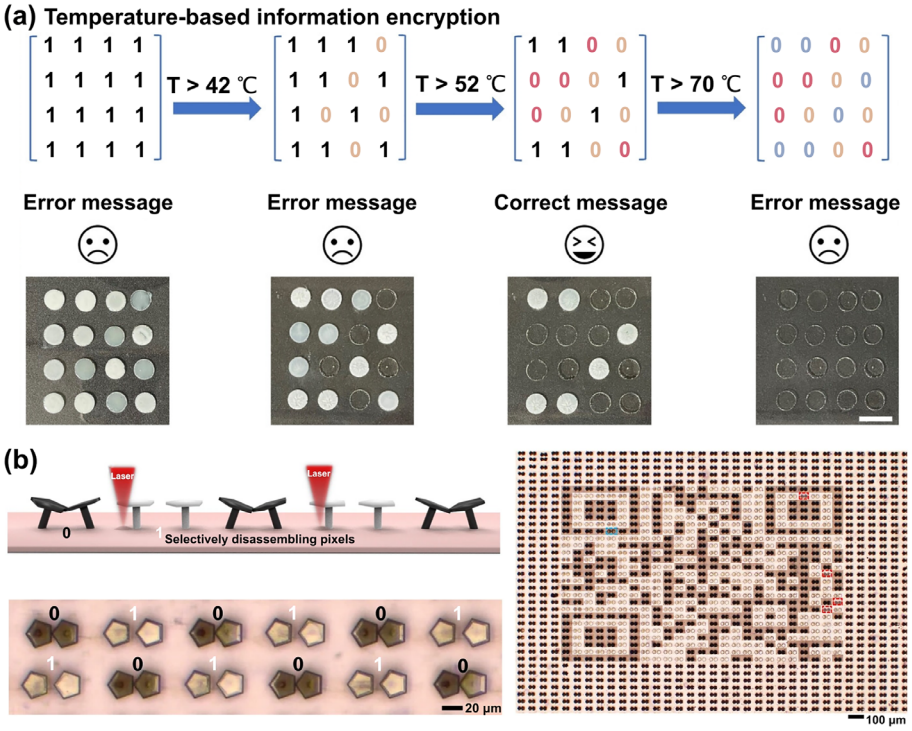

Figure 21. a) Temperature-based information encryption. Reproduced with permission.[17] Copyright 2023, John Wiley and Sons. b) Applications of microactuation systems driven by artificial goosebumps. Reproduced with permission.[18] Copyright 2024, Springer Nature.

and fluorescent/phosphorescent imaging,[323,329–331] among others, to address the challenges posed by false information and data leakage. Integrating various anti-counterfeiting methods or multiple stimuli that activate decryption makes it more difficult to duplicate information, thereby enhancing the overall security level.[332–336] LCEs can change their shapes and colors in response to external stimuli such as temperature, light, or mechanical pressure, thereby effectively concealing or revealing information in different states. The temperature-based encryption and anti-counterfeiting by using the transparency change caused by the phase transition of multi-domain LCEs were fabricated.[17] At room temperature, the LCE points appear opaque, while the colors become colorless when the temperature exceeds the T_{NI}. All points display the same color, indicating an error message (**Figure 21a**). As the temperature increases, the corresponding points become transparent, suggesting the correct information. If users do not maintain the correct temperature range, they will register the wrong information, thereby protecting data security. A novel data storage method by using a micro-driving technique was developed,[18] featuring a controllable switch between dark and bright mushroom structures, which can be activated globally and locally with a programmable laser on a uniform dual-component pixel "canvas" (Figure 21b). By programming various laser parameters, information can be encoded into bi-assembly pixels. Complex patterns, such as a QR code containing the message "Hello MPI-IS", can be written by programming the laser. This approach allows for accurate, localized, and controllable manipulation of microstructures, paving the way for advancements in programmable micromachine development.

7.2. Force Sensors

Mechanochromism refers to the tunability of structural color [73,337–340] achieved by mechanically modifying the lattice constant of the nanostructure, which is similar to the color-changing observed in chameleons. CLCEs are a representative class of mechanochromic self-assembling materials that function without human intervention and have been widely applied in strain sensors.[60,267,290] Human–machine interaction also acts as a vital communication link between users and specific devices or virtual environments, facilitating intuitive, efficient, and seamless interactions for task execution.[341–343] An interactive system by leveraging real-time optoelectronic dual-signal sensing with the capabilities of interactive cholesteric liquid crystal elastomers (iCLCEs) was developed (**Figure 22a**).[60] This system integrates iCLCEs with a display module, a bespoke capacitance acquisition, a transmission unit, and other components. When the iCLCEs are pressed, they generate optical and capacitive signals. These capacitive signals can be captured by a multi-channel data acquisition system and transmitted in real time to the host computer. By integrating an array of RGB (red/green/blue) iCLCEs with the multi-channel data acquisition circuitry, a sensing system for game controllers has been developed. For example, the red, green, and blue iCLCEs are affixed to the back of the hand to align with the three lanes in a customized obstacle course running game. When the finger touches the sensor, the car will turn to the road with the same color as the sensor to avoid the roadblock. This arrangement allows for seamless control of the movement of the car in the game. Using CLCE membranes, a strain sensor capable of distinguishing deformations with different

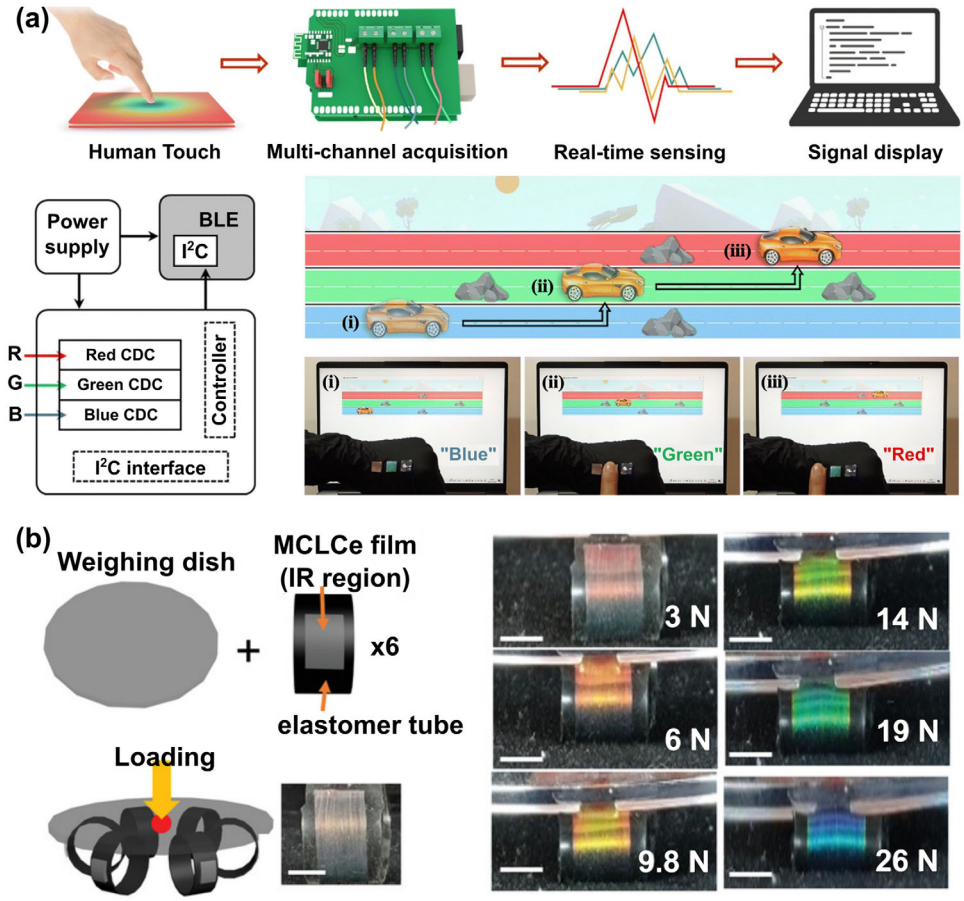

Figure 22. a) Applications of iCLCEs in human-interactive systems. Reproduced with permission.[60] Copyright 2014, Royal Society of Chemistry. b) The color change of MCLCE film on spatial weight. Reproduced with permission.[290] Copyright 2022, John Wiley and Sons.

curvatures was designed by integrating a phase-stabilization process of LC oligomers into highly stretchable and uniformly consistent main-chain CLCEs (MCLCEs), such as in-plane and out-of-plane bending and complex 3D deformation.[290] Six silicone tubes support the weighing dish in this configuration, with CLCE membranes conformally positioned on the outer surface of the elastomeric tubes in the NIR region (Figure 22b). The weight applied to the weighing dish causes the elastomeric tubes to deform vertically, resulting in uniaxial bending of the CLCE membranes. As the weight increases, the elastomeric tubes flatten, resulting in compressive strain in the CLCE membranes and a blue shift in color. The straightforward concept presented can be applied in areas such as wearable devices, displays, and soft robotics.

7.3. Material Transportation

Recent research has investigated soft continuum robots, which exhibit distinct and appealing properties, including a high degree of freedom and excellent biocompatibility.[344–347] Scientists have fabricated various cylindrical soft actuators, such as octopus-inspired robotic tentacles,[348,349] trunk-inspired robotic hands,[350] and worm-inspired designs.[351] However, the majority of soft actuators are powered by pneumatic or hydraulic systems, which necessitate large external control mechanisms and intricate internal channels to achieve various functions.[352,353] Thus, there is urgent demand for the construction of soft actuators using stimuli-responsive materials,[354] which could simplify the manufacturing and assembly process while reducing control requirements. The twisting soft robots made of thermal-responsive LCE can be used for cargo transport, debris cleaning, and self-rolling (**Figure 23a**).[181] Light-fueled self-oscillators based on soft actuating materials can be applied for pumping and coupling (Figure 23b).[355] A soft gripper using tubular actuators as the primary building blocks was developed (Figure 23c).[24] The electronically controlled soft gripper is constructed with three tubular actuators, which are initially attached to a circular plate, and then the plate is connected to an artificial muscle membrane made of LCEs. A microcontroller is employed to modulate the voltage applied to each actuator, enabling precise control over their deformation. Through the selective actuation of the heated wires inside each tubular actuator, the gripper can grasp, lift, and even twist the caps of small bottles on its own without the need for extra external control. This approach demonstrates significant potential for automation in soft robotics applications. LCEs are capable of generating large, reversible contractions, making them ideal for use as artificial muscles. The liquid metal LCE fibers that can achieve maximum shrinkage rates comparable to

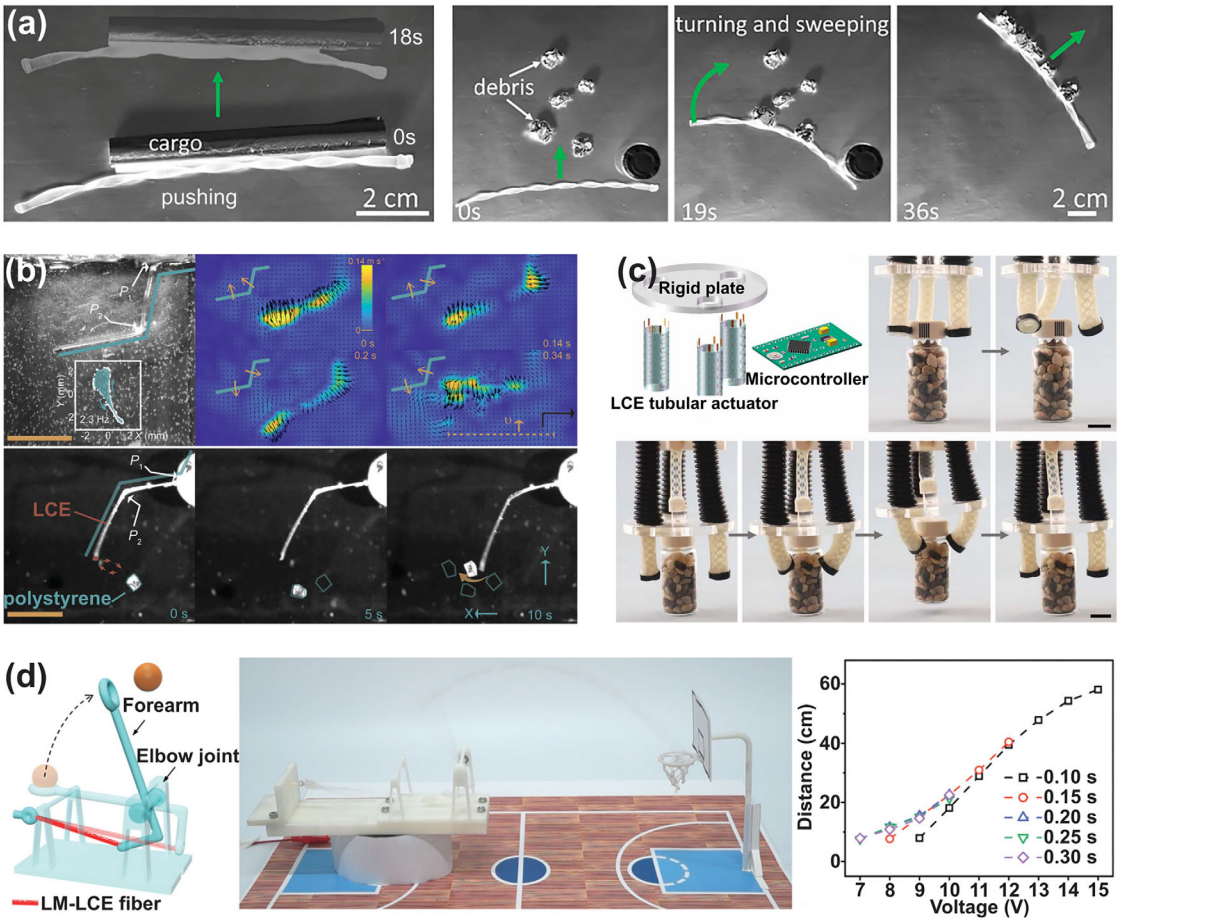

Figure 23. a) Demonstration of cargo transport using an alumina tube. Reproduced with permission.[181] Copyright 2022, National Academy of Sciences. b) Demonstration of autonomous fluid pumping and transport of micro-objects. Reproduced with permission.[355] Copyright 2023, John Wiley and Sons. c) A multifunctional gripper made up of LCE tubular actuators. Reproduced with permission.[24] Copyright 2019, The American Association for the Advancement of Science. d) Liquid metal LCE (LM-LCE) fiber actuator firing operation. Reproduced with permission.[285] Copyright 2021, John Wiley and Sons.

human skeletal muscle were obtained, which can mimic rapid and significant contractions of the human triceps in an artificial arm (Figure 23d).[285] Human triceps are the active muscles used in the basketball throwing motion, which contract quickly to move the forearm and throw the ball. Similar to the triceps, the liquid metal LCE fibers can also be activated by pulsed voltage, which causes contractions that can propel the artificial arm to execute the throw. By modulating the voltage at different pulse durations, the desired throwing distance can be precisely controlled. Under specific pulsed voltage conditions, the ball is accurately launched into the hoop, demonstrating the effectiveness of this biomimetic approach in robotic applications. Liquid metal LCE fibers, with their outstanding contraction ratio and speed, enhance their performance as artificial muscles for rapid movements and are expected to expand the range of demanding applications for soft robots.

He and coworkers[356] developed a self-oscillator comprising two antagonistic photo-active layers with an inactive interlayer, which delivers an output power density of 33 W kg^{-1}. This performance is 275 times greater than other configurations. These oscillators enable operation across a wide range of wavelengths and combine various functions, such as proprioceptive actuation and energy harvesting. The resulting high-performance flapping motion enables various locomotion modes, as demonstrated by a wing that attains a thrust-to-weight ratio of 0.32. This research paves the way for autonomous, sustained, and untethered actuation in high-performance robotics. He and coworkers[234] also designed a light-responsive soft actuator with an engineered asymmetry and dynamic structure, integrating two unique internal feedback loops governed by intrinsic bifurcation. Consequently, the actuator is capable of dynamically switching among three motion modes—tracking, undulation, and oscillation—while independently adjusting to changes in environmental conditions like light intensity, temperature, and viscosity. Moreover, this multimodal functionality broadens the range of environmental interactions, paving the way for applications in areas like fluid dynamics, electronics, and environmental monitoring, beyond just locomotion. This advancement in physical intelligence represents a significant step forward in the evolution of next-generation autonomous soft robotics, paving the way for systems with enhanced autonomy and unprecedented adaptive capabilities.

Ho, Kim, and coworkers[357] conceptualized a self-locked thermo-mechano feedback system for autonomous motility and energy generation. This system utilizes typically wasted low-grade heat to fuel a soft device capable of sustained, untethered multimodal locomotions, which exhibits innately resilient locomotion, synchronizing self-regulated temperature fluctuations with mechanical mobility without external stimulus change. This synergy enables the simultaneous harvesting of thermo-mechanical energy at the intersection of pyro- and piezoelectric mechanisms. This untethered soft material executes precise movements—like translational oscillation, directional rolling, and bidirectional rotation—with rapid changes and dynamic reactions, all without external power. The study establishes a foundation for the emerging field of multi-gait soft energy robotics, while also promoting developments in thermo-mechano-electrical transduction and waste heat harvesting. To advance active optics and photonics, Lu and coworkers[358] developed crosslinked LC actuators in which microstructural design and macroscopic shape engineering are seamlessly integrated. Leveraging the elastic and optical anisotropies of their twisted nematic LC structure, these actuators achieve significant heat-induced bending. This capability demonstrates programmable motions and self-oscillations, which contribute to the achievements of dynamic 2D beam steering and sustained light field modulation. These actuators will find applications in autonomous active optics, photonic systems, and self-governing robotics, all leveraging thermo-mechanical-optical transduction.

8. Conclusion and Perspectives

By integrating the anisotropic characteristics of mesogens with the entropy elasticity of loosely crosslinked polymer networks, LCEs display appealing stimuli-responsive behaviors, making them highly promising for applications in actuators, soft robotics, biomedicine, optical devices, and more. In this review, we summarize the achievements of the responsive LCEs in terms of thermal-responsive LCEs (thermochromic LCEs, thermal-induced shape changes, and thermal-induced soft actuators), photo-responsive LCEs (photochromic CLCEs, photo-induced shape changes, photo-induced soft actuators, and photo-induced microactuators), electrical-responsive LCEs (electrochromic CLCEs, electro-induced shape changes, and electro-induced soft actuators), and others. Subsequently, we discuss the practical applications of responsive LCEs in information encryption, force sensors, and material transportation, which show significant potential for further development of advanced functional materials. Finally, this review concludes with an outlook on the applications, current challenges, and future high-performance LCEs endowed with remarkable photophysical properties. The main challenges and potential future research aspects in this area are discussed below.

First, one major challenge is expanding the fundamental knowledge of chemistry and physics of these materials, as well as their stimulus-responsive mechanisms. To achieve this, it is critical for scientists to collaborate with each other to define the possible applications, which will eventually steer the development and analysis of the materials. In this regard, LC polymer networks that respond to stimuli present a promising candidate for constructing practical functional devices. As outlined in this review, various responses to multiple stimuli have already been reported. Building upon the fundamental understanding of responsive LCEs, future research that takes advantage of the ability to pattern the director's profile of these materials holds potential for creating engineered materials free of creases or interconnections, with promising applications in haptic displays, lab-on-chip devices, aerospace, and optics.

Second, broadening the use of 4D printing LCEs can pave the way for new opportunities. Unlike traditional processing methods, 4D printing offers significant potential and versatility by allowing both global programming of mesogen alignment within a uniform material and localized modification of material composition through multi-material or hybrid printing techniques. Furthermore, circularly polarized grating devices could be fabricated via direct ink writing (DIW) printing by switching between right- and left-handed CLCE inks. By printing CLCE inks with different selective bands on a single object, it is possible to produce a flexible and stretchable photonic device capable of full-band reflection, which holds great potential for use in flexible displays and adaptive electronics. With ongoing advancements in materials science and manufacturing methods, we anticipate that 4D printing will unlock new opportunities for innovative LCE devices, featuring programmable stimuli-responsive characteristics and optimized 3D structures in the near future. Applying 4D printing to LCEs opens up new possibilities to simultaneously control mesogen alignment and 3D geometry, offering improved potential and practicality in developing 4D-printed LCE structures with tailored stimuli-responsive characteristics.

Third, another challenge with most synthetic actuating materials is their slow response time—only elastomers and ferroelectric polymers can respond quickly, while other materials have slower response times. To enhance the actuation rates, it is necessary to either reduce the object's size for quicker heating/cooling and swelling or utilize elastic instabilities like snap buckling. Another key concern is the repeatability and accuracy of synthetic material movements. The movement precision is constrained by both the relaxation process rate and creep, which becomes more pronounced at elevated temperatures. As a result, the best repeatability can be obtained with entirely elastic materials, like chemically crosslinked elastomers. In contrast, the non-crosslinked polymers can exhibit good repeatability within specific time intervals, such as between relaxation times and the polymer chain relaxation time.

Fourth, living actuating organisms like muscle cells, bacteria, and sperm possess much lower stiffness than polymers, with their mechanical properties resembling those found in hydrogels. A key feature of living actuating entities is their capacity to utilize the energy stored in chemical bonds for movement, a capability not available to polymers. Living materials are viscoelastic rather than purely elastic, suggesting that the deformations are either delayed or not fully reversible. A potential direction for advancing actuating synthetic materials could involve efforts to make them more similar to living materials. Specifically, a potential avenue for further research might focus on increasing the movement amplitude through the integration of external stimuli, such as electrical or optical triggers. In this scenario, the force produced by each stimulus could be amplified, resulting in a synergistic effect. It can be concluded that the potential interplay between material advancement and technology to develop materials

with a range of length scales and multi-stimulus responsiveness will significantly increase the possibilities in this field.

The integration of computational modeling and simulation methods into LCE design offers an effective strategy for predicting and enhancing their performance under various conditions. Finite Element Analysis (FEA) enables the forecasting of intricate, large-scale deformations and mechanical behavior when subjected to stimuli like heat or light, facilitating the strategic design of soft robots and actuators. On the atomic and molecular scale, Molecular Dynamics (MD) simulations offer a deeper understanding of the molecular interactions and dynamics that influence the fundamental properties of LCEs, allowing for the creation of materials with more tailored behaviors. Machine Learning (ML) techniques are capable of processing extensive datasets to identify hidden patterns, forecasting optimal molecular structures, and processing parameters to attain desired properties. Ultimately, these methods influence the future development of LCEs by enabling greater precision in controlling their stimuli-responsive properties, thereby expanding their potential for applications in fields such as soft robotics, smart fabrics, and adaptive surfaces. The ability to scale synthesis and processing is a crucial factor for the future of LCEs. In terms of synthesis, this involves transitioning from batch chemical synthesis into flasks to continuous flow reactors, which can consistently produce kilogram-scale quantities of LCE precursors. For processing, techniques like 3D printing are paramount, enabling the creation of complex, monolithic LCE actuators. We anticipate the use of LCEs in 3D printing through the fused filament fabrication (FFF) method. Due to their ability to undergo thermally induced bond exchange, LCEs can plastically deform under stress at elevated temperatures, making them suitable for extrusion into aligned filaments and 3D printing into functional objects. FFF is considered a more cost-effective and efficient 3D printing approach than direct ink writing, as it does not require UV crosslinking. Developing robust and automated fabrication tools that integrate alignment control (e.g., through scalable magnetic or surface shear fields) with these forming processes will be the cornerstone for bringing LCEs from the lab to the market.

Acknowledgements

J.L. and H.Y.J. contributed equally to this work. This work was supported by the National Key Research and Development Program of China (No. 2022YFA1405000), the National Natural Science Foundation of China (Nos. 62375141, T2488302), the Major Project of Natural Science Foundation of Jiangsu Province (No. 20243067), the National Natural Science Foundation of China (No. 62405142), the Natural Science Foundation of Jiangsu Province (No. BK20240656), the China Postdoctoral Science Foundation (No. 2024M761391), Special Funding for Chinese Postdoctoral Fellows (No. 2025T180229), Jiangsu Innovation Team Program, and the Fundamental Research Fund for the Central Universities.

Conflict of Interest

The authors declare no conflict of interest.

Keywords

liquid crystal elastomer, shape change, soft actuator, stimuli-responsive behavior

Received: September 22, 2025
Revised: November 2, 2025
Published online:

[1] I. Apsite, S. Salehi, L. Ionov, *Chem. Rev.* **2022**, *122*, 1349.
[2] X. Liu, M. Gao, J. Chen, S. Guo, W. Zhu, L. Bai, W. Zhai, H. Du, H. Wu, C. Yan, Y. Shi, J. Gu, H. J. Qi, K. Zhou, *Adv. Funct. Mater.* **2022**, *32*, 2203323.
[3] P. Rothemund, Y. Kim, R. H. Heisser, X. Zhao, R. F. Shepherd, C. Keplinger, *Nat. Mater.* **2021**, *20*, 1582.
[4] J. Liu, Z. P. Song, J. Wei, J. J. Wu, M. Z. Wang, J. G. Li, Y. Ma, B. X. Li, Y. Q. Lu, Q. Zhao, *Adv. Mater.* **2024**, *36*, 2306834.
[5] J. Liu, X. Zhou, X. Tang, Y. Tang, J. Wu, Z. Song, H. Jiang, Y. Ma, B. Li, Y. Lu, Q. Li, *Adv. Funct. Mater.* **2024**, *35*, 2414086.
[6] J. Liu, J. J. Wu, J. Wei, Z. J. Huang, X. Y. Zhou, J. Y. Bao, R. C. Lan, Y. Ma, B. X. Li, H. Yang, Y. Q. Lu, Q. Zhao, *Angew. Chem., Int. Ed.* **2024**, *63*, 202319536.
[7] J. Liu, Z. P. Song, L. Y. Sun, B. X. Li, Y. Q. Lu, Q. Li, *Responsive Mater.* **2023**, *1*, 20230005.
[8] J. Li, H. K. Bisoyi, J. Tian, J. Guo, Q. Li, *Adv. Mater.* **2019**, *31*, 1807751.
[9] W. Kang, Y. Tang, X. Meng, S. Lin, X. Zhang, J. Guo, Q. Li, *Angew. Chem., Int. Ed.* **2023**, *62*, 202311486.
[10] Y. Wu, M. Li, Z. G. Zheng, Z. Q. Yu, W. H. Zhu, *J. Am. Chem. Soc.* **2023**, *145*, 12951.
[11] J. Gao, Y. Tang, D. Martella, J. Guo, D. S. Wiersma, Q. Li, *Responsive Mater.* **2023**, *1*, 20230008.
[12] Y. Yang, X. Zhang, C. Valenzuela, R. Bi, Y. Chen, Y. Liu, C. Zhang, W. Li, L. Wang, W. Feng, *Matter.* **2024**, *7*, 2091.
[13] M. Rogóż, H. Zeng, C. Xuan, D. S. Wiersma, P. Wasylczyk, *Adv. Opt. Mater.* **2016**, *4*, 1689.
[14] M. Pilz da Cunha, S. Ambergen, M. G. Debije, E. F. G. A. Homburg, J. M. J. den Toonder, A. P. H. J. Schenning, *Adv. Sci.* **2020**, *7*, 1902842.
[15] C. Zhu, Y. Lu, L. Jiang, Y. Yu, *Adv. Funct. Mater.* **2021**, *31*, 2009835.
[16] R. Lan, X. G. Hu, J. Chen, X. Zeng, X. Chen, T. Du, X. Song, H. Yang, *Responsive Mater.* **2024**, *2*, 20230030.
[17] H. Q. Wang, Y. Tang, Z. Y. Huang, F. Z. Wang, P. F. Qiu, X. Zhang, C. H. Li, Q. Li, *Angew. Chem., Int. Ed.* **2023**, *62*, 202313728.
[18] M. Zhang, A. Pal, X. Lyu, Y. Wu, M. Sitti, *Nat. Mater.* **2024**, *23*, 560.
[19] S. Li, Y. Tang, Q. Fan, Z. Li, X. Zhang, J. Wang, J. Guo, Q. Li, *Light Sci. Appl.* **2024**, *13*, 140.
[20] H. Tian, Z. Wang, Y. Chen, J. Shao, T. Gao, S. Cai, *ACS Appl. Mater. Interfaces.* **2018**, *10*, 8307.
[21] Q. He, Z. Wang, Z. Song, S. Cai, *Adv. Mater. Technol.* **2019**, *4*, 1800244.
[22] N. Torras, K. E. Zinoviev, J. Esteve, A. Sánchez-Ferrer, *J. Mater. Chem. C.* **2013**, *1*, 5183.
[23] J. Lv, Y. Liu, J. Wei, E. Chen, L. Qin, Y. Yu, *Nature* **2016**, *537*, 179.
[24] Q. He, Z. Wang, Y. Wang, A. Minori, M. T. Tolley, S. Cai, *Sci. Adv.* **2019**, *5*, aax5746.
[25] C. Ohm, M. Brehmer, R. Zentel, *Adv. Mater.* **2010**, *22*, 3366.
[26] M. Pilz da Cunha, M. G. Debije, A. P. H. J. Schenning, *Chem. Soc. Rev.* **2020**, *49*, 6568.
[27] R. S. Kularatne, H. Kim, J. M. Boothby, T. H. Ware, *J. Polym. Sci., Part B: Polym. Phys.* **2017**, *55*, 395.
[28] Z. Wen, K. Yang, J. M. Raquez, *Molecules* **2020**, *25*, 1241.
[29] T. J. White, D. J. Broer, *Nat. Mater.* **2015**, *14*, 1087.
[30] R. Zheng, Y. Wei, Z. C. Zhang, Z. Y. Wang, L. L. Ma, Y. Wang, L. Huang, Y. Q. Lu, *Responsive Mater* **2023**, *1*, 20230017.
[31] Q. Li, *Liquid Crystals Beyond Displays: Chemistry, Physics, and Applications*, John Wiley & Sons, Inc, Hoboken, NJ, USA **2012**.

[32] Q. Li, *Nanoscience with Liquid Crystals: From Self-Organized Nanostructures to Applications*, Springer, Heidelberg, Germany **2014**.
[33] F. Reinitzer, *Liq. Cryst.* **1989**, *5*, 7.
[34] S. K. Prasad, *Angew. Chem., Int. Ed.* **2012**, *51*, 10708.
[35] P. J. Collings, M. Hird, *Introduction to Liquid Crystals: Chemistry and Physics*, CRC Press, Boca Ratonn, USA **2019**.
[36] X. Zhang, Y. Xu, C. Valenzuela, X. Zhang, L. Wang, W. Feng, Q. Li, *Light Sci. Appl.* **2022**, *11*, 223.
[37] L. Wang, A. M. Urbas, Q. Li, *Adv. Mater.* **2020**, *32*, 1801335.
[38] H. K. Bisoyi, Q. Li, *Chem. Rev.* **2022**, *122*, 4887.
[39] H. K. Bisoyi, Q. Li, *Chem. Rev.* **2016**, *116*, 15089.
[40] J. Liu, Y. M. Qing, J. J. Wu, J. Q. Tian, C. B. Feng, X. Y. Zhou, Y. Ma, B. X. Li, Y. Q. Lu, Q. Li, *Responsive Mater.* **2025**, *3*, 70020.
[41] R. Song, J. Lv, *Responsive Mater.* **2025**, 70022, https://doi.org/10.1002/rpm2.7002.
[42] H. Wermter, H. Finkelmann, *e-Polymers.* **2001**, *1*, 013.
[43] P. Beyer, E. M. Terentjev, R. Zentel, *Macromol. Rapid Commun.* **2007**, *28*, 1485.
[44] Z. Zhang, J. Li, R. Zhang, R. Chen, Y. Zhang, T. Wang, K. L. Yang, J. Zhu, *Responsive Mater.* **2024**, *2*, 20240021.
[45] X. Pang, L. Qin, B. Xu, Q. Liu, Y. Yu, *Adv. Funct. Mater.* **2020**, *30*, 2002451.
[46] M. Chen, B. Yao, M. Kappl, S. Liu, J. Yuan, R. Berger, F. Zhang, H.-J. Butt, Y. Liu, S. Wu, *Adv. Funct. Mater.* **2020**, *30*, 1906752.
[47] Z. Liu, H. K. Bisoyi, Y. Huang, M. Wang, H. Yang, Q. Li, *Angew. Chem., Int. Ed.* **2022**, *61*, 202115755.
[48] W. Shen, J. Liu, B. Du, H. Zhuo, S. Chen, *J. Mater. Chem. A.* **2021**, *9*, 15087.
[49] A. D. Auguste, J. W. Ward, J. O. Hardin, B. A. Kowalski, T. C. Guin, J. D. Berrigan, T. J. White, *Adv. Mater.* **2018**, *30*, 1802438.
[50] X. Cheng, T. Miao, H. Ma, J. Zhang, Z. Zhang, W. Zhang, X. Zhu, *Small.* **2021**, *17*, 2103177.
[51] H. Finkelmann, H. J. Kock, G. Rehage, *Makromol. Chem., Rapid Commun.* **1981**, *2*, 317.
[52] M. Warner, P. Bladon, E. M. Terentjev, *J. Phys. II.* **1994**, *4*, 93.
[53] E. M. Terentjev, *J. Phys.: Condens. Matter.* **1999**, *11*, R239.
[54] T. H. Ware, J. S. Biggins, A. F. Shick, M. Warner, T. J. White, *Nat. Commun.* **2016**, *7*, 10781.
[55] J. S. Biggins, M. Warner, K. Bhattacharya, *Phys. Rev. Lett.* **2009**, *103*, 037802.
[56] J. Gao, M. Tian, Y. He, H. Yi, J. Guo, *Adv. Funct. Mater.* **2021**, *32*, 2107145.
[57] S. Zhang, C. Sun, J. Zhang, S. Qin, J. Liu, Y. Ren, L. Zhang, W. Hu, H. Yang, D. Yang, *Adv. Funct. Mater.* **2023**, *33*, 2305364.
[58] J. Liu, S. Zhang, Z. Wang, X. Xia, J. Zhang, Y. Yu, Y. Xiao, Y. Ren, J. Chen, B. Yang, W. Xie, W. Hu, H. Yang, *Nat. Commun.* **2024**, *15*, 10367.
[59] S. Li, K. H. Yu, I. Garcia, S. H. Nah, H. N. T. Chui, Z. Tian, S. Yang, *Adv. Funct. Mater.* **2024**, *35*, 2413965.
[60] J. Ma, Y. Yang, X. Zhang, P. Xue, C. Valenzuela, Y. Liu, L. Wang, W. Feng, *Mater. Horiz.* **2024**, *11*, 217.
[61] G. N. Mol, K. D. Harris, C. W. M. Bastiaansen, D. J. Broer, *Adv. Funct. Mater.* **2005**, *15*, 1155.
[62] J. Wu, S. Yao, H. Zhang, W. Man, Z. Bai, F. Zhang, X. Wang, D. Fang, Y. Zhang, *Adv. Mater.* **2021**, *33*, 2106175.
[63] H. E. Fowler, P. Rothemund, C. Keplinger, T. J. White, *Adv. Mater.* **2021**, *33*, 2103806.
[64] Y. Wang, J. Liu, S. Yang, *Appl. Phys. Rev.* **2022**, *9*, 011301.
[65] J. Zhang, Y. Guo, W. Hu, R. H. Soon, Z. S. Davidson, M. Sitti, *Adv. Mater.* **2021**, *33*, 2006191.
[66] Y. Wu, S. Zhang, Y. Yang, Z. Li, Y. Wei, Y. Ji, *Sci. Adv.* **2022**, *8*, abo6021.
[67] Z. Wang, K. Li, Q. He, S. Cai, *Adv. Mater.* **2019**, *31*, 1806849.
[68] H. Yu, T. Ikeda, *Adv. Mater.* **2011**, *23*, 2149.
[69] W. Liu, L. X. Guo, B. P. Lin, X. Q. Zhang, Y. Sun, H. Yang, *Macromolecules* **2016**, *49*, 4023.
[70] S. Palagi, A. G. Mark, S. Y. Reigh, K. Melde, T. Qiu, H. Zeng, C. Parmeggiani, D. Martella, A. Sanchez Castillo, N. Kapernaum, F. Giesselmann, D. S. Wiersma, E. Lauga, P. Fischer, *Nat. Mater.* **2016**, *15*, 647.
[71] J. E. Stumpel, C. Wouters, N. Herzer, J. Ziegler, D. J. Broer, C. W. M. Bastiaansen, A. P. H. J. Schenning, *Adv. Opt. Mater.* **2014**, *2*, 459.
[72] L. T. de Haan, J. M. N. Verjans, D. J. Broer, C. W. M. Bastiaansen, A. P. H. J. Schenning, *J. Am. Chem. Soc.* **2014**, *136*, 10585.
[73] R. Kizhakidathazhath, Y. Geng, V. S. R. Jampani, C. Charni, A. Sharma, J. P. F. Lagerwall, *Adv. Funct. Mater.* **2020**, *30*, 1909537.
[74] P. Lv, X. Yang, H. K. Bisoyi, H. Zeng, X. Zhang, Y. Chen, P. Xue, S. Shi, A. Priimagi, L. Wang, W. Feng, Q. Li, *Mater. Horiz* **2021**, *8*, 2475.
[75] H. Kim, J. A. Lee, C. P. Ambulo, H. B. Lee, S. H. Kim, V. V. Naik, C. S. Haines, A. E. Aliev, R. Ovalle-Robles, R. H. Baughman, T. H. Ware, *Adv. Funct. Mater.* **2019**, *29*, 1905063.
[76] C. Wang, K. Sim, J. Chen, H. Kim, Z. Rao, Y. Li, W. Chen, J. Song, R. Verduzco, C. Yu, *Adv. Mater.* **2018**, *30*, 1706695.
[77] X. Yang, Y. Chen, X. Zhang, P. Xue, P. Lv, Y. Yang, L. Wang, W. Feng, *Nano Today* **2022**, *43*, 101419.
[78] S. Ma, X. Li, S. Huang, J. Hu, H. Yu, *Angew. Chem., Int. Ed.* **2019**, *58*, 2655.
[79] Y. Yu, M. Nakano, T. Ikeda, *Nature* **2003**, *425*, 145.
[80] C. L. van Oosten, C. W. M. Bastiaansen, D. J. Broer, *Nat. Mater.* **2009**, *8*, 677.
[81] A. Potekhina, C. Wang, *Appl. Phys. Lett.* **2021**, *118*, 241903.
[82] S. Iamsaard, S. J. Aßhoff, B. Matt, T. Kudernac, J. J. L. M. Cornelissen, S. P. Fletcher, N. Katsonis, *Nat. Chem.* **2014**, *6*, 229.
[83] J. J. Wie, M. R. Shankar, T. J. White, *Nat. Commun.* **2016**, *7*, 13260.
[84] S. Nocentini, D. Martella, D. S. Wiersma, C. Parmeggiani, *Soft Matter* **2017**, *13*, 8590.
[85] K. M. Lee, M. L. Smith, H. Koerner, N. Tabiryan, R. A. Vaia, T. J. Bunning, T. J. White, *Adv. Funct. Mater.* **2011**, *21*, 2913.
[86] K. M. Lee, T. J. Bunning, T. J. White, *Adv. Mater.* **2012**, *24*, 2839.
[87] K. Kumar, C. Knie, D. Bléger, M. A. Peletier, H. Friedrich, S. Hecht, D. J. Broer, M. G. Debije, A. P. H. J. Schenning, *Nat. Commun.* **2016**, *7*, 11975.
[88] T. J. White, N. V. Tabiryan, S. V. Serak, U. A. Hrozhyk, V. P. Tondiglia, H. Koerner, R. A. Vaia, T. J. Bunning, *Soft Matter.* **2008**, *4*, 1796.
[89] S. K. Ahn, T. H. Ware, K. M. Lee, V. P. Tondiglia, T. J. White, *Adv. Funct. Mater.* **2016**, *26*, 5819.
[90] J. Ma, Y. Yang, C. Valenzuela, X. Zhang, L. Wang, W. Feng, *Angew. Chem., Int. Ed.* **2022**, *61*, 202116219.
[91] S. U. Kim, Y. J. Lee, J. Liu, D. S. Kim, H. Wang, S. Yang, *Nat. Mater.* **2022**, *21*, 41.
[92] J. Weilepp, P. Stein, N. Aßfalg, H. Finkelmann, P. Martinoty, H. R. Brand, *Europhys. Lett.* **1999**, *47*, 508.
[93] N. A. Traugutt, R. H. Volpe, M. S. Bollinger, M. O. Saed, A. H. Torbati, K. Yu, N. Dadivanyan, C. M. Yakacki, *Soft Matter* **2017**, *13*, 7013.
[94] A. Greve, H. Finkelmann, *Macromol. Chem. Phys.* **2001**, *202*, 2926.
[95] C. Ahn, X. Liang, S. Cai, *Extreme Mech. Lett.* **2015**, *5*, 30.
[96] M. H. Li, P. Keller, *Philosophical Transactions of the Royal Society A: Mathematical, Physical and Engineering Sciences.* **2006**, *364*, 2763.
[97] D. J. Broer, *Molecular Crystals and Liquid Crystals.* **1995**, *261*, 513.
[98] D. Liu, D. J. Broer, *Langmuir.* **2014**, *30*, 13499.
[99] K. M. Herbert, H. E. Fowler, J. M. McCracken, K. R. Schlafmann, J. A. Koch, T. J. White, *Nat. Rev. Mater.* **2022**, *7*, 23.
[100] M. O. Saed, A. Gablier, E. M. Terentjev, *Chem. Rev.* **2022**, *122*, 4927.
[101] X. Wan, L. Luo, Y. Liu, J. Leng, *Adv. Sci.* **2020**, *7*, 2001000.
[102] M. Chen, M. Gao, L. Bai, H. Zheng, H. J. Qi, K. Zhou, *Adv. Mater.* **2023**, *35*, 2209566.
[103] Y. Chi, Y. Li, Y. Zhao, Y. Hong, Y. Tang, J. Yin, *Adv. Mater.* **2022**, *34*, 2110384.

[104] B. Jin, S. Yang, *Adv. Funct. Mater.* **2023**, *33*, 2304769.
[105] J. Zhao, L. Zhang, J. Hu, *Adv. Intell. Syst.* **2021**, *4*, 2100065.
[106] T. Zang, J. Wang, G. Yan, X. Lu, J. Hu, H. Xia, Y. Zhao, *Adv. Mater.* **2025**, *37*, 08694.
[107] A. van Oosterhout, M. A. Robertson, J. Paik, *Nat. Rev. Bioeng.* **2025**, 1, https://doi.org/10.1038/s44222-025-00359-6.
[108] A. Rešetič, *Commun. Chem.* **2024**, *7*, 56.
[109] E. M. Terentjev, *Macromolecules.* **2025**, *58*, 2792.
[110] Y. Li, T. Liu, V. Ambrogi, O. Rios, M. Xia, W. He, Z. Yang, *ACS Appl. Mater. Interfaces.* **2022**, *14*, 14842.
[111] Z. Pei, Y. Yang, Q. Chen, E. M. Terentjev, Y. Wei, Y. Ji, *Nat. Mater.* **2014**, *13*, 36.
[112] A. Gablier, M. O. Saed, E. M. Terentjev, *Macromolecules.* **2020**, *53*, 8642.
[113] W. Zou, X. Lin, E. M. Terentjev, *Adv. Mater.* **2021**, *33*, 2101955.
[114] H. Liang, S. Zhang, Y. Liu, Y. Yang, Y. Zhang, Y. Wu, H. Xu, Y. Wei, Y. Ji, *Adv. Mater.* **2022**, *35*, 2202462.
[115] M. O. Saed, A. Gablier, E. M. Terentjev, *Adv. Funct. Mater.* **2023**, *34*, 2307202.
[116] X. Chen, M. A. Dam, K. Ono, A. Mal, H. Shen, S. R. Nutt, K. Sheran, F. Wudl, *Science* **2002**, *295*, 1698.
[117] B. Zhang, Z. A. Digby, J. A. Flum, P. Chakma, J. M. Saul, J. L. Sparks, D. Konkolewicz, *Macromolecules* **2016**, *49*, 6871.
[118] A. Erice, A. Ruiz de Luzuriaga, J. M. Matxain, F. Ruipérez, J. M. Asua, H.-J. Grande, A. Rekondo, *Polymer.* **2018**, *145*, 127.
[119] D. J. Fortman, J. P. Brutman, C. J. Cramer, M. A. Hillmyer, W. R. Dichtel, *J. Am. Chem. Soc.* **2015**, *137*, 14019.
[120] R. L. Snyder, D. J. Fortman, G. X. De Hoe, M. A. Hillmyer, W. R. Dichtel, *Macromolecules* **2018**, *51*, 389.
[121] L. Li, X. Chen, J. M. Torkelson, *Macromolecules.* **2019**, *52*, 8207.
[122] W. Denissen, G. Rivero, R. Nicolay, L. Leibler, J. M. Winne, F. E. Du Prez, *Adv. Funct. Mater.* **2015**, *25*, 2451.
[123] P. Zheng, T. J. McCarthy, *J. Am. Chem. Soc.* **2012**, *134*, 2024.
[124] Y.-X. Lu, Z. Guan, *J. Am. Chem. Soc.* **2012**, *134*, 14226.
[125] S. Billiet, K. De Bruycker, F. Driessen, H. Goossens, V. Van Speybroeck, J. M. Winne, F. E. Du Prez, *Nat. Chem.* **2014**, *6*, 815.
[126] M. M. Obadia, B. P. Mudraboyina, A. Serghei, D. Montarnal, E. Drockenmuller, *J. Am. Chem. Soc.* **2015**, *137*, 6078.
[127] P. Chakma, Z. A. Digby, M. P. Shulman, L. R. Kuhn, C. N. Morley, J. L. Sparks, D. Konkolewicz, *ACS Macro Lett.* **2019**, *8*, 95.
[128] M. T. Brannum, A. M. Steele, M. C. Venetos, L. T. J. Korley, G. E. Wnek, T. J. White, *Adv. Opt. Mater.* **2019**, *7*, 1801683.
[129] K. R. Schlafmann, M. S. Alahmed, K. L. Lewis, T. J. White, *Adv. Funct. Mater.* **2023**, *33*, 2305818.
[130] A. Kotikian, C. McMahan, E. C. Davidson, J. M. Muhammad, R. D. Weeks, C. Daraio, J. A. Lewis, *Sci. Robot.* **2019**, *4*, aax7044.
[131] K. Liu, F. Hacker, C. Daraio, *Sci. Robot.* **2021**, *6*, abf5116.
[132] J. Küpfer, H. Finkelmann, *Makromol. Chem., Rapid Commun.* **1991**, *12*, 717.
[133] M. J. Ford, C. P. Ambulo, T. A. Kent, E. J. Markvicka, C. Pan, J. Malen, T. H. Ware, C. Majidi, *Proc. Natl. Acad. Sci. USA* **2019**, *116*, 21438.
[134] T. H. Ware, M. E. McConney, J. J. Wie, V. P. Tondiglia, T. J. White, *Science* **2015**, *347*, 982.
[135] H. Aharoni, Y. Xia, X. Zhang, R. D. Kamien, S. Yang, *Proc. Natl. Acad. Sci. USA* **2018**, *115*, 7206.
[136] M. E. Prévôt, S. Ustunel, E. Hegmann, *Materials* **2018**, *11*, 377.
[137] Y. Wang, R. Yin, L. Jin, M. Liu, Y. Gao, J. Raney, S. Yang, *Adv. Funct. Mater.* **2023**, *33*, 2210614.
[138] A. W. Hauser, D. Liu, K. C. Bryson, R. C. Hayward, D. J. Broer, *Macromolecules* **2016**, *49*, 1575.
[139] S. Li, G. Librandi, Y. Yao, A. J. Richard, A. Schneider-Yamamura, J. Aizenberg, K. Bertoldi, *Adv. Mater.* **2021**, *33*, 2105024.
[140] K. Kim, Y. Guo, J. Bae, S. Choi, H. Y. Song, S. Park, K. Hyun, S.-K. Ahn, *Small.* **2021**, *17*, 2100910.
[141] B. A. Kowalski, V. P. Tondiglia, T. Guin, T. J. White, *Soft Matter* **2017**, *13*, 4335.
[142] B. Ni, G. Liu, M. Zhang, P. Keller, M. Tatoulian, M. H. Li, *CCS Chem* **2021**, *4*, 847.
[143] C. P. Ambulo, J. J. Burroughs, J. M. Boothby, H. Kim, M. R. Shankar, T. H. Ware, *ACS Appl. Mater. Interfaces.* **2017**, *9*, 37332.
[144] A. Kotikian, R. L. Truby, J. W. Boley, T. J. White, J. A. Lewis, *Adv. Mater.* **2018**, *30*, 1706164.
[145] X. Peng, S. Wu, X. Sun, L. Yue, S. M. Montgomery, F. Demoly, K. Zhou, R. R. Zhao, H. J. Qi, *Adv. Mater.* **2022**, *34*, 2204890.
[146] N. A. Traugutt, D. Mistry, C. Luo, K. Yu, Q. Ge, C. M. Yakacki, *Adv. Mater.* **2020**, *32*, 2000797.
[147] Z. Wang, Z. Wang, Y. Zheng, Q. He, Y. Wang, S. Cai, *Sci. Adv.* **2020**, *6*, abc0034.
[148] A. Kotikian, A. A. Watkins, G. Bordiga, A. Spielberg, Z. S. Davidson, K. Bertoldi, J. A. Lewis, *Adv. Mater.* **2024**, *36*, 2310743.
[149] M. K. McBride, M. Hendrikx, D. Liu, B. T. Worrell, D. J. Broer, C. N. Bowman, *Adv. Mater.* **2017**, *29*, 1606509.
[150] Z. C. Jiang, Y. Y. Xiao, L. Yin, L. Han, Y. Zhao, *Angew. Chem., Int. Ed.* **2020**, *59*, 4925.
[151] Y. Wu, Y. Yang, X. Qian, Q. Chen, Y. Wei, Y. Ji, *Angew. Chem., Int. Ed.* **2020**, *59*, 4778.
[152] M. K. McBride, A. M. Martinez, L. Cox, M. Alim, K. Childress, M. Beiswinger, M. Podgorski, B. T. Worrell, J. Killgore, C. N. Bowman, *Sci. Adv.* **2018**, *4*, aat4634.
[153] D. W. Hanzon, X. He, H. Yang, Q. Shi, K. Yu, *Soft Matter* **2017**, *13*, 7061.
[154] X. Zhou, Y. Sheng, G. Chen, H. Wan, L. Lu, H. Xing, J. Huang, Z. Zhu, Y. Wang, H. Bao, J. Wu, Q. Zhao, T. Xie, N. Zheng, *Nat. Commun.* **2025**, *16*, 7536.
[155] H. Xu, H. Liang, Y. Yang, Y. Liu, E. He, Z. Yang, Y. Wang, Y. Wei, Y. Ji, *Nat. Commun.* **2024**, *15*, 7381.
[156] Y. Yao, E. He, H. Xu, Y. Liu, Z. Yang, Y. Wei, Y. Ji, *Nat. Commun.* **2023**, *14*, 3518.
[157] R. C. P. Verpaalen, M. Pilz da Cunha, T. A. P. Engels, M. G. Debije, A. P. H. J. Schenning, *Angew. Chem., Int. Ed.* **2020**, *59*, 4532.
[158] G. Chen, B. Jin, Y. Shi, Q. Zhao, Y. Shen, T. Xie, *Adv. Mater.* **2022**, *34*, 2201679.
[159] S. Chen, Y. Cao, M. Sarparast, H. Yuan, L. Dong, X. Tan, C. Cao, *Adv. Mater. Technol.* **2020**, *5*, 1900837.
[160] Z. Liu, R. Zhang, Y. Xiao, J. Li, W. Chang, D. Qian, Z. Liu, *Mater. Horiz* **2021**, *8*, 1783.
[161] S. Gantenbein, K. Masania, W. Woigk, J. P. W. Sesseg, T. A. Tervoort, A. R. Studart, *Nature* **2018**, *561*, 226.
[162] H. C. Astley, T. J. Roberts, *Biol. Lett.* **2011**, *8*, 386.
[163] H. C. Astley, T. J. Roberts, *J. Exp. Biol.* **2014**, *217*, 4372.
[164] M. J. Schwaner, D. C. Lin, C. P. McGowan, *J. Exp. Biol.* **2018**, *221*, jeb186700.
[165] E. Queathem, *J. Insect Physiol.* **1991**, *37*, 129.
[166] M. Gomez, D. E. Moulton, D. Vella, *Nat. Phys.* **2017**, *13*, 142.
[167] S. Ma, P. Xue, Y. Tang, R. Bi, X. Xu, L. Wang, Q. Li, *Responsive Mater.* **2024**, *2*, 20230026.
[168] Y. Kim, J. van den Berg, A. J. Crosby, *Nat. Mater.* **2021**, *20*, 1695.
[169] J. Jeon, J. C. Choi, H. Lee, W. Cho, K. Lee, J. G. Kim, J. W. Lee, K. I. Joo, M. Cho, H. R. Kim, J. J. Wie, *Mater. Today.* **2021**, *49*, 97.
[170] K. Korner, A. S. Kuenstler, R. C. Hayward, B. Audoly, K. Bhattacharya, *Proc. Natl. Acad. Sci. USA* **2020**, *117*, 9762.
[171] H. Arazoe, D. Miyajima, K. Akaike, F. Araoka, E. Sato, T. Hikima, M. Kawamoto, T. Aida, *Nat. Mater.* **2016**, *15*, 1084.
[172] B. Gorissen, D. Melancon, N. Vasios, M. Torbati, K. Bertoldi, *Sci. Robot.* **2020**, *5*, abb1967.
[173] S. Yan, L. Wu, Y. Wen, J. Sun, J. Zhou, *Responsive Mater.* **2025**, *3*, 20240035.

[174] M. R. Shankar, M. L. Smith, V. P. Tondiglia, K. M. Lee, M. E. McConney, D. H. Wang, L. S. Tan, T. J. White, *Proc. Natl. Acad. Sci. USA* **2013**, *110*, 18792.
[175] M. Li, S. Lv, J. Zhou, *S. Mater. Struct* **2014**, *23*, 125012.
[176] T. S. Hebner, K. Korner, C. N. Bowman, K. Bhattacharya, T. J. White, *Sci. Adv.* **2023**, *9*, ade1320.
[177] Y. Xia, G. Cedillo-Servin, R. D. Kamien, S. Yang, *Adv. Mater.* **2016**, *28*, 9637.
[178] T. Kamal, S. Y. Park, *Chem. Commun.* **2014**, *50*, 2030.
[179] A. H. Gelebart, D. J. Mulder, M. Varga, A. Konya, G. Vantomme, E. W. Meijer, R. L. B. Selinger, D. J. Broer, *Nature* **2017**, *546*, 632.
[180] H. Shahsavan, A. Aghakhani, H. Zeng, Y. Guo, Z. S. Davidson, A. Priimagi, M. Sitti, *Proc. Natl. Acad. Sci. USA* **2020**, *117*, 5125.
[181] Y. Zhao, Y. Chi, Y. Hong, Y. Li, S. Yang, J. Yin, *Proc. Natl. Acad. Sci. USA* **2022**, *119*, 2200265119.
[182] A. Clement, M. Babaei, J. Phadikar, D. W. Lee, A. A. Skandani, M. R. Shankar, *Extreme Mech. Lett.* **2021**, *47*, 101362.
[183] Y. Zhao, Y. Hong, F. Qi, Y. Chi, H. Su, J. Yin, *Adv. Mater.* **2023**, *35*, 2370047.
[184] N. Tamaoki, *Adv. Mater.* **2001**, *13*, 1135.
[185] Y. Yang, Q. Li, H. Zhang, H. Liu, X. Ji, B. Z. Tang, *Adv. Mater.* **2021**, *33*, 2105418.
[186] R. Aleisa, J. Feng, Z. Ye, Y. Yin, *Angew. Chem., Int. Ed.* **2022**, *61*, 202203700.
[187] X. Le, H. Shang, H. Yan, J. Zhang, W. Lu, M. Liu, L. Wang, G. Lu, Q. Xue, T. Chen, *Angew. Chem., Int. Ed.* **2021**, *60*, 3640.
[188] M. Chen, Y. Hou, R. An, H. J. Qi, K. Zhou, *Adv. Mater.* **2024**, *36*, 2303969.
[189] S. H. Choi, J. H. Kim, J. Ahn, T. Kim, Y. Jung, D. Won, J. Bang, K. R. Pyun, S. Jeong, H. Kim, Y. G. Kim, S. H. Ko, *Nat. Mater.* **2024**, *23*, 834.
[190] J. Gao, M. Tian, Y. He, H. Yi, J. Guo, *Adv. Funct. Mater.* **2022**, *32*, 2107145.
[191] A. M. Martinez, M. K. McBride, T. J. White, C. N. Bowman, *Adv. Funct. Mater.* **2020**, *30*, 2003150.
[192] Y. Huang, H. K. Bisoyi, S. Huang, M. Wang, X. M. Chen, Z. Liu, H. Yang, Q. Li, *Angew. Chem., Int. Ed.* **2021**, *60*, 11247.
[193] Y. S. Zhang, S. A. Jiang, J. D. Lin, C. R. Lee, *J. Mater. Chem. C.* **2020**, *8*, 5517.
[194] Y. Li, Y. Teixeira, G. Parlato, J. Grace, F. Wang, B. D. Huey, X. Wang, *Soft Matter* **2022**, *18*, 6857.
[195] Z. Zhang, W. Wang, M. O'Hagan, J. Dai, J. Zhang, H. Tian, *Angew. Chem., Int. Ed.* **2022**, *61*, 202205758.
[196] O. S. Bushuyev, M. Aizawa, A. Shishido, C. J. Barrett, *Macromol. Rapid Commun.* **2018**, *39*, 1700253.
[197] W. Wu, L. Yao, T. Yang, R. Yin, F. Li, Y. Yu, *J. Am. Chem. Soc.* **2011**, *133*, 15810.
[198] Z. Jiang, M. Xu, F. Li, Y. Yu, *J. Am. Chem. Soc.* **2013**, *135*, 16446.
[199] J. Guillen Campos, C. Tobin, S. Sandlass, M. Park, Y. Wu, M. Gordon, J. Read de Alaniz, *Adv. Mater.* **2024**, *36*, 2404932.
[200] C. Ma, W. Lu, X. Yang, J. He, X. Le, L. Wang, J. Zhang, M. J. Serpe, Y. Huang, T. Chen, *Adv. Funct. Mater.* **2018**, *28*, 1704568.
[201] Z. Li, P. Liu, X. Ji, J. Gong, Y. Hu, W. Wu, X. Wang, H. Q. Peng, R. T. K. Kwok, J. W. Y. Lam, J. Lu, B. Z. Tang, *Adv. Mater.* **2020**, *32*, 1906493.
[202] S. Wei, W. Lu, X. Le, C. Ma, H. Lin, B. Wu, J. Zhang, P. Theato, T. Chen, *Angew. Chem., Int. Ed.* **2019**, *58*, 16243.
[203] Y. Yao, C. Yin, S. Hong, H. Chen, Q. Shi, J. Wang, X. Lu, N. Zhou, *Chem. Mater.* **2020**, *32*, 8868.
[204] K. S. Sarkisyan, D. A. Bolotin, M. V. Meer, D. R. Usmanova, A. S. Mishin, G. V. Sharonov, D. N. Ivankov, N. G. Bozhanova, M. S. Baranov, O. Soylemez, N. S. Bogatyreva, P. K. Vlasov, E. S. Egorov, M. D. Logacheva, A. S. Kondrashov, D. M. Chudakov, E. V. Putintseva, I. Z. Mamedov, D. S. Tawfik, K. A. Lukyanov, F. A. Kondrashov, *Nature* **2016**, *533*, 397.
[205] M. Yang, Y. Xu, X. Zhang, H. K. Bisoyi, P. Xue, Y. Yang, X. Yang, C. Valenzuela, Y. Chen, L. Wang, W. Feng, Q. Li, *Adv. Funct. Mater.* **2022**, *32*, 2201884.
[206] G. Long, Y. Deng, W. Zhao, G. Zhou, D. J. Broer, B. L. Feringa, J. Chen, *J. Am. Chem. Soc.* **2024**, *146*, 13894.
[207] M. Irie, *Chem. Rev.* **2000**, *100*, 1685.
[208] M. Irie, T. Fukaminato, K. Matsuda, S. Kobatake, *Chem. Rev.* **2014**, *114*, 12174.
[209] Z. G. Zheng, Y. Li, H. K. Bisoyi, L. Wang, T. J. Bunning, Q. Li, *Nature* **2016**, *531*, 352.
[210] Y. Zhao, T. Ikeda, *Smart Light-Responsive Materials : Azobenzene-Containing Polymers and Liquid Crystals*, John Wiley & Sons, Inc, Hoboken, NJ, USA **2009**.
[211] H. M. D. Bandara, S. C. Burdette, *Chem. Soc. Rev.* **2012**, *41*, 1809.
[212] Z. G. Zheng, Y. Q. Lu, Q. Li, *Adv. Mater.* **2020**, *32*, 1905318.
[213] H. K. Bisoyi, Q. Li, *Acc. Chem. Res.* **2014**, *47*, 3184.
[214] H. Zeng, M. Lahikainen, L. Liu, Z. Ahmed, O. M. Wani, M. Wang, H. Yang, A. Priimagi, *Nat. Commun.* **2019**, *10*, 5057.
[215] C. Chen, P. Shi, Z. Liu, S. Duan, M. Si, C. Zhang, Y. Du, Y. Yan, T. J. White, R. Kramer-Bottiglio, M. Sitti, T. Iwasaki, X. He, *Sci. Robot.* **2025**, *10*, ads1292.
[216] Z. Zhang, J. Zhao, H. Chen, D. Chen, *Appl. Bionics Biomech.* **2017**, *2017*, 1.
[217] C. Zhang, W. Zou, L. Ma, Z. Wang, *Rob. Auton. Syst.* **2020**, *124*, 103362.
[218] Y. Wu, J. K. Yim, J. Liang, Z. Shao, M. Qi, J. Zhong, Z. Luo, X. Yan, M. Zhang, X. Wang, R. S. Fearing, R. J. Full, L. Lin, *Sci. Robot.* **2019**, *4*, aax1594.
[219] J. S. Koh, E. Yang, G. P. Jung, S. P. Jung, J. H. Son, S. I. Lee, P. G. Jablonski, R. J. Wood, H. Y. Kim, K. J. Cho, *Science* **2015**, *349*, 517.
[220] M. Duduta, F. Berlinger, R. Nagpal, D. R. Clarke, R. J. Wood, F. Z. Temel, *IEEE Rob. Autom. Lett.* **2020**, *5*, 3868.
[221] R. Chen, Z. Yuan, J. Guo, L. Bai, X. Zhu, F. Liu, H. Pu, L. Xin, Y. Peng, J. Luo, L. Wen, Y. Sun, *Nat. Commun.* **2021**, *12*, 7028.
[222] J. Zhao, J. Zhang, D. McCoul, Z. Hao, S. Wang, X. Wang, B. Huang, L. Sun, *Soft Robot* **2019**, *6*, 713.
[223] N. W. Bartlett, M. T. Tolley, J. T. B. Overvelde, J. C. Weaver, B. Mosadegh, K. Bertoldi, G. M. Whitesides, R. J. Wood, *Science* **2015**, *349*, 161.
[224] M. Loepfe, C. M. Schumacher, U. B. Lustenberger, W. J. Stark, *Soft Robot* **2015**, *2*, 33.
[225] Z. Liu, J. Liu, H. Wang, X. Yu, K. Yang, W. Liu, S. Nie, W. Sun, Z. Xie, B. Chen, S. Liang, Y. Guan, L. Wen, *IEEE Rob. Autom. Lett.* **2020**, *5*, 3291.
[226] S. Li, D. Rus, *IEEE/ASME Trans. Mechatron.* **2019**, *24*, 447.
[227] E. W. Hawkes, C. Xiao, R. A. Peloquin, C. Keeley, M. R. Begley, M. T. Pope, G. Niemeyer, *Nature* **2022**, *604*, 657.
[228] S. Zhang, X. Hu, M. Li, U. Bozuyuk, R. Zhang, E. Suadiye, J. Han, F. Wang, P. Onck, M. Sitti, *Sci. Adv.* **2023**, *9*, adf9462.
[229] H. Li, J. Wang, *ACS Appl. Mater. Interfaces.* **2019**, *11*, 10218.
[230] Y. Hu, J. Liu, L. Chang, L. Yang, A. Xu, K. Qi, P. Lu, G. Wu, W. Chen, Y. Wu, *Adv. Funct. Mater.* **2017**, *27*, 1704388.
[231] K. Yu, X. Ji, T. Yuan, Y. Cheng, J. Li, X. Hu, Z. Liu, X. Zhou, L. Fang, *Adv. Mater.* **2021**, *33*, 2104558.
[232] C. Ahn, X. Liang, S. Cai, *Adv. Mater. Technol.* **2019**, *4*, 1900185.
[233] X. Zhou, G. Chen, B. Jin, H. Feng, Z. Chen, M. Fang, B. Yang, R. Xiao, T. Xie, N. Zheng, *Adv. Sci.* **2024**, *11*, 2402358.
[234] C. Chen, Z. Liu, P. Shi, Y. Zhao, S. Duan, Y. Du, Y. Yan, M. Si, T. Iwasaki, X. He, *Nat. Commun.* **2025**, *16*, 7630.
[235] W. Wang, Q. Liu, I. Tanasijevic, M. F. Reynolds, A. J. Cortese, M. Z. Miskin, M. C. Cao, D. A. Muller, A. C. Molnar, E. Lauga, P. L. McEuen, I. Cohen, *Nature* **2022**, *605*, 681.
[236] Z. Ren, M. Zhang, S. Song, Z. Liu, C. Hong, T. Wang, X. Dong, W. Hu, M. Sitti, *Sci. Adv.* **2022**, *8*, abq2345.

[237] S. Tottori, L. Zhang, F. Qiu, K. K. Krawczyk, A. Franco-Obregón, B. J. Nelson, *Adv. Mater.* **2012**, *24*, 811.
[238] M. Wehner, R. L. Truby, D. J. Fitzgerald, B. Mosadegh, G. M. Whitesides, J. A. Lewis, R. J. Wood, *Nature* **2016**, *536*, 451.
[239] H. W. Huang, M. S. Sakar, A. J. Petruska, S. Pané, B. J. Nelson, *Nat. Commun.* **2016**, *7*, 12263.
[240] X. Hu, I. C. Yasa, Z. Ren, S. R. Goudu, H. Ceylan, W. Hu, M. Sitti, *Sci. Adv.* **2021**, *7*, abe8436.
[241] Q. Liu, W. Wang, M. F. Reynolds, M. C. Cao, M. Z. Miskin, T. A. Arias, D. A. Muller, P. L. McEuen, I. Cohen, *Sci. Robot.* **2021**, *6*, abe6663.
[242] B. J. Nelson, I. K. Kaliakatsos, J. J. Abbott, *Annu. Rev. Biomed. Eng.* **2010**, *12*, 55.
[243] F. A. Mohd Ghazali, M. N. Hasan, T. Rehman, M. Nafea, M. S. Mohamed Ali, K. Takahata, *J. Micromech. Microeng.* **2020**, *30*, 073001.
[244] X. Yan, Q. Zhou, M. Vincent, Y. Deng, J. Yu, J. Xu, T. Xu, T. Tang, L. Bian, Y. X. J. Wang, K. Kostarelos, L. Zhang, *Sci. Robot.* **2017**, *2*, aaq1155.
[245] K. I. Jang, K. Li, H. U. Chung, S. Xu, H. N. Jung, Y. Yang, J. W. Kwak, H. H. Jung, J. Song, C. Yang, A. Wang, Z. Liu, J. Y. Lee, B. H. Kim, J. H. Kim, J. Lee, Y. Yu, B. J. Kim, H. Jang, K. J. Yu, J. Kim, J. W. Lee, J. W. Jeong, Y. M. Song, Y. Huang, Y. Zhang, J. A. Rogers, *Nat. Commun.* **2017**, *8*, 15894.
[246] Y. Kim, H. Yuk, R. Zhao, S. A. Chester, X. Zhao, *Nature* **2018**, *558*, 274.
[247] M. Hippler, E. Blasco, J. Qu, M. Tanaka, C. Barner-Kowollik, M. Wegener, M. Bastmeyer, *Nat. Commun.* **2019**, *10*, 232.
[248] M. Lahikainen, H. Zeng, A. Priimagi, *Soft Matter* **2020**, *16*, 5951.
[249] W. Hu, G. Z. Lum, M. Mastrangeli, M. Sitti, *Nature* **2018**, *554*, 81.
[250] H. Gu, Q. Boehler, H. Cui, E. Secchi, G. Savorana, C. De Marco, S. Gervasoni, Q. Peyron, T. Y. Huang, S. Pane, A. M. Hirt, D. Ahmed, B. J. Nelson, *Nat. Commun.* **2020**, *11*, 2637.
[251] M. Lahikainen, H. Zeng, A. Priimagi, *Nat. Commun.* **2018**, *9*, 4148.
[252] S. Li, M. M. Lerch, J. T. Waters, B. Deng, R. S. Martens, Y. Yao, D. Y. Kim, K. Bertoldi, A. Grinthal, A. C. Balazs, J. Aizenberg, *Nature.* **2022**, *605*, 76.
[253] C. W. Moon, J. E. Park, M. Park, Y. Kim, K. Narasimha, J. K. Hyun, S. J. Park, *ACS Appl. Mater. Interfaces.* **2021**, *13*, 1555.
[254] H. N. Umh, S. Yu, Y. H. Kim, S. Y. Lee, J. Yi, *ACS Appl. Mater. Interfaces.* **2016**, *8*, 15802.
[255] Y. J. Quan, Y. G. Kim, M. S. Kim, S. H. Min, S. H. Ahn, *ACS Nano* **2020**, *14*, 5392.
[256] M. Kolle, A. Lethbridge, M. Kreysing, J. J. Baumberg, J. Aizenberg, P. Vukusic, *Adv. Mater.* **2013**, *25*, 2239.
[257] D. Li, R. R. Jiang, S. K. Chen, J. M. Wu, X. Dong, X. L. Wang, Y. Z. Wang, F. Song, *Chem. Eng. J.* **2023**, *453*, 139835.
[258] S. Foland, B. Swedlove, H. Nguyen, J. B. Lee, *J. Microelectromech. Syst.* **2012**, *21*, 1117.
[259] S. Banisadr, J. Chen, *Sci. Rep.* **2017**, *7*, 17521.
[260] S. Nam, D. Wang, G. Lee, S. S. Choi, *Nanophotonics* **2022**, *11*, 2139.
[261] J. A. H. P. Sol, R. F. Douma, A. P. H. J. Schenning, M. G. Debije, *Adv. Mater. Technol.* **2023**, *8*, 2200970.
[262] W. Shi, X. Zhang, R. Han, H. Li, H. Cao, Y. Chen, D. Wang, Z. Yang, W. He, *Liq. Cryst.* **2022**, *49*, 153.
[263] S. T. Kim, H. Finkelmann, *Macromol. Rapid Commun.* **2001**, *22*, 429.
[264] I. Kundler, H. Finkelmann, *Macromol. Rapid Commun.* **1995**, *16*, 679.
[265] J. Schmidtke, S. Kniesel, H. Finkelmann, *Macromolecules* **2005**, *38*, 1357.
[266] S. Nam, D. Wang, C. Kwon, S. H. Han, S. S. Choi, *Adv. Mater.* **2023**, *35*, 2302456.
[267] W. Zhang, H. Tian, T. Liu, H. Liu, F. Zhao, X. Li, C. Wang, X. Chen, J. Shao, *Mater. Horiz* **2023**, *10*, 2024.
[268] Y. Xiao, J. Mao, Y. Shan, T. Yang, Z. Chen, F. Zhou, J. He, Y. Shen, J. Zhao, T. Li, Y. Luo, *Nanoscale* **2020**, *12*, 7514.
[269] Z. S. Davidson, H. Shahsavan, A. Aghakhani, Y. Guo, L. Hines, Y. Xia, S. Yang, M. Sitti, *Sci. Adv.* **2019**, *5*, aay0855.
[270] A. Chortos, E. Hajiesmaili, J. Morales, D. R. Clarke, J. A. Lewis, *Adv. Funct. Mater.* **2020**, *30*, 1907375.
[271] E. Hajiesmaili, D. R. Clarke, *Nat. Commun.* **2019**, *10*, 183.
[272] P. Li, Y. Wang, U. Gupta, J. Liu, L. Zhang, D. Du, C. C. Foo, J. Ouyang, J. Zhu, *Adv. Funct. Mater.* **2019**, *29*, 1901908.
[273] S. Shian, K. Bertoldi, D. R. Clarke, *Adv. Mater.* **2015**, *27*, 6814.
[274] B. Aksoy, H. Shea, *Adv. Funct. Mater.* **2020**, *30*, 2001597.
[275] C. Zhang, B. Jin, X. Cao, Z. Chen, W. Miao, X. Yang, Y. Luo, T. Li, T. Xie, *Adv. Mater.* **2022**, *34*, 2206393.
[276] C. Zhang, G. Chen, K. Zhang, B. Jin, Q. Zhao, T. Xie, *Adv. Mater.* **2024**, *36*, 2313078.
[277] Y. Chen, H. Zhao, J. Mao, P. Chirarattananon, E. F. Helbling, N. S. P. Hyun, D. R. Clarke, R. J. Wood, *Nature* **2019**, *575*, 324.
[278] G. Li, X. Chen, F. Zhou, Y. Liang, Y. Xiao, X. Cao, Z. Zhang, M. Zhang, B. Wu, S. Yin, Y. Xu, H. Fan, Z. Chen, W. Song, W. Yang, B. Pan, J. Hou, W. Zou, S. He, X. Yang, G. Mao, Z. Jia, H. Zhou, T. Li, S. Qu, Z. Xu, Z. Huang, Y. Luo, T. Xie, J. Gu, et al., *Nature* **2021**, *591*, 66.
[279] X. Ji, X. Liu, V. Cacucciolo, M. Imboden, Y. Civet, A. El Haitami, S. Cantin, Y. Perriard, H. Shea, *Sci. Robot.* **2019**, *4*, aaz6451.
[280] C. Tang, B. Du, S. Jiang, Q. Shao, X. Dong, X. J. Liu, H. Zhao, *Sci. Robot.* **2022**, *7*, abm8597.
[281] A. Chortos, J. Mao, J. Mueller, E. Hajiesmaili, J. A. Lewis, D. R. Clarke, *Adv. Funct. Mater.* **2021**, *31*, 2010643.
[282] H. Liu, H. Tian, J. Shao, Z. Wang, X. Li, C. Wang, X. Chen, *ACS Appl. Mater. Interfaces.* **2020**, *12*, 56338.
[283] S. Schuhladen, F. Preller, R. Rix, S. Petsch, R. Zentel, H. Zappe, *Adv. Mater.* **2014**, *26*, 7247.
[284] Y. Y. Xiao, Z. C. Jiang, X. Tong, Y. Zhao, *Adv. Mater.* **2019**, *31*, 1903452.
[285] J. Sun, Y. Wang, W. Liao, Z. Yang, *Small*. **2021**, *17*, 2103700.
[286] G. Yang, L. Dong, M. Ren, B. Cui, X. Yuan, X. Wang, Y. Li, W. Li, G. Qiao, Y. Shao, W. Li, X. Wang, P. Xu, H. Fang, J. Di, Q. Li, *Nano Lett.* **2024**, *24*, 9608.
[287] S. Wu, Y. Hong, Y. Zhao, J. Yin, Y. Zhu, *Sci. Adv.* **2023**, *9*, adf8014.
[288] K. Hisano, S. Kimura, K. Ku, T. Shigeyama, N. Akamatsu, A. Shishido, O. Tsutsumi, *Adv. Funct. Mater.* **2021**, *31*, 2170298.
[289] P. Zhang, G. Zhou, L. T. de Haan, A. P. H. J. Schenning, *Adv. Funct. Mater.* **2021**, *31*, 2007887.
[290] W. C. Han, Y. J. Lee, S. U. Kim, H. J. Lee, Y. S. Kim, D. S. Kim, *Small.* **2023**, *19*, 2206299.
[291] Y. Geng, R. Kizhakidathazhath, J. P. F. Lagerwall, *Nat. Mater.* **2022**, *21*, 1441.
[292] Y. Yang, J. Wang, L. Wang, Q. Wu, L. Ling, Y. Yang, S. Ning, Y. Xie, Q. Cao, L. Li, J. Liu, Q. Ling, J. Zang, *Sci. Adv.* **2022**, *8*, abq1456.
[293] Y. Guo, H. Shahsavan, M. Sitti, *Adv. Mater.* **2020**, *32*, 2002753.
[294] Z. Liu, J. Liao, L. He, Q. Gui, Y. Yuan, H. Zhang, *Polym. Chem.* **2020**, *11*, 6047.
[295] S. V. Fridrikh, E. M. Terentjev, *Phys. Rev. E.* **1999**, *60*, 1847.
[296] X. Zhou, B. Jin, Z. Zhu, J. Wu, Q. Zhao, G. Chen, *Angew. Chem., Int. Ed.* **2024**, *63*, 202409182.
[297] E. P. A. van Heeswijk, L. Yang, N. Grossiord, A. P. H. J. Schenning, *Adv. Funct. Mater.* **2020**, *30*, 1906833.
[298] Y. Kim, X. Zhao, *Chem. Rev.* **2022**, *122*, 5317.
[299] L. Wang, Y. Kim, C. F. Guo, X. Zhao, *J. Mech. Phys. Solids.* **2020**, *142*, 104045.
[300] T. Wang, H. Ugurlu, Y. Yan, M. Li, M. Li, A. M. Wild, E. Yildiz, M. Schneider, D. Sheehan, W. Hu, M. Sitti, *Nat. Commun.* **2022**, *13*, 4465.
[301] C. Zhou, Y. Yang, J. Wang, Q. Wu, Z. Gu, Y. Zhou, X. Liu, Y. Yang, H. Tang, Q. Ling, L. Wang, J. Zang, *Nat. Commun.* **2021**, *12*, 5072.
[302] T. Xu, J. Zhang, M. Salehizadeh, O. Onaizah, E. Diller, *Sci. Robot.* **2019**, *4*, aav4494.

[303] J. Zhang, Z. Ren, W. Hu, R. H. Soon, I. C. Yasa, Z. Liu, M. Sitti, *Sci. Robot.* **2021**, *6*, abf0112.
[304] Y. Li, H. Yu, K. Yu, X. Guo, X. Wang, *Adv. Funct. Mater.* **2021**, *31*, 2100338.
[305] Y. Sun, L. Wang, Z. Zhu, X. Li, H. Sun, Y. Zhao, C. Peng, J. Liu, S. Zhang, M. Li, *Adv. Mater.* **2023**, *35*, 2302824.
[306] M. del Pozo, C. Delaney, C. W. M. Bastiaansen, D. Diamond, A. P. H. J. Schenning, L. Florea, *ACS Nano* **2020**, *14*, 9832.
[307] R. Lan, J. Sun, C. Shen, R. Huang, L. Zhang, H. Yang, *Adv. Funct. Mater.* **2019**, *29*, 1900013.
[308] X. Zhao, Y. Chen, B. Peng, J. Wei, Y. Yu, *Angew. Chem., Int. Ed.* **2023**, *62*, 202300699.
[309] Y. Liu, B. Xu, S. Sun, J. Wei, L. Wu, Y. Yu, *Adv. Mater.* **2017**, *29*, 1604792.
[310] O. M. Wani, R. Verpaalen, H. Zeng, A. Priimagi, A. P. H. J. Schenning, *Adv. Mater.* **2019**, *31*, 1805985.
[311] Y. Song, Z. Li, M. Zadan, J. Wang, S. Kumar, C. Majidi, *Nat. Commun.* **2025**, *16*, 7292.
[312] X. Zheng, Q. Ma, Y. Tao, Y. Huang, M. Li, H. Ji, *ACS Appl. Mater. Interfaces.* **2023**, *15*, 13609.
[313] X. Wang, N. Zhao, B. Qin, J. Xu, W. Yang, C. Li, L. Sun, J. Zhang, *Macromol. Chem. Phys.* **2020**, *221*, 2000071.
[314] Y. Zhang, B. Yuan, Y. Shi, X. Chen, Z. Wang, L. He, B. Wang, J. Xiao, M. Yu, Y. Gao, L. Zhang, C. Zou, R. Lan, H. Yang, *Mater. Horiz.* **2025**, *12*, 2014.
[315] Y. Zhu, J. Huang, H. Mi, Z. Xu, Y. Ai, S. Gong, C. Li, M. Wang, L. Chen, *Angew. Chem., Int. Ed.* **2025**, *64*, 202421915.
[316] H. Huang, H. Li, J. Yin, K. Gu, J. Guo, C. Wang, *Adv. Mater.* **2023**, *35*, 2211117.
[317] Y. Qi, L. Song, C. Zhou, S. Zhang, *Adv. Mater.* **2023**, *35*, 2210753.
[318] J. Lou, *Mater. Today* **2024**, *75*, 1.
[319] B. Liu, C. L. Yuan, H. L. Hu, H. Wang, Y. W. Zhu, P. Z. Sun, Z. Y. Li, Z. G. Zheng, Q. Li, *Nat. Commun.* **2022**, *13*, 2712.
[320] R. Arppe, T. J. Sørensen, *Nat. Rev. Chem.* **2017**, *1*, 0031.
[321] J. Bai, Z. Shi, X. Jiang, *Adv. Funct. Mater.* **2023**, *33*, 2301797.
[322] B. Liu, C. L. Yuan, H. Hu, P. Sun, L. H. Yu, Z. G. Zheng, *J. Mater. Chem. C.* **2022**, *10*, 16924.
[323] K. Zhang, X. Zhou, S. Li, L. Zhao, W. Hu, A. Cai, Y. Zeng, Q. Wang, M. Wu, G. Li, J. Liu, H. Ji, Y. Qin, L. Wu, *Adv. Mater.* **2023**, *35*, 2370315.
[324] H. Yang, S. Li, J. Zheng, G. Chen, W. Wang, Y. Miao, N. Zhu, Y. Cong, J. Fu, *Adv. Mater.* **2023**, *35*, 2301300.
[325] J. Zhang, H. Shen, X. Liu, X. Yang, S. L. Broman, H. Wang, Q. Li, J. W. Y. Lam, H. Zhang, M. Cacciarini, M. B. Nielsen, B. Z. Tang, *Angew. Chem., Int. Ed.* **2022**, *61*, 202208460.
[326] S. Zeng, D. Zhang, W. Huang, Z. Wang, S. G. Freire, X. Yu, A. T. Smith, E. Y. Huang, H. Nguon, L. Sun, *Nat. Commun.* **2016**, *7*, 11802.
[327] R. Lin, Y. Qi, D. Kou, W. Ma, S. Zhang, *Adv. Funct. Mater.* **2022**, *32*, 2207691.
[328] S. Zeng, Z. Yang, Z. Hou, C. Park, M. D. Jones, H. Ding, K. Shen, A. T. Smith, H. X. Jin, B. Wang, H. Jiang, L. Sun, *Proc. Natl. Acad. Sci. USA* **2022**, *119*, 2118991119.
[329] H. Li, X. Xue, Y. Cao, H. Cheng, A. Luo, N. Guo, H. Li, G. Xie, Y. Tao, R. Chen, W. Huang, *J. Am. Chem. Soc.* **2023**, *145*, 7343.
[330] J. Wei, C. Liu, J. Duan, A. Shao, J. Li, J. Li, W. Gu, Z. Li, S. Liu, Y. Ma, W. Huang, Q. Zhao, *Nat. Commun.* **2023**, *14*, 627.
[331] Z. H. Zhao, P. C. Zhao, S. Y. Chen, Y. X. Zheng, J. L. Zuo, C. H. Li, *Angew. Chem., Int. Ed.* **2023**, *62*, 202301993.
[332] L. Bai, Y. Jin, X. Shang, H. Jin, W. Zeng, L. Shi, *Chem. Eng. J.* **2023**, *456*, 141082.
[333] F. Zhang, Q. Li, C. Wang, D. Wang, M. Song, Z. Li, X. Xue, G. Zhang, G. Qing, *Adv. Funct. Mater.* **2022**, *32*, 2204487.
[334] X. Yang, C. Valenzuela, X. Zhang, Y. Chen, Y. Yang, L. Wang, W. Feng, *Matter.* **2023**, *6*, 1278.
[335] H. Zhang, Q. Li, Y. Yang, X. Ji, J. L. Sessler, *J. Am. Chem. Soc.* **2021**, *143*, 18635.
[336] Y. Jiang, J. Ma, Z. Ran, H. Zhong, D. Zhang, N. Hadjichristidis, *Angew. Chem., Int. Ed.* **2022**, *61*, 202208516.
[337] F. Fu, L. Shang, Z. Chen, Y. Yu, Y. Zhao, *Sci. Robot.* **2018**, *3*, aar8580.
[338] L. Minati, F. Benetti, A. Chiappini, G. Speranza, *Colloids Surf. A.* **2014**, *441*, 623.
[339] P. Zhao, B. Li, Z. Tang, Y. Gao, H. Tian, H. Chen, *Smart Mater. Struct.* **2019**, *28*, 075037.
[340] M. Li, H. Tan, L. Jia, R. Zhong, B. Peng, J. Zhou, J. Xu, B. Xiong, L. Zhang, J. Zhu, *Adv. Funct. Mater.* **2020**, *30*, 2000008.
[341] G. Gao, F. Yang, F. Zhou, J. He, W. Lu, P. Xiao, H. Yan, C. Pan, T. Chen, Z. L. Wang, *Adv. Mater.* **2020**, *32*, 2004290.
[342] J. Park, D. Kang, H. Chae, S. K. Ghosh, C. Jeong, Y. Park, S. Cho, Y. Lee, J. Kim, Y. Ko, J. J. Kim, H. Ko, *Sci. Adv.* **2022**, *8*, abj9220.
[343] M. Zhu, Z. Sun, Z. Zhang, Q. Shi, T. He, H. Liu, T. Chen, C. Lee, *Sci. Adv.* **2020**, *6*, aaz8693.
[344] D. Rus, M. T. Tolley, *Nature* **2015**, *521*, 467.
[345] M. T. Tolley, R. F. Shepherd, B. Mosadegh, K. C. Galloway, M. Wehner, M. Karpelson, R. J. Wood, G. M. Whitesides, *Soft Robot* **2014**, *1*, 213.
[346] F. Ilievski, A. D. Mazzeo, R. F. Shepherd, X. Chen, G. M. Whitesides, *Angew. Chem., Int. Ed.* **2011**, *50*, 1890.
[347] C. Christianson, N. N. Goldberg, D. D. Deheyn, S. Cai, M. T. Tolley, *Sci. Robot.* **2018**, *3*, aat1893.
[348] R. V. Martinez, J. L. Branch, C. R. Fish, L. Jin, R. F. Shepherd, R. M. D. Nunes, Z. Suo, G. M. Whitesides, *Adv. Mater.* **2013**, *25*, 205.
[349] C. Laschi, M. Cianchetti, B. Mazzolai, L. Margheri, M. Follador, P. Dario, *Adv. Robot.* **2012**, *26*, 709.
[350] M. W. Hannan, I. D. Walker, *J. Robotic. Syst.* **2003**, *20*, 45.
[351] S. Seok, C. D. Onal, K. J. Cho, R. J. Wood, D. Rus, S. Kim, *IEEE/ASME Trans. Mechatron.* **2013**, *18*, 1485.
[352] D. Drotman, M. Ishida, S. Jadhav, M. T. Tolley, *IEEE/ASME Trans. Mechatron.* **2019**, *24*, 78.
[353] C. D. Onal, D. Rus, *Bioinspir. Biomim.* **2013**, *8*, 026003.
[354] S. M. Mirvakili, I. W. Hunter, *Adv. Mater.* **2018**, *30*, 1704407.
[355] Z. Deng, H. Zhang, A. Priimagi, H. Zeng, *Adv. Mater.* **2024**, *36*, 2209683.
[356] Y. Zhao, Z. Liu, P. Shi, C. Chen, Y. Alsaid, Y. Yan, X. He, *Nat. Mater.* **2025**, *24*, 116.
[357] X.-Q. Wang, C. F. Tan, K. H. Chan, X. Lu, L. Zhu, S.-W. Kim, G. W. Ho, *Nat. Commun.* **2018**, *9*, 3438.
[358] R. Zheng, L. Ma, W. Feng, J. Pan, Z. Wang, Z. Chen, Y. Zhang, C. Li, P. Chen, H. K. Bisoyi, B. Li, Q. Li, Y. Lu, *Adv. Funct. Mater.* **2023**, *33*, 2301142.

Jiao Liu received her Ph.D. degree in Advanced Materials and Liquid Crystal Institute (AMLCI) at Kent State University in 2022. She is currently an assistant professor at Nanjing University of Posts and Telecommunications. Her research focuses on circularly polarized luminescent liquid crystal materials, chiral liquid crystal elastomer, lyotropic liquid crystals, and stimuli-responsive soft matter.

Hao-Yi Jiang is currently a graduate student at Nanjing University of Posts and Telecommunications. His research mainly focuses on lyotropic liquid crystals, biological detection based on liquid crystals, and oblique helicoidal cholesteric liquid crystals.

Bing-Xiang Li received his Ph.D. degree in Chemical Physics from the Advanced Materials and Liquid Crystal Institute at Kent State University in 2019. He is currently a professor at Nanjing University of Posts and Telecommunications. His current research spans from liquid crystals, stimuli-responsive soft matter, active matter, to biological physics.

Yan-Qing Lu received both his B.S. and Ph.D. degrees from Nanjing University, China, in 1991 and 1996, respectively. He has 5 years of experience in the telecom industry in the United States and China. He is currently a Changjiang Distinguished Professor at Nanjing University and a Fellow of the Optical Society of America and the Chinese Optical Society. His research interests include liquid crystal photonics, fiber optics, and nonlinear optics.

Quan Li is Distinguished Chair Professor and Director of Institute of Advanced Materials at Southeast University. He held appointments in the USA, Germany, and France. Li received his Ph.D. from the Chinese Academy of Sciences in Shanghai, where he was promoted to the youngest Full Professor in February 1998. He is a Fellow of the Royal Society of Chemistry. He has been elected as a member of the European Academy of Sciences and the European Academy of Sciences and Arts. He has also been honored as Professor and Chair Professor at ten universities. His current research interest spans from stimuli-responsive smart soft matter, advanced photonics, and optoelectronic materials for energy harvesting and energy saving to functional biocompatible materials, biomedical materials, and nanoparticles to nanoengineering and device fabrication.